MITTEILUNGEN AUS DEM GEOLOGISCHEN INSTITUT DER EIDG.TECHNISCHEN HOCHSCHULE
UND DER UNIVERSITÄT ZÜRICH
Neue Folge
Nr. 241

Stefan M. Schmid

Laboratory experiments on rheology and deformation mechanisms in calcite rocks and their application to studies in the field

Zürich 1982

PREFACE

This contribution was submitted as a Habilitationsschrift to the president of the ETH Zürich in June 1981. I wish to thank the members of the committee, Profs. M.S.Paterson, J.G.Ramsay and A.B.Thompson for their support.

VORWORT

Dieser Beitrag wurde dem Präsidenten der ETH Zürich im Juni 1981 als Habilitationsschrift vorgelegt. Ich danke den Mitgliedern des begutachtenden Kommittees, den Professoren M.S.Paterson, J.G.Ramsay und A.B.Thompson für ihre Unterstützung.

CONTENTS

ABSTRACT

First, the major deformation mechanisms and associated flow laws will be discussed. Great importance is attributed to the grain size which can have a profound effect on the rheological behaviour of a rock: at high stresses small grain sizes have a hardening effect, at low stresses they have a weakening effect. The microstructures and crystallographic preferred orientations (textures) of experimentally deformed rocks will be presented as a basis of comparison with naturally deformed rocks.

The microfabric of some calcite tectonites from the Helvetic nappes of Switzerland will be analysed and attempts are made to interpret the deformation mechanisms operative in these rocks. It is argued that the flow stresses operative may be relatively large in some environments ($>$1000bar) and extremely low in other cases, such as the Lochseiten mylonite ($<$100bar).

The strain softening mechanism operative in the calc-mylonites is interpreted to be the result of grain size reduction by dynamic recrystallization inducing a change in deformation mechanism towards superplastic flow.

The mechanics of overthrusting in the case of the Glarus overthrust will be re-discussed in the light of the more recent laboratory results. As a consequence of the very low relative strength of the mylonite as compared to the thrust block, strain is localized within the mylonite layer during the final phase of thrusting. Models of gravity spreading, always based on the assumption of a yielding thrust block, are rejected for this final phase of thrusting.

ZUSAMMENFASSUNG

Zuerst werden die wichtigsten Verformungsmechanismen und die damit verbundenen Fliessgesetze diskutiert. Der Korngrösse wird grosse Bedeutung beigemessen in Bezug auf das rheologische Verhalten des Gesteins: unter hohen Spannungen erhöht eine kleine Korngrösse die Festigkeit, unter niedrigen Spannungen ist die Fliessgrenze herabgesetzt in feinkörnigen Gefügen. Die Mikrostrukturen und die kristallographisch bevorzugte Einregelung (Textur) experimenteller Proben werden beschrieben in Hinsicht auf einen Vergleich mit natürlich verformten Gesteinen.

Das Gefüge einiger Kalk-Tektonite aus den helvetischen Decken der Schweiz wird analysiert und es wird versucht, die aktiven Verformungsmechanismen zu interpretieren. Die Fliessspannungen werden als relativ hoch eingeschätzt in einigen Fällen ($>$1000bar), währenddem in anderen Fällen (so im Lochseitenkalk) extrem niedrige Fliesspannungen abgeleitet werden ($<$100bar).

Der Mechanismus der Herabsetzung der Fliesspannung in den Kalk-Myloniten wird als das Resultat dynamischer Rekristallisation gedeutet, einer Korngrössenreduktion, welche einen Wechsel im Verformungsmechanismus zu superplastischem Fliessen herbeiführt.

Die Mechanik im Falle der Glarner Hauptüberschiebung wird erneut diskutiert im Lichte neuer Laboruntersuchungen. In Folge der sehr niedrigen relativen Fliesspannung im Mylonit, verglichen mit der Festigkeit im Ueberschiebungsblock, wird die Verformung beschränkt auf den Mylonithorizont während der finalen Phase der Ueberschiebung. "Gravity spreading"-Modelle, welche immer auf der Annahme eines Ueberschiebungsblockes oberhalb der Fliessgrenze basieren, werden abgelehnt für diese finale Ueberschiebungsphase.

I. INTRODUCTION

In discussions with field oriented structural geologists an experimental geologist often notes criticism in regard to the applicability of experimental results in the study of naturally deformed rocks. The critics often point out that the laboratory experiments which have to be performed under controlled and therefore necessarily simple conditions are unadequate to throw light on the more complex processes in geological environments. In another branch of earth sciences however, namely petrology, experimental results are more widely applied and no geologist would question the great impact experimental petrology has had on the interpretation of field petrological data.

It is not the aim of this study to analyse the reasons for the relatively modest impact experimental rock deformation has had in structural geology but it may be mentionned that this state of affairs has certainly to do with (i) the great difficulty in performing geologically relevant deformation experiments (the load has to be applied through a moving piston, while the specimen is held at high pressure and temperature) and (ii) the temptation of the field geologists to choose particularly difficult areas not really suitable for the study of fundamental processes of rock deformation.

An attempt is made here to bridge this gap between experimental and field studies. Thereby the discussion concentrates on ductile deformation of calcite rocks. It will become evident how little we know about many aspects of rock creep, particularly about solid-fluid interactions during deformation. At the same time there exist important results from laboratory experiments which await application to field problems.

Some of the results presented here have already been published in separate specialized contributions. It was felt necessary however to summarize these results and to put them into a larger context, especially what the applications to field geological problems are concerned. Extending the laboratory results into natural rock deformation is not an easy task because nearly all the constraints in a well controlled experiment are lost and as a consequence the wellknown uncertainty takes over which makes geology to a descriptive and sometimes speculative, but at the same time to such an exciting branch of science.

II. FLOW LAWS AND DEFORMATION MECHANISMS IN CALCITE ROCKS

A. Some general remarks concerning flow laws

If we consider a solid under constant differential stress σ, then its flow- or strain-rate $\dot{e}$ is dictated by three factors primarily and we can generally write

$$\dot{e} = \dot{e}\ (\ \sigma\ ,\ e\ ,\ T\ )$$

where the stress difference σ (determined as $\sigma_1 - \sigma_2$) and briefly referred to as "stress" throughout this contribution) the strain e and the temperature T are the most important quantities which determine the resulting strain rate. Striktly speaking such a simple flow law is only valid provided that all the other factors such as pressure, H_2O content, grain size etc. are held constant or can be assumed to have no major influence on the material properties. During the first stages of deformation the strain rate strongly depends on strain (primary creep), after a few percent of strain the rate of deformation slows down to a stationary value. The rock is then said to be in steady state and ideally strain has no influence on the strain rate any more. We will see later that strain can alter the material properties and thereby invalidate the assumption of steady state. At this point it is important to say that the concept of steady state is used here merely to imply flow at constant stress and strain rate.

For thermally activated creep one can emprically derive flow laws from a series of experiments on the same rock, valid for steady state flow only. They are usually presented in the form of

$$\dot{e} = \dot{e}_0 \exp {}^{-H}/RT \quad f\ (\sigma)$$

where $\dot{e}_0$ is a material dependent constant, H is the apparent activation energy for creep and R is the Gas Constant. The stress dependence can adequately be described in most cases by either

$$f(\sigma) = \exp \, {}^{\sigma}/\sigma_o \qquad \text{(exponential creep law)}$$

or

$$f(\sigma) = \sigma^n \qquad \text{(power creep law)}$$

where the constants σ_o and n determine the stress sensitivity of the strain rate. Because in most cases the parameter n is found to be greater than unity rocks deviate from linear viscous behaviour.

There is no single flow law for all conditions of stress and temperature, simply because the deformation mechanism is a function of stress and temperature as well. Associated with each of these deformation mechanisms is a different flow law. It is usual to sub-divide the stress-temperature space into different fields by means of a deformation mechanism map (Ashby and Verrall 1978 and fig. 1). Whithin each of these fields a particular mechanism is dominant.

Such deformation mechanism maps are normally calculated from first principles by assuming specific microdynamical models. Experiments often merely provide numbers for the various material dependent constants in the theoretical flow laws. The field of diffusional creep (Nabarro-Herring and Coble creep) in particular is postulated on theoretical grounds because this mechanism has not been experimentally observed in the case of rocks and minerals so far. Even creep of ice, as observed at temperatures just below the melting point and at very low stresses seems not to conform to the model of diffusional creep.

The primary aim of these deformation mechanism maps is to outline the expected conditions of appearance of given deformation mechanisms outside the range of $\dot{e}$ - σ - T - conditions accessible to the experimentalist. The main problem in the application of the laboratory data is the enormous gap between geological strain rates of the order of $10^{-10}\,\mathrm{sec}^{-1}$ to $10^{-15}\,\mathrm{sec}^{-1}$ (involving time spans of between 30 and 3 million years for 10 percent shortening strain) and the laboratory strain rates between usually 10^{-2} and $10^{-7}sec^{-1}$. As illustrated in fig. 1 one has a high chance of crossing a boundary between deformation mechanism fields by extrapolating down to lower strain rates and consequently to lower stresses at any given temperature. Therefore a flow law observed at high stresses under laboratory strain rates can be extrapolated over a limited range of strain rates and stresses only. It is also seen from fig. 1 that the deformation mechanism fields essentially depend on stress. In order to explore the flow behaviour at low stresses the experimentalist is forced to elevate the temperature beyond the range of temperatures expected under natural conditions (Paterson 1976). Thus, elevated temperatures are essentially used as a "trade off" for unattainably slow geological strain rates. Once a flow law has been established at high temperatures and low stresses the geologist has to extrapolate down to lower temperatures, along a path which is less likely to cross deformation mechanism boundaries.

B. Flow laws in calcite rocks

From the now relatively numerous studies on flow laws of different calcite rocks (e.g. Heard 1963, Heard and Raleigh 1972, Rutter 1970 and 1974, Schmid, Boland and Paterson 1977, Schmid Paterson and Boland 1980) it can be inferred that there is no unique flow law valid for all calcite rocks (table 1).
Apart from strain rate, temperature and stress, grain size appeares to be a parameter of high importance. A comparison between coarse grained marbles (grain sizes of 200-300 μm) and finegrained limestone (grain size of less than 10 μm) shows that the relative strength of these monomineralic rocks is largely dependent on grain size (fig. 2). When considering this influence of grain size on the rheological properties we have to distinguish between (i) a high stress environment at relatively low T and high $\dot{e}$, where a small grain size leads to a relatively higher flow stress and (ii) a low stress environment where the finegrained rock flows at a relatively lower flow stress. This contrasting influence of grain size on the strength results from the fact that different deformation mechanisms are operative at different stress levels.

Unfortunately we have little information so far on the influence of two other potentially important factors such as (i) the influence of fluid phases on the rheological properties and (2) the role of impurities and second phase minerals in calcite rocks.

1) The high stress region

At room temperature the brittle-ductile transition in calcite rocks can be observed to be mainly a function of the effective confining pressure, that is, the difference between confining pressure and the internal fluid pressure (Rutter 1974). The flow stress within the ductile field never reaches a constant (steady state) value because of continued work hardening with increasing strain. The flow stress at an arbitrary chosen strain (usually the 10 percent strain level is chosen) is mainly a function of effective confining pressure and largely independent of strain rate.

The influence of effective confining pressure on the strength indicates that friction between cohesionless surfaces is at least partially controlling the strength of the material. Because no fractures are visible macroscopically nor under the optical microscope for rocks deformed in the ductile field, these microcracks presumably mainly follow the grain boundaries and part of the strain is achieved by frictionally controlled grain boundary sliding. This pressure dependent type of ductile flow is sometimes referred to as cataclastic flow. However, abundant twinning within grains is observed at the same time (fig. 3), indicating that intragranular deformation accommodates a large fraction of total strain even in the pressure sensitive region in the case of calcite rocks.

At temperatures higher than around $400^{\circ}C$ under laboratory strain rates ductile deformation is fully achieved by intracrystalline crystal plastic deformation, i.e. by dislocation glide and twinning. Effective pressure ceases to be an important parameter. Rutter (1974) observed that both confining pressure and pore pressure have no longer a significant effect on the rheological properties. At the same time the flow behaviour of rocks becomes thermally activated and this goes hand in hand with the strength becoming strain rate sensitive. Empirically the σ - $\dot{e}$ - relationship is best described by an exponential stress dependence of strain rate (see page 6 and table 1). The same relationship can be derived from first principles by assuming that the strain rate is controlled by the resistance to glide (low temperature plasticity of Ashby and Verall 1978, see fig. 1, occasionally also referred to as dislocation glide). The motion of dislocations through the crystal lattice is obstructed by energy barriers of different sorts (impurities for example) and these obstacles can only be overcome at a certain rate which is temperature sensitive.

At room temperature as well as in the 400-500^{o}C temperature region the strength of calcite is grain size dependent in the sense that a small grain size leads to higher flow stresses at constant temperature and strain rate. Olsson (1974) systematically investigated the dependence of the yield stress σ_y on grain size in the range of 20 - 300^{o}C and found the following empirical relationship:

$$\sigma_y = \sigma_o + k\, d^{-1/2}$$

where σ_o and k are constants and d is the grain size. This grain size dependence is known as the Hall-Petch law in metallurgy (Nicolas and Poirier 1976). The hardening effect of a small grain size is due to the fact that grain boundaries are obstacles to the free propagation of slip and twinning. The shear strain produced by the conservative motion of dislocations or by twinning within a particular grain cannot simply be accommodated by the neighbouring grains. These strain incompatibilities near grain boundaries are nicely illustrated by the lensoid shaped deformation twins in calcite which are typical for experimentally and naturally deformed calcite rocks (fig. 4). The constriction of twins at grain boundaries implies that twinning can only occommodate strain in the grain interior whereas the grain boundary region deforms by slip mechanisms which are relatively harder to operate at low temperatures (Turner et al. 1954). Hence, in a finegrained limestone the strength of the polycrystalline aggregate will largely be determined by the resistance to glide (or cracking in the cataclastic domain) near the tip of a twin lamella. In the coarse grained marble however the local stress concentrations at grain boundaries (illustrated by fig. 6) will have a small effect only on the bulk strength of the aggregate.

The fact that twinning is more effective in coarse grained materials is illustrated by the observation of Rutter (1970) that finegrained Solnhofen limestone does not twin any more at and above 400^{o}C (and below stresses of 2-3kb) whereas marbles (Heard and Raleigh 1972, Schmid Paterson and Boland 1980) still deform by twinning up to temperatures of 600-700^{o}C (and down to stresses of about 1 kb).

It seems therefore that the critical grain size below which no twinning occurs is stress dependent. The grain size in the matrix of oolitic limestones, experimentally deformed for other purposes by Schmid and Paterson (1977), is highly variable and the minimum grain size below which no twinning occurs was determined as a function of stress observed at 10 percent strain for some of these specimens. In fig. 5 these results are plotted together with the transition stresses for twinning observed in Solnhofen limestone and Carrara marble. The trend for the minimum grain size for twinning to be stress dependent is confirmed but the scatter is considerable. This scatter is partly due to the fact that the presence or absence of twins in any grain depends on the orientaion of the twin planes in respect to the applied stress field and that there is no absolutely sharp boundary between the twinning and non-twinning fields. If further experimental studies could establish a better correlation and if it can be demonstrated that the effects of strain, strain rate and temperature are unimportant, such a correlation could well serve as a paleostress indicator.

2) The intermediate stress region

Below 2kb in the case of Solnhofen limestone and below 1 -1.4kb in marbles a power law dependence (see page 6 and table 1) best describes the rheological behaviour. At the same time the relative strength of calcite rocks becomes largely grain size independent (fig. 2). The activation energies for creep (table 1) are now near the experimentally determined activation energy for diffusion of carbon and oxygen in calcite (88 kcal mole^{-1}, Anderson 1969). This correspondence in activation energies is a general one for many materials (Kirby and Raleigh 1973) and is consistent with a model of Weertman (1968) assuming that the flow rate is controlled by climb of dislocations (i.e. a process involving diffusion) out of their glide plane. Thus, climb is the rate controlling step although glide still accommodates most of the bulk strain in the grains.

Climb allows the dislocations to aggregate along subgrain boundaries within the old grains (fig. 7). By a process of progressive misorientation of subgrains first proposed by Hobbs (1968) to explain dynamic (or syntectonic) recrystallization the subgrains eventually individualize into an equiaxed mosaic of new grains (fig. 8). This type of recrystallization called in situ - recrystallization by Poirier and Nicolas (1975) or rotation recrystallization by Guillope and Poirier (1979) is distinct from a nucleation and growth mechanism which may also occur during deformation. Both the migration of dislocations into dislocation walls (recovery) and syntectonic recrystallization oppose the effect of work hardening and lead to a steady state situation by keeping the dislocation density at a constant value which is stress dependent.

Theoretically the determination of dislocation density under the transmission electron microscope can lead to a paleostress determination. Schmid, Paterson and Boland (1980) showed however that small strains introduced into experimentally deformed specimens during cooling under pressure lead to an increase in dislocation density. The dislocation density in naturally deformed calcite may therefore not be used to deduce stresses during steady state flow if small strains during cooling and uplifting are likely to have altered the dislocation density (Briegel and Goetze 1978).

Twiss (1977) has shown theoretically that dislocation density can be related to subgrain size and hence that the subgrain size also may be used to determine paleostresses. This method of paleostress determination is more reliable because grain size is more likely to survive cooling and uplift. The sizes of both optically visible subgrains (subgrains on a TEM scale are much smaller) and grains recrystallized by the mechanism of subgrain rotation on specimens of experimentally deformed marble (Schmid, Paterson and Boland 1980) was measured and found to be inversly proportional to the flow stress and the following empirical relationship between stress and grain size d was found

$$\log \sigma = \log K + b \log d$$

where log K = 3.67 $\pm$ 0.07 if stress is given in bars and grain size is measured in μm, and where b = -1.01 $\pm$ 0.05. This stress dependence of the recrystallized grain size (fig. 10) as a result of recovery and syntectonic recrystallization is likely to record the deviatoric stress during the main act of deformation in which the geologist is usually interested. Similar relationships were found in minerals such as olivine, quartz and halite by Post (1973 and 1977), Kohlstedt et al. (1976), Mercier et al. (1977), Guillope and Poirier (1979) and Ross et al. (1980).

Another mechanism of recrystallization was found to occur in Carrara marble at elevated temperatures. It is driven by grain boundary migration and leads to considerable grain growth at the highest temperatures (fig. 9). Guillope and Poirier (1979) refer to this type of recrystallizaion as "migration recrystallization". For halite these authors found that the grain size produced by migration recrystallization is stress dependent as well. The grain size at a given stress level however is roughly an order of magnitude larger than that for rotation recrystallization.

The possibility of more than one recrystallization mechanism makes the application of recrystallized grain size paleostress determinations difficult. It has to be ensured that the mechanism in the natural case is the same as the mechanism operative in the laboratory. Also one has to be able to exclude the possibility of subsequent grain growth under static conditions. Furthermore, in chapter V the possibility of a recrystallization induced change in deformation mechanism away from power law creep will be discussed. In such a case the established stress - grain size relationship breaks down too.

3) The low stress region

Three different mechanisms can be expected to operate in the low stress region: (i) pressure solution mechanisms (ii) creep by solid state diffusion and (iii) creep by grain boundary sliding. All of them are strongly grain size dependent, but in contrast to the high stress region a small grain size leads to a relatively lower flow stress at constant strain rate. The first two of these mechanisms lead to linear viscous behaviour.

Rutter (1976) proposed a deformation mechanism map for calcite (fig. 11) by taking into account creep by solid state diffusion (Nabarro-Herring and Coble creep) on the one hand and pressure solution on the other hand. Unfortunately both these mechanisms have not yet been experimentally observed to operate in calcite rocks.

There is ample evidence in naturally deformed rocks that pressure solution is a common deformation mechanism at relatively low temperatures. In Rutter's model for pressure solution the rate of deformation is mainly controlled by the normal stress across a grain boundary, the concentration of the solution outside the interface between two grains and by the grain boundary diffusivity in the presence of a fluid film at the grain boundary. It has to be emphazised that Rutters model applies to pressure solution at the scale of individual grains only. In natural rock deformation solution transfer often occurs on a much bigger scale and in such cases the flow law derived from this model does not apply.

Creep by solid state diffusional mass transfer has not yet been observed experimentally in rock materials. At moderate temperatures, where fluids are present in rocks the solution transfer model leads to higher strain rates than the solid state diffusion model (fig. 11). From this figure it is also evident that pressure solution mechanisms are extremely difficult to produce under laboratory conditions because they operate at low stresses and temperatures only, i.e. at very slow strain rates. By increasing the temperature at low stresses in order to produce measurable strain rates other mechanisms with a higher activation energy, such as solid state diffusional creep or grain boundary sliding will operate. Another interesting feature of fig. 11 is that the flow stress at a given strain rate is nearly temperature insensitive within the field of pressure solution. Rutter (1976) points out that this feature results from the competing effects of (i) decreasing solubility of calcite with increasing temperature and (ii) increasing pressure sensitivity of solubility with increasing temperature. At the same time the diffusivity within a grain boundary water film is not expected to be very temperature sensitive.

The third mechanism likely to operate at low stresses is grain boundary sliding leading to superplastic behaviour. The notion of superplasticity is a phenomenological one and implies extreme ductility in extension of materials. In this very broad sense all highly deformed rocks such as mylonites could be called superplastic. Superplastic deformation in the usual narrow sense however is additionally characterized by (i) a low value of the parameter n in the flow law of the form $\dot{e} \propto \sigma^n$, with $1 < n < 3$ and (ii) by the observation that the grains remain equiaxed even after large amounts of strain. Most authors regard grain boundary sliding as the prime strain producing mechanism during superplastic flow (Edington et al. 1976). Microdynamical models for superplastic flow usually assume that the strain rate at any given temperature and stress is not controlled by the viscous resistance to sliding at the grain boundaries but rather by the slowest event during the process of grain boundary sliding and grain swopping, namely the minor changes in shape the grains have to undergo in order to slide past each other and to change neighbours (fig. 12). Ball and Hutchinson (1969) proposed that dislocations pile up at unfavourably positioned grain boundaries and that these dislocations escape by climb into the grain boundaries. An alternative model by Ashby and Verrall (1973) proposes local diffusional mass transfer.

Superplastic flow of finegrained Solnhofen limestone has been observed by Schmid, Boland and Paterson (1977) to be the dominant deformation mechanism below stresses of 400 bar at $900^{0}C$ and below 1000 bar at $600^{0}C$. An observed value of 1.7 for the stress exponent n as well as the observation of extensive grain boundary sliding using the split cylinder technique provide strong evidence that superplastic flow is the dominant deformation mechanism in calcite at low stresses. No evidence for Coble creep was found.

Figs. 13 and 14 are deformation mechanism maps entirely based on empirically determined flow laws (table 1). In these maps the field of diffusional creep dominating at low stresses in Rutters deformation mechanism map (fig. 10) has been replaced by the experimentally determined flow law for superplastic behaviour. It is interesting to note that the observed flow law for superplastic creep does not differ drastically from Rutters theoretical predictions based on an entirely different mechanism, namely diffusional creep.

III. THE MICROFABRIC OF EXPERIMENTALLY DEFORMED CALCITE ROCKS

A. Microstructure

Early work on experimental deformation of calcite single crystals (Turner et al. 1954) showed that twinning is easier than r-glide at low temperatures and that the critical resolved shear stress for r-glide, being very temperature sensitive, eventually becomes lower than that for twinning on e at increased temperatures. The same trend was observed for polycrystalline Carrara marble where twinning is dominant above 1000 bar differential stress, corresponding to temperatures of less than 600-700^{o}C at laboratory strain rates (fig. 15) and where twinning is absent in the low stress-high temperature region (fig. 9). Schmid, Paterson and Boland (1980) showed that the transition from dominantly twinning to dominantly glide coincides with the transition from an exponential stress dependence of strain rate to a power law stress dependence. The power law region, where intracrystalline glide predominates,can be subdivided into (i) a stress range of 200-1000 bars where polygonization with the typical development of equiaxed subgrains is confined to the grain boundary region of original grains and where undulose extinction and prismatic subgrains are found in the grain interior ("core-mantle structure") (fig. 16) and (ii) a low stress region below 200 bar where a polygonal network of equiaxed grains penetrates entire grains (fig. 17). This change in microstructure within the power law region again goes hand in hand with a change in the form of the flow law from high values of the stress exponent n between 7 and 8 at high stresses to a lower value of n around 3 to 4 at the lower stresses. Grain boundary sliding between recrystallized grains was found to occur but there is no evidence for grain boundary sliding as a major strain producing mechanism in the marble.

The microstructural development in finegrained Solnhofen limestone is quite distinct from that described for Carrara marble. As mentionned earlier, the small grain size in this limestone prohibits twinning and indeed no twinning is observed in Solnhofen limestone under conditions where the marble still deforms by twinning (fig. 18). Also does the change from an exponential into a power law flow law not coincide with the transition from twinning to glide.

As grain boundary sliding becomes predominant at low stresses the microstructure changes markedly: the grains remain equiaxed even after large strains and no optically visible strain features can be detected (fig. 19). The grain boundaries which are serrated in the undeformed material have equilibrated into a polygonal network with straight boundaries, indicating that the grain boundaries became mobile. This mobility of grain boundaries helps in accommodating grain boundary sliding. Measurements on grain shape have shown that the amount of strain as recorded by the shape anisotropy of the grains amounts to only about $^1/3$ of the total strain imposed (Schmid Boland and Paterson 1977), suggesting that grain boundary sliding predominates but that there might be a component of intracrystalline dislocation creep as well.

The fact that grain shape no longer reflects total strain in the superplastic regime is of importance to the development of schistosity and lineations in rocks. These macroscopic fabric elements often reflect grain shape and the intensity of schistosity and/or lineation is expected to be a very poor qualitative indicator of the magnitude of total strain once a rock deforms by grain boundary sliding.

Another important characteristic of superplastic flow is that the microfabric is very stable up to large strains. This is not the case for twinning and dislocation glide where a strong crystallographic preferred orientation as well as a shape anisotropy of the grains develops. This leads to strain hardening in coaxial deformation and possibly to strain softening in simple shear. If Coble creep is envisaged as a deformation mechanism then the grains become progressively elongate and this leads to an increase in the length of the diffusion path between the sites of sources and sinks of the diffusing vacancies. This means that the material eventually work hardens after large strains. Thus, grain boundary sliding is the only mechanism leading to steady state deformation over very large amounts of strain (with the possible exeption of dislocation creep accompanied by continuous dynamic recrystallization).

B. Texture

A similar correspondence between flow law and deformation mechanism on the one hand and microfabric development on the other hand is observed when the type and degree of lattice preferred orientation (here referred to as texture) is measured. Casey et al. (1978) found that basically three types of textures can be found in experimentally deformed limestone and marble:

type 1: A strong preferred orientation of compression directions near c and e for twinned calcite rocks (fig. 20)

type 2: A maximum near a, extending towards h with a second maximum near e for specimens deformed by intracrystalline glide (fig. 21).

type 3: A concentration of compression directions perpendicular to c for the superplastic regime (fig. 22). Here the degree of preferred orientation is significantly weaker than in the two previous types after the same amount of shortening.

Texture development elegantly reflects the predominant deformation mechanisms for the experimentally deformed rocks. However, texture analysis is a more difficult tool in evaluating deformation mechanisms in naturally deformed rocks because the texture is also strongly dependent on the shape of the finite strain ellipsoid as well as on the deformation path. This will be illustrated when the textures of naturally deformed rocks will be discussed.

The type 1 textures seem to be mainly caused by twinning. Twinning on e produces a reorientaion of the crystallographic axes not only through external rotations but also by a complete reorientation of the twinned domain such that the compression axis becomes to lie somewhere near the c-axis in terms of an inverse pole figure presentation such as fig. 20. Lister (1978) found that the Taylor-Bishop-Hill analysis of texture development does not allow for a successfull simulation of the type 1 texture. This method of texture simulation treats twinning on e like glide on e and hence does not allow for a reorientation of the lattice within the twinned domain mentionned above. Wenk et al. (1973) came to the conclusion that an e-maximum type of preferred orientation can also be explained by the simultaneous operation of two r-glide planes, based on applying the Calnan and Clews (1950, 1951a,b) analysis to calcite.

The type 2 texture has been remarkably well simulated by Lister (1978) when activating mainly r- and f-glide and in addition e-glide to a minor extent.

According to Lister (1978) the type 3 textures are best interpreted in terms of slip on r and f, but no activity at all on the e-planes. The fact that this texture is weaker than the type 1 and type 2 textures agrees well with the observation that grain boundary sliding is the dominant deformation mechanism. The strain contribution from glide on r and f is small and the texture is continuously randomized by grain rotations.

IV. THE MICROFABRIC OF NATURALLY DEFORMED CALCITE ROCKS

Calcite is very susceptible for annealing under elevated temperatures. Griggs et al. (1960) investigated the effects of annealing recrystallization on calcite aggregates and single crystals in the laboratory. Annealing recrystallization starts at temperatures around 500^{o}C and the amount of recrystallization depends on the strain induced prior to annealing. High strains induce a high difference in free energy between the initial and the recrystallized state via the stored strain energy in the form of dislocations. Griggs et al. (1960) found that annealing times between 15 and 120 minutes had no effect on the amount of recrystallization. Under geological time spans however it is likely that the threshold temperature is even lower than 500^{o}C.

Griggs et al. (1960) demonstrated that annealing recrystallization substantially alters the microstructure to a granoblastic or porphyroblastic microstructure typical for marbles and that the texture tends to become random with traces of the original preferred orientation left.

A classical example of a very intensely deformed but completely annealed calcite rock is Carrara marble. The effects of annealing are so strong in this rock that it serves as an "undeformed" starting material in experimental rock deformation.

This extreme sensitivity to the effects of annealing recrystallization has its advantages and disadvantages in field geological problems. It is a great disadvantage of course that the traces of deformation and dynamic (syntectonic) recrystallization are completely wiped out in high metamorphic terrains. The effects of annealing recrystallization start to predominate within the greenschist facies rocks in the case of calcite. Therefore studies of deformation mechanisms on the basis of the microfabric are limited to unmetamorphic or lower greenschist metamorphic terrains such as the Helvetic nappes in the Alps. The advantage however lies in the fact that late postmetamorphic deformations can easily be demonstrated if they affect a highly metamorphosed marble. In a region along the Insubric line strongly deformed calc-mylonites (Fliesskalke, Gansser 1968) are very widespread and they are good indicators for post-lepontine tectonic events.

Deformation during higher metamorphic grade is well recorded in the microfabric of quartz where especially the texture still records the kinematic framework during deformation, even under amphibolite facies conditions (Simpson 1981). The fact that calcite is very abundant in low grade environments whereas quartz is abundant in high grade terrains is very fortunate in that it provides the field geologist with enough microfabric evidence under all metamprphic conditions if he chooses the appropriate mineral species for his studies.

A. Pressure solution

It is well known that pressure solution, i.e. stress induced diffusional mass transport in a "wet" environment via solution and redeposition, is a very important deformation mechanism in limestones (Durney 1972, Ramsay 1981). Because of the difficulties in activating this deformation mechanism under laboratory strain rates there are hardly any experimental data to be compared with field observations. For this reason the emphazis of this contribution will be given to other deformation mechanisms although they are by no means the only important mechanisms.

Another difficulty associated with pressure solution stems from the very large domains which have to be considered because the sites of solution and redeposition are often very distant in space. Mostly the transport path goes over many grains in the aggregate, for example from a stylolite to a calcite vein. This situation does not correspond to the pressure solution model of Rutter (1976) and long distance transport mechanisms are very difficult to simulate in the laboratory because of the small specimen sizes.

Under favourable circumstances however solution and redeposition on the scale of individual grains, corresponding to the model of Rutter (1976), can be observed in nature. Fig. 23 illustrates diffusional mass transport in a crinoidal limestone from the schistes lustrés in Corsica. The high impurity content in the crinoidal fragments contrasts with the clean areas of overgrowth. Solution takes place along the stylolites.

It is interesting to note in fig. 23 that the light coloured domains of redeposition occur in a direction which is not at 90^0 but oblique to the plane of orientation of the stylolites. Fig. 24 shows a mica-rich domain within the same section and in an identical orientation to the micrograph of fig. 23 and with asymmetric crenulation folds. The axial plane of the microfolds suggests a direction of maximum finite shortening oblique to the normal to the stylolites in fig. 23 but parallel to the elongate domains of redeposition. This suggests that stylolite orientation is not controlled by the orientation of the finite strain axes.

B. Intracrystalline plasticity and grain boundary sliding

1) The regional setting of the rocks described

The discussion of naturally deformed rocks will focus on two types of calcite tectonites: (i) limestones deformed to high plastic strains and with a well developed foliation and stretching lineation and (ii) calc-mylonites. Well developed foliation and stretching lineation are found only in deeper structural levels within the Helvetic nappe pile, our main area of investigations. They are found along the inverted limb of the Morcles nappe and in the parautochthonous cover of the infrahelvetic nappes in Eastern Switzerland (Milnes and Pfiffner 1977) and in the Saasberg-Schuppe situated between the main Glarus thrust plane below and the Verrucano sediments of the Freiberge above. In the normal limb of the Morcles nappe and in higher tectonic levels of the Helvetic nappes in general pressure solution mechanisms are readily detectable in the field in the form of stylolites on one hand and fibrous deposits in "pressure shadows" and veins on the other hand (Durney and Ramsay 1973). The traces of intracrystalline plasticity are not so easy to detect at relatively low strains typical for these structural levels and it remains uncertain as to how much they contribute to the total strain in the rocks. It is certain however that the relative contribution by pressure solution to total strain is significantly higher in the higher structural levels (Ramsay 1981). The reasons for having dominantly intracrystalline plasticity in the lower parts of the Helvetic nappes can be interpreted in two ways by making use of the deformation mechanism map in fig. 11, proposed by Rutter (1976):

(i) The increased temperatures in the lower structural levels favour intracrystalline plasticity as a consequence of the vastly different temperature sensitivity of strain rates for the two mechanisms.

(ii) Total strain in the inverted limb of the Morcles nappe frequently is orders of magnitude higher than in the normal limb and it could be argued that strain rates and consequently stresses were substantially higher as well. In this case mainly gradients in strain rate and stress would be responsible for the observed change in the dominant deformation mechanism.

Here the second interpretation is favoured because with a mere increase in temperature we would expect a change from pressure solution mechanisms into diffusional creep such as Nabarro-Herring or Coble creep according to fig. 11, or into superplastic flow according to the deformation mechanism maps of figs. 13 and 14 . Only an increase in the magnitude of strain rate and stress can bring about the change towards intracrystalline plasticity.

The stresses necessary to induce this change are largely dependent on grain size and are in excess of 100 bars for coarse grained calcite rocks and in excess of 1000 bars for grain sizes around 10 μm (figs. 13 and 14). Because many limestone formations such as the Upper Jurassic Malm are very finegrained we would expect large stresses in excess of 1kb in these deeper structural levels of the Helvetic nappes if dislocation glide or creep are the dominant deformation mechanisms.

The occurrence of calc-mylonites is mainly restricted to the Helvetic nappes east of the Reuss valley. They accompany the Glarus overthrust where they are known as Lochseitenkalk (Schmid 1975). They are not limited to that particular thrust however and the same type of rock occurs also along second order thrusts at deeper levels, such as the base of the infrahelvetic Griesstock nappe (Frey 1965) and at nappe boundaries within the the Helvetic thrust block such as the contact between the Mürtschen- and Axen-nappes (Schindler 1959).

The tectonic style of the Helvetic nappes changes rather abruptly along strike across the Reuss valley as well

(Trümpy 1969). West of the Reuss valley fold nappes with large inverted limbs predominate. The strain in these inverted limbs is pervasive and high throughout the stratigraphic succession which is usually well preserved. East of the Reuss valley the sedimentary cover of the nappes is basically in an upright position, apart from minor second order folds. The base of the nappe units is often marked with a calc-mylonite.

Whereas the process of mylonitization occurs in situ along some of the second order thrusts, the Lochseiten calc-mylonite along the main Glarus overthrust is allochthonous in the sense that it is not derived from the footwall (Flysch units) nor from the overriding unit (Verrucano). The field evidence suggests that these calc-mylonites flow much more readily than the country rocks, including neighbouring unmylonitized limestones which are locally present along the main Glarus thrust (Schmid 1975). This obviously demands an explanation which accounts for the reduction in flow strength during mylonitization (work softening) such as to keep deformation concentrated along mylonite layers rather than spread it over the entire stratigraphic succession as is the case in the western parts of the Helvetic nappes.

2) Calcite tectonites with a well developed foliation and stretching lineation

To some extent the microstructures and textures of some of these rock types have already been discussed in Schmid, Casey and Starkey (1981) and for additional information, particularly on the detailed texture descriptions in the form of orientation distribution functions (ODF) the reader is referred to this contribution.

a) Microstructures

In some of the rock types along the inverted limb of the Morcles nappe the amount of strain can be estimated from strain markers such as the Tertiary limestone conglomerates unconformably overlaying mid-Cretaceous limestones (Badoux 1972).
It is somewhat surprising that the aspect ratios of the individual grains in these conglomerates by no means record the high amount of strain in the rock (typically around 50:10:1).
As shown in fig. 25 taken from one of these conglomerates the amount of strain recorded by the aspect ratio of the grains rarely exceeds 1:1.5 in the X-Z-section.

Another striking feature is that the flattening plane of the grains often does not coincide with the macroscopically well developed foliation plane (fig.26). Typically, the plane of flattening in the individual grains is at an angle of $<45^{o}$ to the macroscopic foliation. This deflection of the grain flattening plane from the foliation, i.e. the supposed plane of finite flattening in the rock, is systematically related to the sense of shear (northward thrust of the core and normal limb in the Morcles nappe over the inverted limb) according to fig. 27. Another obliquity can be oberved between foliation plane and the position of the c-axis point maximum in the texture of many of these rocks (fig. 34). The c-axis point maximum is often deflected into a direction subparallel to the normal to the flattening plane of the individual grains in the microstructure and, as a consequence, oblique to the finite plane of flattening (foliation).

It could be argued that large amounts of grain boundary sliding are reponsable for this discrepancy between the type of strain recorded by the individual grains and the bulk strain in the rock. However the fact that (i) a strong texture is observed at the same time and (ii) that twinning is pervasive in some of these specimens (figs. 26 and 28) suggests that intracrystalline plasticity rather than grain boundary sliding is the predominant deformation mechanism. In this case grain boundary migration would cause the observed discrepancy between strain recorded by grain shape and strain in the bulk rock. Two kinds of driving forces for grain boundary migration can be envisaged: (i) the difference in stored plastic strain energy of neighbouring grains and (ii) the minimization of the surface energy stored at grain boundaries by restoring highly elongated grains back into near-isometric shapes.

In view of the observation that in many cases the grain boundaries are fairly straight and well equilibrated (figs. 25, 29 and 33) and because of the sense of obliquity between individual grains and the macroscopic foliation being systematically related to the sense of shear the second interpretation is favoured (with the exception of the microstructure in figs. 26 and 28, where local differences in stored plastic energy may be at least partially responsable for the highly serrated grain boundaries). Following this second interpretation the grain shape would record the last increments of strain only along a rotational deformation path such as simple shear. This interpretation in terms of a rotational deformation path can also offer a good explanation for the obliquity between texture and foliation as mentioned above and discussed in Schmid, Casey and Starkey (1981) and shown in fig. 34.

With the exception of the specimen shown in figs. 26 and 28 twinning is restricted to the odd larger grain (fossil fragments etc.) in the microstructure (figs. 30,31 and 32). The critical minimum grain size for twinning seems to be around 50 μm in the Morcles area and this minimum grain size for twinning can be potentially used for paleostress estimates. Fig. 5 suggests that such a relationship exists and although the calibration is subject to refinements one is tempted to infer a fairly high stress in the order of 2kb for the inverted limb of the Morcles nappe on the basis of fig. 5 and the observed minimum grain size for twinning at around 50 μm. The microstructure of figs. 26 and 28 again form an exception and here the stresses may have been higher.

Are such high stresses to be reconciled with reasonable strain rates if one takes the existing flow laws on calcite rocks? As mentioned earlier the transition from pressure solution into intracrystalline plasticity rather than into grain boundary sliding mechanisms and/or diffusional creep demands high stresses at small grain sizes. A stress of 2kb would yield a value for the strain rate of around $10^{-11}sec^{-1}$ by taking the flow law for Solnhofen limestone in regime 2 (table 1) to be valid for an extrapolation down to temperatures of 350°C.

Another method of stress determination , the size of recrystallized grains (fig. 10) cannot be widely used in these rocks because recrystallization by subgrain rotation can only rarely be observed to be operative in some of the bigger grains. In fig. 32 the size of the subgrains within the large calcite grain however agrees with the size of around 20 μm in the finegrained matrix. If one takes this grain size in the matrix to be the result of dynamic recrystallization by subgrain rotation rather than by surface energy driven grain boundary migration as suggested above one arrives at a stress estimate around 250 bar on the basis of fig. 10.

If this substantially lower stress estimate is correct one would expect superplastic flow to be the predominant deformation mechanism and this was rejected earlier on the basis of the textural and microstructural observations. Subgrain formation illustrated in fig. 32 would have to be ascribed to a late episode in a continuous deformation process under decreasing stresses.

In conclusion it is tentatively suggested that the stresses are in excess of 1kb during the main deformational event in these rocks and that the strain rates were in the order of $10^{-11} sec^{-1}$. The rather lengthy discussion demonstrated the difficulties in arriving at an internally consistent estimation of stresses and strain rates. Part of the difficulty clearly arrives from the fact that both stresses and strain rates obviously have to change with time. It is thus very dangerous to simply use one of the lines of evidence, such as the paleostress estimate on the basis of grain size, in isolation.

b) Textures

Fig. 34 summarizes the main types of preferred orientation patterns found in these rocks. In contrast to the texture results obtained on the experimentally deformed material, where three distinct types of textures, corresponding to different deformation mechanisms were found, there is basically only one type of texture in all the rocks studied so far: a single maximum for simultaneously c- and e - poles. A single maximum pattern for simultaneously c and e is possible because the angle between these two crystal directions is only 26^{0} and because the point maxima are rather broad. These c- and e- maxima are either positioned near the foliation normal or they are deflected from this direction in a systematic way in respect to the sense of shear as inferred from the field geological evidence (i.e. they are deflected from the position of the foliation normal "against" the sense of shear, see fig. 34a,b and Schmid, Casey and Starkey (1981).

Apart from this single maximum for c and e which is common to all the measured natural specimens there are significant differences in the alignment of all the other crystal directions and in the symmetry of these pole figures. The types of textures such as illustrated in fig. 34 can be summarized into two subtypes:

subtype a:

The crystal directions other than c and e form small circles (in the case of the rhomb r) or great circles (in the case of the a-axis which is perpendicular to c) around the c- and e-maximum positions. Thus, the texture has a high degree of axial symmetry. As shown in fig. 34a this axial symmetry of the texture however may be oblique to the macroscopic fabric axes. Because twinning is pervasive in the specimen presented in figs. 26 and 28, Schmid, Casey and Starkey (1981) interpreted the obliquity by concluding that the texture reflects the final increments along a rotational strain path such as simple shear. In this case the texture would be more or less symmetric in respect to the stress axis and oblique to the axes of finite strain. This is because twinning produces a very rapid reorientation of the crystallographic axes within the twinned domains. Thus, the obliquity of the c- and e-axis point maxima could be used to gain information on the strain path (co-axial vs. non-coaxial). In some other cases the same type of texture is found to be symmetric with the finite strain axes indicating locally coaxial deformation (Schmid, Casey and Starkey, 1981).

subtype b:

The crystal directions other than c and e form distinct maxima (fig. 34b). The poles to r tend to be positioned in a strong maximum near the foliation normal and in a secondary maximum at some angle $< 45^{o}$ to the lineation. The a-directions no longer define a more or less homogeneously populated great circle but tend to align into a maximum in the X-Z-plane of the strain ellipsoid, at some small angle to the lineation. If again simple shear is invoked from the fact that the texture is oblique to the macroscopic fabric axes and if the shear strain is assumed to be high, the pole figure for r, i.e. the dominant glide system in the absence of twinning, can be interpreted in terms of a stable end orientation in simple shear (fig. 35). One of the r-poles (r_1) is aligned such as to bring the r_1-plane into coincidence with the shear plane in the bulk rock and r_1 then operates syntetically with the sense of shear in the rock; the secondary maximum r_2 corresponds to r-planes operating antithetically to the sense of shear in the rock. A version of this type of texture, but symmetric in respect to the macroscopic fabric axes is illustrated in fig. 34c. Again, there are two maxima for the poles to r, but this time they are symmetrically disposed in relation to the foliation normal. This texture suggests conjugate shear on two r-planes along a coaxial deformation path.

Microstructurally the two subtypes described above are different in regard to the abundance of twinning. The specimens of subtype a are strongly twinned (figs. 26 and 28) whereas the specimens of subtype b only occasionally show twinning (figs. 29 and 33). Thus, it is suggested that the subtype b specimens deformed in an environment where glide on r was very important.

Looking at the c-axis pole figures alone it appears however that both subtypes a and b correspond to the type of texture found in the experimentally deformed material where twinning is important and where the compression axis is aligned with the c- and e- pole directions (type 1 texture). How can this be reconciled with the fact that no twinning is observed in the specimens of subtype b, whereas for the experimentally deformed material twinning seemed to be the obvious explanation for this texture? The following explanations are possible:

(i) Twinning was active during the early stages in the deformation and because twinning in all the grains went to completion no twin boundaries are visible any more. In this case the natural textures of subtype b would correspond to the type 1 textures described in the chapter on experimental textures.

(ii) We do not know the effects of the deformation path on the texture development before experiments or simulations along a non-coaxial strain path are available. It is possible, that subtype b corresponds to the type 2 texture of the experimentally deformed material and that the strain path has a more profound effect on the development of the texture than intuitively would be assumed.

(iii) The naturally deformed material in the case of subtype b does not correspond to any of the experimentally produced textures because the relative magnitudes of the critical resolved shear stresses for the activation of various slip systems (such as r- and f-glide) are different in the naturally deformed specimens due to the lower temperatures and strain rates or because so far undetected slip systems were active in nature.

The first explanation is rather unlikely to hold because of the fact that the twins can still be observed in the case of some of the specimens such as those with subtype a textures. The strong alignment of r-planes in subtype b specimens emprically suggests that r-glide is important indeed and in this case the second or third or a combination of explanations is to be preferred.

In the case of the subtype a textures twinning is certainly largely responsable for the texture development and the subtype a textures can easily be correlated with the experimentally produced type 1 textures.

3) Calc-mylonites

The macrosopic appearance of the mylonites is characterized by a lamination produced by darker, finegrained domains alternating with lighter, coarsegrained domains, usually a few millimetres thick (Schmid 1975). The mylonitic foliation is either wavy or even folded but never ideally planar in appearance like the cleavage planes of the rocks described in the earlier section. Another macroscopic difference from the rocks described in the previous section is the absence of a stretching lineation. In a more southerly area around Flims the calc-mylonite along the main Garus thrust can take on a marble-like appearance and the lamination becomes less marked.

a) The process of mylonitization, illustrated in a detailled profile

Because the calc-mylonites along the main Glarus overthrust are allochthonous in respect to the country rocks a detailed profile to illustrate progressive mylonitization was taken elsewhere, namely through the nappe boundary between the Axen- and Mürtschen-nappes south of the Klöntalersee (Glarus, coord. 720 350/ 209 350). There, Lower Cretaceous Oehrlikalk is the youngest preserved formation of the Mürtschen nappe and is progressively mylonitized and overridden by the oldest formation at the base of the Axen nappe, the Mid-Jurassic Dogger formation (fig. 36). The ferruginous, quartz-bearing limestone of the Dogger formation hardly shows any traces of deformation in thin section and behaved as a fairly rigid body at least during nappe emplacement. Some minor open folds are found near the thrust contact (fig. 36) but on a big scale the entire sedimentary pile up to the Cretaceous is in an upright position within the Axen nappe (the same applies to the Mürtschen nappe in this area, see profile F, table II in Schindler 1959). No brittle type thrust surface is found at the very contact between the mylonitized Oehrlikalk and the Dogger formation.

The following description of the microstructures within the Oehrlikalk formation runs from bottom to top (compare fig. 36):

At 3 metres below the contact to the base of the Dogger the Oehrlikalk still has its original sedimentary microstructure preserved. Fig. 37 shows slightly flattened ooids in a sparitic matrix. Thus, the spectrum of grain sizes present in the starting material is very wide. Figs. 38 and 39 illustrate again that only the larger grains of the sparitic matrix deform by twinning whereas the smaller grains within ooids remain untwinned. Fig. 40 illustrates the formation of subgrains throughout one of the coarse grained matrix grains which is unsuitably oriented for twinning. Subgrain formation and recrystallization by subgrain rotation (fig. 40) are more often observed in untwinned grains deforming by glide alone.

At 2 metres below the contact the coarser grains are more heavily twinned and new grains of a very small grain size (in the order of 1 μm and hence at the limit of optical resolution) nucleate (fig. 41). The process of recrystallization by nucleation is different from recrystallization by subgrain rotation (figs. 40 and 42) and leads to a much smaller grain size. Some of the twins are very broad and lensoid shaped and they show evidence for twin boundary migration (fig. 43). The similarity with some of the experimentally deformed marble specimens is remarkable.

Only at 1 metre below the contact do the limestones start to exhibit the typical mylonitic foliation and the following descriptions apply to this mylonitized horizon. Fig. 44 taken from one of the few large original grains left over, illustrates the beginning of granulation by nucleation recrystallization, preferably localized along old traces of twin boundaries. In fig. 45 one of these surviving old grains is surrounded by a totally recrystallized matrix. Fig. 46 illustrates that recrystallization by subgrain rotation occurs at the same time, producing a larger grain size. Figs. 47 and 48 show the typical end product of this progressive grain size reduction: the larger grains are so heavily twinned that the twin boundaries have a rather diffuse appearance. The matrix grains mostly have a grain size of 1 or a few µm .

Along the same profile the textures of some of the specimens have been measured (fig. 36). The pole figures are presented in a projection plane perpendicular to the mylonitic foliation with the direction of supposed tectonic transport (north) oriented at the margin of the pole figure (no lineation is observed). One of the specimens (7978) was taken from 2 metres below the contact in unmylonitized limestone and two specimens are from within the mylonite band at 20 cm from the contact (7975) and from the very contact (7974 in fig. 36).

Two features are somewhat surprising: (i) the intensity of the texture is unaffected by the mylonitization process and the texture of the mylonites is no stronger than in many of the tectonites described in the previous section and (ii) the symmetry of the pole figures roughly coincides with the macroscopic foliation (in specimen 7975 the e-axis point maximum is somewhat oblique to the foliation but in a sense opposite to what would be expected for the sense of shear inferred from a northward transport of the Axen nappe, compare fig. 34a and b).

The first feature, the weak texture, can be ascribed to the fact that dynamic recrystallization leads to a grain size reduction and that this in turn induces a change in deformation mechanism towards predominantly grain boundary sliding in the finegrained domains (this change in deformation mechanism will be more extensively discussed in a later chapter). The larger and heavily twinned old grains would then be strongly oriented, but grain boundary sliding in the matrix would tend to randomize the texture in the total rock, as measured by the X-ray method.

The high symmetry can be interpreted to indicate that shearing is concentrated in the finegrained recrystallized laminae and that the coarse grained relict grains, determining the bulk texture to a large extent (because X-rays measure the bulk intensity to which these domains largely contribute) , behave rather passively during shear. The coarse grained domains could record either an earlier deformation history or a local deformation history which deviates from the deformation path of the bulk rock.

All of the pole figures conform to the types of textures illustrated in fig. 34 for the calcite tectonites: specimen 7978 corresponds to subtype b and the two other specimens are somewhere intermediate between the two subtypes illustrated in fig. 34.

b) The microfabric of calc-mylonites from the main Glarus overthrust

In the central and more northern areas the microstructure is remarkably similar to the microstructures described in the previous section. Twin boundary migration and nucleation recrystallization can be observed in relatively undeformed domains such as syntectonic calcite veins (fig. 49). Recrystallization by subgrain rotation, mainly concentrated in grain boundary regions is also observed (fig. 50). Again, the grain size produced by nucleation recrystallization is much smaller. As a consequence the grain size of the fully recrystallized matrix is very variable (figs. 51 and 52), usually 10 µm and less. Fig. 53 shows large flattened old grains surrounded by a fully recrystallized matrix with near isometric grain shapes.

In a more southerly area south of Segnes Pass the rocks are almost fully recrystallized and only rarely are old twinned grains preserved (fig. 54). Subgrain rotation is now the only recognizable mechanism of recrystallization (fig. 55) und thus the average grain size is larger (fig. 56) in fully recrystallized domains. This gives the rock the marble-like macroscopic apearance. In some cases there is evidence for subsequent growth and late twinning, postdating recrystallization and grain growth (fig. 57).

Figs. 58 and 59 illustrate an analoguous microstructural development in a specimen of marble collected in the Valpellin Series of the Dent Blanche nappe. This marble was post-metamorphically deformed and the central part of a marble horizon is completely recrystallized to a calc-mylonite.

The texture of one of the mylonites from the Glarus overthrust was measured and published in Schmid, Casey and Starkey (1981, specimen 63). The type of texture is the same as for the mylonites described in the previous section, the <u>c</u> and <u>e</u>- maxima are perpendicular to the foliation. Fig. 61 illustrates the texture of one of the mylonites from the southern area along the overthrust, where recrystallization went to completion. The texture is very weak in this rock and this supports the idea that grain boundary sliding is the dominant deformation mechanism once the rock has completely recrystallized.

c) Grain size measurements on subgrains and recrystallized grains

It was pointed out that two different mechanisms of recrystallization were observed in the mylonites: recrystallization by nucleation, not observed in the experimentally deformed material, and recrystallization by subgrain rotation, observed to be stress dependent in the experimentally deformed rocks.

Table 2 summarizes the grain size measurements for those specimens only where recrystallization demonstrably occurred by subgrain rotation. Similarly to the experimentally deformed material the grain size of fully recrystallized grains and subgrains was found to be equal. The average maximum grain diameter parallel to two perpendicular directions was measured for 20-50 grains in each specimen. No correction for the true 3-dimensional shape was made since the grain size determinations in the experimental material (fig. 10) were not corrected for cut-effects either.

The grain sizes listed in table 2 are remarkably similar over all the specimens and therefore a mean of all the mean values (6.5 μm) was chosen to estimate the stress during subgrain formation and recrystallization. By using the relationship illustrated in fig. 10 one obtains a differential stress of around 700 bar. Does this indicate that the basal shear stress in the mylonite during nappe emplacement was around 350 bar (by taking the maximum shear stress which is half the stress difference) ?

In the following chapters it will be argued that the recrystallization induced change in deformation mechanism towards superplastic flow by grain boundary sliding will be associated with work softening. The stress determination based on recrystallized grain size clearly can be valid for that part of the deformation only which occurred during the initial phase of deformation by intracrystalline plasticity. Once the rock deforms by grain boundary sliding, the grain size no more reflects stress. Thus, the differential stress of 700 bars is taken to indicate the peak stress before work softening occurred and another, lower estimate of stress, based on an extrapolation of the flow law for superplastic creep will be produced in chapter VI.

4) Summary and discussion

One of the main purposes of this chapter was the demonstration of the remarkable similarities in the microstructural development with increasing strain between laboratory and natural rock deformation. This indicates that the deformation mechanisms operating at high temperatures (500-1000^{o}C) and at laboratory strain rates are indeed basically the same mechanisms which operate at much lower temperatures in a geological environment at slow strain rates. The approach of using high temperatures as a "trade off" for slow strain rates is thus justified.

The stress estimates, although at best semi-quantitative, suggest high stresses operating during deformation of the calcite tectonites in the lower structural levels of the Helvetic nappes such as the inverted limb of the Morcles nappe. The strain and consequently the strain rate gradients in this part of the Helvetic nappes seem to be related to stress gradients.

Deformation in eastern Switzerland is often much more strongly localized in narrow mylonite bands. These calc-mylonites show evidence for a reduction in grain size by dynamic recrystallization with increasing strain, which in turn induces work softening. It will be argued in the next chapters that the strength of these calc-mylonites must have been extremely low.

At this stage it is difficult to explain the different response of the rocks to stress in western and eastern parts of the Helvetic nappes. These differences could be due to (i) facies changes such as the presence or absence of clastic sediments such as the Verrucano formation in eastern Switzerland, (ii) changes in the big scale tectonic configuration and in the exact way deformation is transfered from basement to cover, or (iii) by changes in the deformation mechanisms in the calcite rocks due to different environmental parameters such as displacement rates of microplates or changes in metamorphic grade. Although the last interpretation cannot be proved to be correct it offers an interesting possibility that the small scale deformation mechanism may dictate the large scale tectonic style.

The symmetry of the texture is a valuable tool in interpreting the strain path (co-axial vs. non co-axial) in the case of a rock with a homogeneous microstructure. In the case of the calc-mylonites however the textures are symmetric in relation to the macroscopic foliation in spite of the fact that these mylonites surely must have deformed along a non co-axial strain path.

V. A MODEL FOR A STRAIN INDUCED CHANGE IN DEFORMATION MECHANISM LEADING TO WORK SOFTENING

As emphazised earlier, any flow law and consequently also the associated deformation mechanism is valid only as long as strain rate at constant stress can be assumed to be independent of strain (steady state concept). Strain is an important variable in geology that does not appear on deformation mechanism maps. It is well known for the work hardening stage of deformation that strain induced changes of the microstructure alter the rheological behaviour of the rock and consequently no deformation mechanism map in the usual sense can be proposed for the work hardening stage.

It is well known to field geologists that strain gradients are accompanied with substantial alterations in the microstructure, even after large strains, i.e. at stages in the deformation which are well beyond the work hardening stage normally restricted to the first few percents of strain. One of the most obvious changes in microstructure occurring in a sequence of rocks undergoing mylonitization is dynamic recrystallization. Provided that the rock deforms by dislocation creep in a power law deformation regime, polygonization into subgrains is to be expected, and eventually the subgrain boundaries will become proper grain boundaries and the rock will have altered its grain size. Thus, mylonitization usually is associated with a grain size reduction.

We have demonstrated earlier that grain size is an important parameter affecting the rheological behaviour of a rock in the high stress region where a reduction in grain size is expected to lead to work hardening as well as in the low stress region on the other hand where we expect work softening as a consequence of a grain size reduction. Figs. 13 and 14 illustrated that any deformation mechanism map is only valid for a particular grain size. It is usefull therefore to alternatively construct a deformation mechanism map with grain size as a variable at constant temperature. This was done in fig. 62 for calcite aggregates by combining the constitutive equations for exponential and power law creep as observed in Carrara marble with those for superplastic flow observed in Solnhofen limestone. Because superplastic flow is grain size dependent, the resulting deformation regime boundary is grain size dependent as well and separates a high stress - large grain size area of predominantly dislocation creep from a low stress - small grain size area of superplastic flow.

Superimposed on this deformation regime map is the curve of stress vs. the size of new grains recrystallizing by a rotation mechanism of dynamic recrystallization (see fig. 10). Strictly speaking this curve should fall within the power law field because this recrystallization by subgrain rotation can only be brought about by dislocation creep and the notion of an "equilibrium grain size" is meaningless in the domain of superplastic flow (Etheridge and Wilkie, 1979). The stress vs. grain size curve however is superimposed on the deformation mechanism map solely for the purpose of demonstrating the following evolution with increasing strain:

A calcite aggregate deforms by a strain rate and under a stress indicated by the position of point A in fig. 62. The position of this point A indicates that the material has a grain size which is larger than the size of the subgrains and recrystallized grains expected to form with increasing strain. The material deforming by dislocation creep at point A will eventually recrystallize to a grain size along a curve which comes to lie within the field of superplasticity. The paths A-B and A-C indicated in fig. 62 indicate two extreme possibilities of what can hypothetically occur if the production of a new grain size by rotation recrystallization would be instantaneous. The path A-B illustrates that under boundary conditions of constant stress an acceleration of strain rate over several orders of magnitude will occur as a consequence of the change in grain size. The path A-C alternatively illustrates a stress drop under the extreme opposite boundary conditions of constant strain rate. This change in rheological behaviour is a consequence of a change in mechanism towards superplasticity and can only occur if the position of the equilibrium grain size curve is inside the superplastic field.

However, it is obvious that instantaneous recrystallization is a very unreasonable assumption for what may occur in nature. As observed in the experiments on Carrara marble and also in many mylonitic rocks the evolution of an equiaxed finegrained aggregate of recrystallized grains will lead to a bimodal grain size distribution. Some fabric domains will be fully recrystallized while the original grain size will be preserved in other domains. This may lead to a situation where both dislocation creep and grain boundary sliding occur simultaneously in different fabric domains. Such a situation can no longer be described by a single point in the diagramm of fig. 62. Initially the fully recrystallized domains will be isolated and will make up a small volume fraction of the rock. Thus, flow will remain stable and can still be defined by the position of point A in fig. 62. As the volume fraction of fully recrystallized material grows, the bulk strain rate of the rock will increase and/or the bulk stress will drop due to the contribution of the superplastically deforming domains to the overall deformation in the rock. The rheology of the bulk rock can then be thought to be given by the position of a point somewhere along the path between A and B or A and C.

In conclusion, dynamic recrystallization will induce a change in microstructure which in turn induces a change in deformation mechanism leading to work softening.

This conclusion apparently contradicts the fact that during experimental deformation of Carrara marble no work softening was observed as a consequence of dynamic recrystallization, even after more than 30 percent shortening (Schmid, Paterson and Boland 1981). However, when a similar deformation regime map is constructed for the 900-1050^{o}C temperature region (the temperatures at which recrystallization occurred in these experiments) one ends up with a different position of the mechanism boundary in stress vs. grain size coordinates due to the different activation energies for creep in dislocation creep and superplastic flow respectively (fig. 64). The mechanism boundary now almost coincides with the position of the equilibrium grain size curve or comes even to lie inside the dislocation creep field. In other words, the new grain size produced by recrystallization does not fall inside the area of dominantly superplastic flow at the high temperatures and therefore no work softening is expected.

Fig. 63 shows a deformation mechanism map for 600^{o}C, a temperature intermediate between the 400^{o}C considered in fig. 62 and the experimental situation. The relative positions of mechanism boundary and equilibrium grain size curve are nearer to each other than in fig. 62 and consequently the effect of work softening is expected to be less pronounced at this higher temperature. From this we conclude that the work softening effect invoked in this chapter is most pronounced at low temperatures.

So far we only discussed the effects of recrystallization by subgrain rotation on the rheology. In the previous chapter part of the recrystallization was interpreted to occur by a nucleation mechanism. We do not know of the grain size of nucleation recrystallized grains is a function of stress too, because this second mechanism was not observed in the experiments. In view of the observation that the grain size produced by nucleation is even smaller, we would expect the effect of work softening to be even more dramatic in the case of the calc-mylonites in the Helvetic nappes.

The same mechanism of work softening presented here may also apply for other rock types. Bouiller and Guegin (1975) describe superplastic mylonites in peridotites and Twiss (1977) interpreted the experiments of Post (1973) in terms of a mechanism change induced by dynamic recrystallization.

Above, work softening as a consequence of a change in deformation mechanism towards grain boundary sliding (superplasticity) was discussed. A similar weakening effect as a consequence of grain size reduction can of course be postulated for transitions into other grain size sensitive deformation mechanisms such as pressure solution or diffusional creep.

VI. THE LOCHSEITEN MYLONITE AND THE MECHANICS OF OVERTHRUSTING FOR THE GLARUS OVERTHRUST

A. The flow strength of the Lochseiten mylonite as expected from laboratory data

The thrust plane of this 35 km long overthrust in the Helvetic nappes of eastern Switzerland is accompanied by a one metre thick calc-mylonite, locally known as the Lochseitenkalk. Hsü (1969) recognized that the displacement of the overthrust block did not take place along a cohesionless frictional thrust plane and proposed that the displacement was taken up by ductile flow of this very thin layer of calc-mylonite. This view was supported by the field observations of Schmid (1975) who also found that during the relatively late phase of thrusting, the so-called Ruchi-phase (Milnes and Pfiffner 1977), the rocks above and below the thrust plane remained essentially rigid. Based on the minimum displacement of 35 km and a maximum available time span of 10 m.y. Schmid (1975) estimated the minimum strain rate in the mylonite to be around $10^{-10}sec^{-1}$. Knowing the minimum strain rate and assuming a temperature of $400^{0}C$ it was tempting to calculate the shear stress at the base of the thrust block from experimentally determined flow laws on calcite rocks.

Schmid (1975) extrapolated the experimentally determined flow laws on Yule marble (Heard 1963) and Solnhofen limestone (Rutter and Schmid 1975) down to the estimated strain rate and came to the conclusion that the extrapolation of the Solnhofen data leads to an unrealistically high basal shear stress in excess of 1 kbar. The data on Yule marble would lead to a more reasonable stress estimate and they were used by Hsü (1969) for a similar extrapolation.

Because the calc-mylonite in question has a grain size similar to that of Solnhofen limestone, whereas Yule marble is much coarser grained, Schmid (1975) preferred to extrapolate the Solnhofen limestone data.

In the light of the more recent experiments on Solnhofen limestone (Schmid, Boland and Paterson 1977) and by consulting the deformation mechanism map of fig. 14 it becomes obvious why the extrapolation of Schmid (1975) was erraneous: the changes in the deformation mechanism towards low stresses and consequently the changes in the flow law along the extrapolation path to the geological strain rates were not considered because no data were available at that time for the low stress behaviour. The laboratory data used for this extrapolation (Rutter 1974, Rutter and Schmid 1975) were obtained at relatively low temperatures (400^{0}-550^{0}C) and at high differential stresses (around 2kb) and it was not only necessary to extrapolate towards lower strain rates but also towards lower stresses.

Before a new extrapolation based on the more recent laboratory data on Solnhofen limestone is presented the assumption that Solnhofen limestone is a good model material for the calc-mylonite needs to be tested. For this purpose two stress relaxation tests were performed on specimens of this mylonite at 600^{0}C and 700^{0}C. The stress relaxation test offers a valuable means for exploring a wide range of stresses and strain rates with a limited number of pilot tests as shown by the results obtained with this method on both Solnhofen limestone (Schmid 1976) and on Carrara marble (Schmid, Paterson and Boland 1980).

The results of these stress relaxation tests are plotted in fig. 65 and they show a good correspondence between the two rock types so far as the slope $n = \partial \log \dot{e} / \partial \log \sigma$ is concerned. Both the 600^{0}C and the 700^{0}C isotherms exhibit the same slope, indicating low values for the parameter n in the low stress region. Such a low value of the parameter n in the power law creep equation was found to be characteristic for superplastic flow in Solnhofen limestone. The strength of the two rock types is very similar at 600^{0}C, whereas at 700^{0}C the Lochseiten mylonite appears to be stronger. In view of the very inhomogeneous nature of the mylonite block used for testing, a big scatter in the strength is expected from specimen to specimen and therefore not too much emphazis should be placed on the exact correspondence in the relative strength between the two rock types. The important result of these pilot tests however is the observation of a transition from high values of the parameter n at high stresses into the low value for n at lower stresses, suggesting that this mylonite deforms superplastically as well at low stresses, like Solnhofen limestone and unlike the coarser grained marbles. As evidenced by fig. 60 the microstructure of this mylonite was not substantially altered during the relaxation test.

The extrapolation can now be made by using the deformation mechanism map for variable grain sizes at 400^{0}C (fig. 62) which is largely based on the Solnhofen limestone data. For grain sizes of 5.9 μm (grain size of Solnhofen limestone) and 1 μm (the grain size of large domains within the Lochseiten mylonite) differential stresses of 240 bar and 10 bar respectively are obtained at strain rates of 10^{-10}sec^{-1}. Superplastic flow is expected to be the dominant deformation mechanism at these small grain sizes. These values of stress and strain rate refer to deformation in a triaxial test and the stress - strain rate relationship for simple shear can be derived by generalizing the flow law following a procedure proposed by Nye (1953) and by rederiving the special case for simple shear. Thereby the experimentally derived flow law at a given grain size and temperature of the form

$$\dot{e} = C\ (\Delta\sigma)^{n}$$

transforms into

$$\dot{\gamma} = C\ 3^{\frac{n+1}{2}}\ \tau^{n}$$

where $\dot{e}$ and σ are the engeneering strain rate and differential stress respectively and where $\dot{\gamma}$ and τ are the shear strain rate and shear stress.

The shear stresses are then calculated to be between 100 bar and 4 bar respectively for grain sizes of 5.9 μm and 1 μm.

B. The mechanics of overthrusting

The classical approach in discussing the mechanics of overthrusting was to assume that the overthrust block remains rigid and that thrusting is possible only provided that no failure occurs in the thrust block. This lead Hubbert and Rubey (1959) to postulate a maximum shear stress at the base of the thrust block below which stability is maintained in terms of the Mohr-Coulomb failure criterion. Both Hsü (1969) and Schmid (1975) used this classical approach exept that they considered the basal the basal shear stress to be determined by the ductile flow in the mylonite rather than by pore pressure assisted frictional resistance. For the calculation of the maximum shear stress at the base of the thrust Hsü and Schmid used the following equation derived by Laubscher (1961, p.244) and allowing for the effects of pore pressure within the thrust block:

$$\tau_{max} = \frac{1}{x}\left\{az + [b + (1-b)\lambda]\frac{\rho g z^2}{2}\right\}$$

where x is the length of the thrust block (35 km), z is the thickness of the thrust block (6 km), ρ g z is the lithostatic pressure, λ the ratio of fluid pressure over the lithostatic pressure and where a and b are the experimentally determined parameters in the Mohr-Coulomb equation ($a = 2\tau_0\sqrt{b}$ and $b = 1 + \sin\phi / 1 - \sin\phi$, if the Mohr-Coulomb equation is written as $\tau = \tau_0 + (1-\lambda) \tan\phi \; \sigma_n'$).
This formula evaluates the maximum permissible shear stress at the base of the thrust block before failure within the thrust block takes place.

Inserting the experimentally determined parameters a and b for the Lower Cretaceous Oehrlikalk (Briegel and Schmid, unpublished data) into this equation yields a maximum shear stress between 630 and 780 bar respectively for values of λ between 1 and 0 (Schmid 1975). Inserting the same parameters determined on Verrucano (Schmid 1975, table 2) yields values between 580 and 930 bars respectively.

The extrapolated basal shear stress of $<$ 100 bar is thus no longer in conflict with the simple stability consideration and if the model of Hubbert and Rubey (1959) is correct, this would mean that no deformation would take place within the thrust block during overthrusting (i.e. during the Ruchi phase, Milnes and Pfiffner 1977).

The serious shortcoming of Hubbert and Rubey`s approach however is that brittle fracture and/or ductile flow can take place within the thrust block and contemporaneous with thrusting in many geological environments. In our case the effects of the Ruchi phase are weak enough to say that most of the deformation during the Ruchi phase was taken up by the mylonite, but the assumption of absolute stability within the thrust block is certainly open to discussion.

A different model was recently proposed by Chapple (1978). The main assumptions are that (i) the thrust block is plastically yielding throughout during the thrust motion (ii) that the basal shear stress is constant and equal to the flow stress in the basal mylonite or decollement horizon and (iii) that the normal and shear stress at the surface are zero. Chapple (1978) considers a wedge shaped thrust block with a surface slope α generally dipping towards the foreland and a slope θ of the basal thrust away from the foreland. Given all the assumptions to be valid and given prescribed slopes α and θ the problem is overdetermined and the following formula 36 in Chapple (1978) expresses the surface slope α as a function of the yield stress K within the thrust block, the ratio χ of the shear stress in the basal layer over the yield stress K, the basal slope θ and the overburden pressure ρ g z :

$$\alpha = \frac{2\,K\,(\frac{\chi}{2} - \theta)}{\rho\, g\, z}$$

For the Glarus case we consider a region south of the culmination of the thrust plane where the basal thrust slopes away from the foreland by an angle of up to 15° (Schmid 1975) or up to even higher angles if corrections for later movements are made. There are considerable difficulties in estimating the yield stress K within the thrust block and therefore both values of 500 and 1000 bars are considered (Chapple 1978 used 1000 bar but this value seems high for the more slaty members within the Verrucano formation). Fig. 66 is a graphical expression of Chapple`s equation and shows the magnitude of the basal shear stress (implicit in the value of $\mathcal{X}$) vs. the expected surface slope α. Fig. 66a refers to a minimum overburden of 6 km and fig. 66b uses a more realistic estimate of 10 km overburden. If the extrapolated value of $<$ 100 bar is taken for the basal shear stress one could conclude that the surface slope α of the thrust block was zero or negative and away from the foreland and that consequently gravity played no role in assisting the nappe motion in the sense of the gravity spreading model. The nappe motion in fact would have to move against the gravitational body forces if α is negative. Fig. 66 also illustrates that this conclusion is relatively unaffected by the exact values of K, θ and overburden, whereas the relative strength within the block and the basal shear stress is very critical.

At this point we have to remember that the derivation of the surface slope α rests on the assumption that the thrust block yields everywhere. If this condition is relaxed the surface slope is no longer dictated by Chapple`s equation. In the case of the Glarus thrust a surface slope away from the foreland would be extremely unlikely at the time of thrusting because the northward transport and deposition of the Molasse pebbles starts long before the initiation of the Ruchi phase. Thus, we conclude (i) that the assumption of simultaneous and pervasive yielding is invalid in the Glarus case and that consequently (ii) that gravity spreading is not effective during the thrusting phase even if a surface slope towards the foreland is available.

For the very initial stage of thrusting during the Calanda phase (Milnes and Pfiffner 1977) no decollement horizon of the kind of the Lochseiten calc-mylonite was available at the base of the future thrust apart from only sporadically developped Carboniferous slates. During this early stage we expect a high basal shear stress and consequently the mechanism of gravity spreading could well have played an important role in the northward motion of the Helvetic nappe pile.

This discussion illustrates the necessity for having good estimates of the rheological properties of the rocks involved. the entire discussion on gravity gliding, gravity spreading and active tectonic push at the rear of a thrust block critically depends on the rheology of both the basal decollement horizon (or mylonite) and the thrust block itself.

ACKNOWLEDGEMENTS

First I want to thank those friends who were actively involved in joint projects on most of the research presented here: J.N.Boland, M.Casey, M.S.Paterson and E.H.Rutter. Their contributions were absolutely vital for the work presented here. I profited from many discussions with W.M.Chapple, O.A.Pfiffner, J.G.Ramsay, C.Simpson J.Starkey and many others. The beautifull illustrations of microstructures were only possible because P.Willies, F.Pirovino and E.Schärli produced excellent ultra-thin sections, and because U.Gerber made such high quality photoprints. I thank J.G.Ramsay for his continuing support. The grant 2.859-0.77 of the Schweizerische Nationalfonds supported the field work in the Helvetic nappes.

REFERENCES

Anderson,T.F.,1969. Self diffusion of carbon and oxygen in calcite by isotope exchange with carbon dioxide. J.Geoph.Res., 74, 3918-3931.

Ashby,M.F.and Verrall.,R.A.,1973. Diffusion-accommodated flow and superplasticity. Acta Met.,21,149-163.

____________________,1978. Micromechanisms of flow and fracture and their relevance to the rheology of the upper mantle. Phil.Trans.R.Soc.Lond.,A,288,59-95.

Badoux,H.,1972. Tectonique de la nappe de Morcles entre Rhône et Lizerne. Mat. Carte Geol. Suisse, NS 143,1-78.

Ball,A.and Hutchinson,M.M.,1969. Superplasticity in the Aluminium-Zinc Eutectoid. Metal Science Journal, 3, 1-7.

Boullier,A.M. and Gueguen,Y.,1975. Origin of some mylonites by superplastic flow. Contr.Min.Pet., 50, 93-104.

Briegel,U. and Goetzte,C., 1978. Estimates of differential stress recorded in the dislocation structure of Lochseiten limestone (Switzerland). Tectonophysics, 48, 61-76.

Calnan,E.A. and Clews,C.J.B.,1950. Deformation textures of face-centred cubic metals. Phil.Mag., 41, 1085-1100.

____________________,1951a. The development of deformation textures in metals: part II. Body-centred cubic metals, Phil.Mag.,42, 616-635.

____________________,1951b. The development of deformation textures in metals: part III. Hexagonal structures. Phil.Mag.,42, 919-931.

Casey,M.,RutterE.H.,Schmid,S.M.,Siddans,A.W.B. and Whalley,J.S., 1978. Texture development in experimentally deformed calcite rocks. Proc. 5th Int. Conf. on Textures of Materials, Aachen, Springer Verlag, Berlin, p.231-240.

Chapple,W.M.,1978. Mechanics of thin-skinned fold-and-thrust belts. Geol.Soc.Am.Bull., 89, 1189-1198.

Durney, D.W.,1972. Solution transfer, an important geological deformation mechanism. Nature, 235, 315-317.

Durney,D.W. and Ramsay,J.G.,1973. Incremental strains measured by syntectonic growths. In: DeJong,K. and Scholten,R. (editors), Gravity and Tectonics, Wiley, New York, 67-96.

Edington,J.W., Melton,K.N. and Cutler,C.P.,1976. Superplasticity. Progr.Mater.Sci.,1,61-158.

Etheridge,M.A. and Wilkie,J.C.,1979. Grainsize reduction, grain boundary sliding and the flow strength of mylonites. Tectonophysics,58,159-178.

Frey,F.,1965. Geologie der östlichen Claridenkette. Vjschr. natf. Ges. Zürich, 110.

Gansser,A.,1968. The Insubric Line, a major geotectonic problem. S.M.P.M., 48, 123-144.

Griggs,D.T., Paterson, M.S., Heard,H.C. and Turner,F.J.,1960. Annealing recrystallization in calcite crystals and aggregates. Geol.Soc.Am. memoir 79, 21-37.

Guillope,M. and Poirier,J.P.,1979. Dynamic recrystallization during creep of single-crystalline halite: An experimental study. J.Geoph.Res., 84, 5557-5567.

Heard,H.C.,1963. Effects of large changes in strain rate in the experimental deformation of Yule marble. J.Geol., 71, 162-195.

Heard,H.C. and Raleigh,C.B.,1972. Steady-state flow in marble at 500-800^{o}C. Geol.Soc.Am.Bull., 83, 935-956.

Hobbs,B.E.,1968. Recrystallization of single crystals of quartz. Tectonophysics, 6, 353-401.

Hsü,K.J.,1969. Statics and kinetics of the Glarus overthrust. Eclogae geol. Helv., 62, 143-154.

Hubbert,M.K. and Rubey,W.W.,1959. Role of fluid pressure in mechanisc of overthrust faulting. Geol.Soc.Am.Bull., 70, 115-166.

Kirby,S.H. and Raleigh,C.B.,1973. Mechanisms of high-temperature, solid-state flow in minerals and ceramics and their bearing on the creep behaviour of the mantle. Tectonophysics, 19, 165-194.

Kohlstedt,D.L., Goetze,C. and Durham,W.B.,1976. Experimental deformation of single-crystal olovine with application to flow in the mantle. In: R.G.S.Strens (editor), Petrophysics: The Physics and Chemistry of Minerals and Rocks. Wiley, New York, 35-49.

Laubscher,H.P.,1961. Die Fernschubhypothese der Jurafaltung. Eclogae geol. Helv., 54, 221-282.

Lister,G.S.,1978. Texture transitions in plastically deformed calcite rocks. Proc. 5th Int. Conf. on Textures of Materials, Aachen, Springer Verlag, Berlin, 199-210.

Mercier,J.C.C., Anderson,D.A. and Carter,N.L.,1977. Stress in the lithosphere: inferences from steady state flow of rocks. Pure Appl. Geophys., 115 (1/2), 199-226.

Milnes,A.G. and Pfiffner,O.A.,1977. Structural development of the Infrahelvetic complex, eastern Switzerland. Eclogae geol. Helv., 70, 83-95.

Nicolas,A. and Poirier,J.P.,1976. Crystalline plasticity and solid state flow in metamorphic rocks. John Wiley, London, 444pp.

Nye,J.F.,1953. The flow law of ice from measurements in glacier tunnels, laboratory experiments and the Jungfrau-firn borehole experiment. Proc.R.Soc.Lond., 219, 477-489.

Olsson,W.A.,1974. Grain size dependence of yield stress in marble. J.Geoph.Res., 79: 4859-4862.

Paterson,M.S.,1976. Some current aspects of experimental rock deformation. Phil.Trans.R.Soc.Lond. A, 283, 163-172.

Poirier,J.P. and Nicolas,A.,1975. Deformation induced recrystallization due to progressive misorientation of subgrains, with special reference to mantle peridotites. J.Geol., 83, 707-720.

Post,R.L.,1973. The flow laws of Mt.Burnet Dunite. PhD-thesis, University of California, Los Angeles.

________ ,1977. High temperature creep of Mt.Durnet Dunite. Tectonophysics, 42, 75-110.

Ramsay,J.G.,1981. Tectonics of the Helvetic nappes. In: Thrust and Nappe Tectonics, K.R.McClay and N.J.Price (editors), Geol.Soc.Special Publication, 9, 293-309.

Ross,J.V., AveLallemant,H.G. and Carter,N.L.,1980. Stress dependence of recrystallized-grain and subgrain size in olivine. Tectonophysics, 70, 39-61.

Rutter,E.H.,1970. An experimental study of the factors affecting the rheological properties of rock in simulated geological environments. PhD-thesis, Imperial College, London.

Rutter,E.H.,1974. The influence of temperature, strain rate and interstitial water in the experimental deformation of calcite rocks. Tectonophysics, 22, 311-334.

__________ ,1976. The kinetics of rock deformation by pressure solution. Phil.Trans.R.Soc.Lond.A., 283-219.

Rutter,E.H. and Schmid,S.M.,1975. An experimental study of unconfined flow of Solnhofen limestone. Bull.geol.Soc.Am., 86, 145-152.

Schindler,C.M.,1959. Zur Geologie des Glärnisch. Beitr.geol.Karte Schweiz, N.F. 107.

Schmid,S.M.,1975. The Glarus overthrust: Field evidence and mechanical model. Eclogae geol. Helv., 68, 247-280.

________ ,1976. Rheological evidence for changes in the deformation mechanism of Solnhofen limestone towards low stresses. Tectonophysics, 31, T21-T28.

Schmid,S.M., Boland,J.N. and Paterson,M.S.,1977. Superplastic flow in finegrained limestone. Tectonophysics, 43, 257-291.

Schmid,S.M. and Paterson,M.S.,1977. Strain analysis in an experimentally deformed oolitic limestone. In:Energetics of Geological Processes, K.Saxena and S.Battacharji (editors), Springer Verlag, New York, 67-93.

Schmid,S.M.,Paterson,M.S. and Boland,J.N.,1980. High temperature flow and danamic recrystallization in Carrara marble. Tectonophysics, 65, 245-280.

Schmid,S.M., Casey,M. and Starkey,J.,1981. The microfabric of calcite tectonites from the Helvetic nappes (Swiss Alps). In: Thrust and Nappe Tectonics, K.R.McClay and N.J.Price (editors). Geol.Soc.Spec.Publication 9, 151-158.

Simpson,C.,1981. Ductile shear zones: a mechanism of rock deformation in the orthogneisses of the Maggia nappe, Ticino. PhD-thesis, ETH Zürich.

Trümpy,R.,1969. Die helvetischen Decken der Ostschweiz: Versuch einer palinspastischen Korrelation und Ansätze zu einer kinematischen Analyse. Eclogae geol. Helv., 62, 105-142.

Turner,F.J.,Griggs,D.T. and Heard,H.,1954. Experimental deformation of calcite crystals. Geol.Soc.Am.Bull., 65, 883-934.

Twiss,R.J.,1977. Theory and applicability of a recrystallized grain size paleopiezometer. In: Stress in the Earth, M.Wyss (editor), reprint from Pageoph., 115, in CCRG, 3, Birkhäuser Verlag, Basel, p. 227-244.

Weertman,J.,1968. Dislocation climb theory of steady state creep. Trans. ASM, 61, 681-694.

Wenk,H.R.,Venkitasubramanyan,C.S. and Baker,D.W.,1973. Preferred orientation in experimentally deformed limestone. Contr. Min.Pet., 38, 81-114.

table 1: Experimentally determined flow laws in calcite rocks.

All equations are given for units in sec, bar, kcal mole^{-1}, K^{o}, μm.

$\dot{e}$ = strain rate, σ = stress difference, T = absolute temperature, R = gas constant

SOLNHOFEN LIMESTONE (grain size 4 um)

Study by	Rutter (1974) const. $\dot{e}$ experiments	Schmid et al. (1977) const. $\dot{e}$ experiments
Temperature range	up to 500^{o}C	600-900^{o}C
confining pressure	1.5 kb	3 kb
Flow law in "regime 1" (low T plasticity)	$\dot{e} = 10^{-0.12} \exp\left(- \frac{47}{R\,T} + \frac{\sigma}{160}\right)$ (1)	
transition stress		1900 bar
Flow law in "regime 2" (high T plasticity)		$\dot{e} = 10^{-1.33} \exp\left(- \frac{71}{R\,T}\right) \sigma^{4.7}$ (2)
transition stress		1000 bar at 600^{o}C / 400 bar at 900^{o}C
Flow law in "regime 3" (superplasticity)		$\dot{e} = 10^{2.7} \exp\left(- \frac{51}{R\,T}\right) \sigma^{1.7}$ (3) or, if grain size d is introduced as a variable: $\dot{e} = 10^{4.98}\, d^{-3} \exp\left(- \frac{51}{R\,T}\right) \sigma^{1.7}$ (4)

table 1 ctd.

CARRARA MARBLE (grain size 200 um)

Study by	Rutter (1974) const. $\dot{e}$ experiments	Schmid et al. (1980) const. $\dot{e}$ experiments	Schmid et al (unpublished) stress relaxation experiments
Temperature range	up to 500°C	600 - 1050°C	600 - 1050°C
confining pressure	1.5 kb	3 kb	3 kb
Flow law in "regime 1" (twinning)	$\dot{e} = 10^{5.8} \exp\left(-\frac{62}{R\,T} + \frac{\sigma}{114}\right)$ (5)		
transition stress		1000 bar	1000 bar
Flow law in "regime 2" (no twinning, high-T plasticity)		$\dot{e} = 10^{-4.5} \exp\left(-\frac{100}{R\,T}\right) \sigma^{7.6}$ (6)	$\dot{e} = 10^{-5.5} \exp\left(-\frac{75}{R\,T}\right) \sigma^{6.0}$ (8)
transition stress		200 bar	200 bar
Flow law in "regime 3" (no twinning, high-T plasticity)		$\dot{e} = 10^{3.9} \exp\left(-\frac{102}{R\,T}\right) \sigma^{4.2}$ (7)	$\dot{e} = 10^{3.8} \exp\left(-\frac{86}{R\,T}\right) \sigma^{2.9}$ (9)

table 1 ctd.

YULE MARBLE (grain size 300 um)

Study by: Heard(1963), Heard and Raleigh (1972), const. $\dot{e}$ experiments in extension. The exponential fits to regime 1 were taken from Rutter (1974)

Temperature range: up to $800^{o}C$

confining pressure: 5 kb

	I-orientation (favourable for twinning)	T-orientation (unfavourable for twinning)
Flow law in "regime 1" (twinning)	$\dot{e} = 10^{7.8} \exp\left(-\frac{62}{R\,T} + \frac{\sigma}{91}\right)$ (10)	$\dot{e} = 10^{7.0} \exp\left(-\frac{57}{R\,T} + \frac{\sigma}{138}\right)$ (12)
transition stress	1100 bar	1400 bar
Flow law in "regime 2" (high-T plasticity)	$\dot{e} = 10^{-12.2} \exp\left(-\frac{62}{R\,T}\right) \sigma^{8.3}$ (11)	$\dot{e} = 10^{-11.3} \exp\left(-\frac{61}{R\,T}\right) \sigma^{7.7}$ (13)

no equivalent of "regime 3" in Carrara marble, probably because of the lower maximum temperature reached in these experiments (at $800^{o}C$ the flow stresses are in excess of 200 bar at laboratory strain rates).

table 2: Measurements of the size of subgrains and recrystallized grains (subgrain rotation mechanism only) for various calc-mylonite specimens in the Glarus area.

specimen	locality	microstructure illustrated in figure	subgrain size	recrystallized grain size
7979	see fig. 36	40	7.7 ± 2.9	6.2 ± 2.2
7978	see fig. 36	42	6.0 ± 1.5	
7975	see fig. 36	46		6.5 ± 2.2
64	Foostock	50		7.1 ± 2.7
116	Ringlspitz	55	6.7 ± 2.6	5.7 ± 1.6
116	Ringlspitz	54		6.6 ± 2.1

For each specimen between 20 and 50 grains were measured. The grain size is defined to be the average maximum grain diameter parallel to two perpendicular directions in a section. The mean value of 6.5 µm indicates a stress around 700 bar at the time of subgrain formation according to fig. 10.

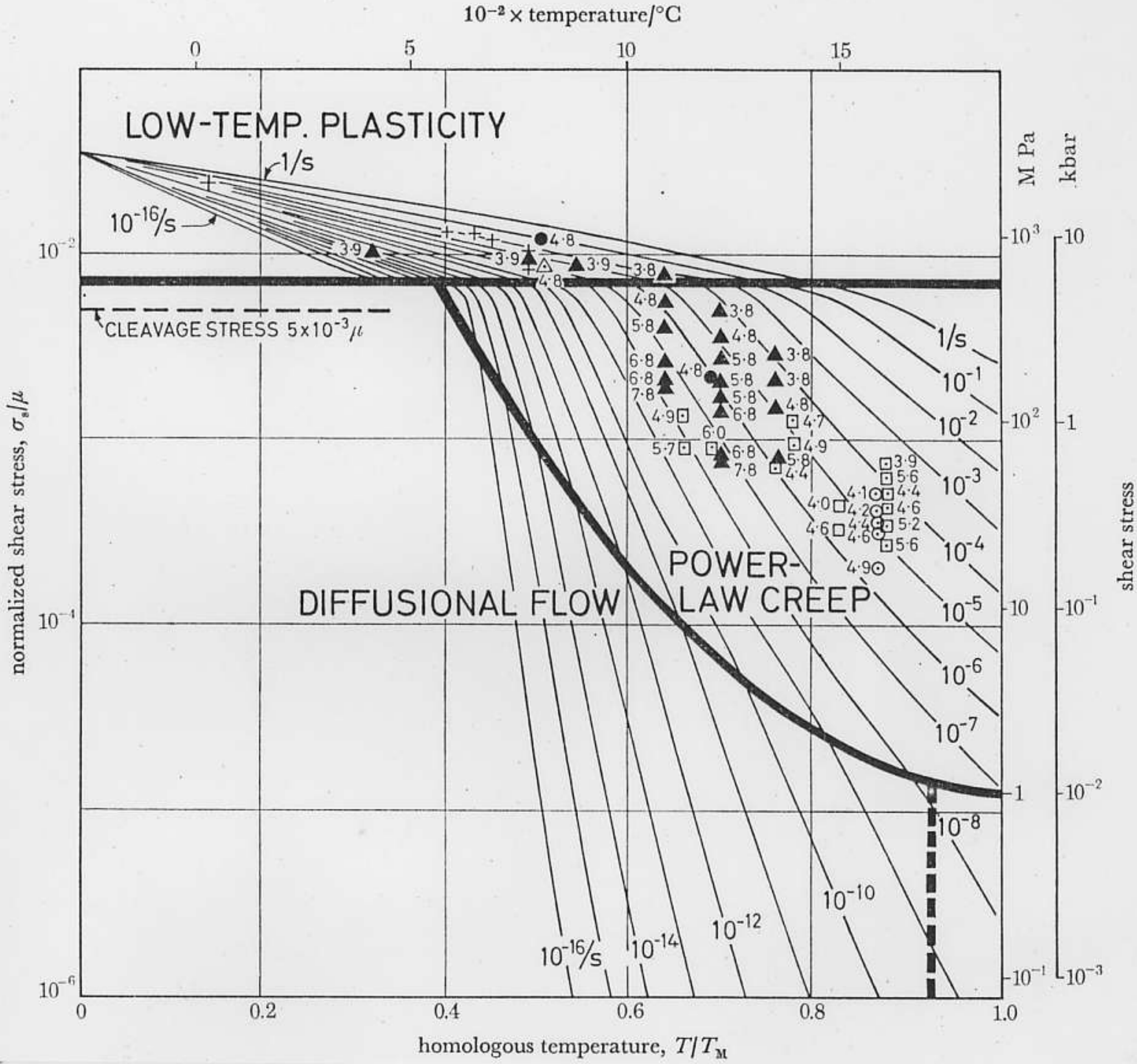

Fig. 1. Deformation mechanism map for olivine taken from Ashby and Verrall (1978, fig. 14). The map is constructed for a grain size of 100 μm and for zero confining pressure. The solid lines delineate mechanism boundaries, superimposed are the strain rate contours. The various symbols indicate the position of experimental results on the map.

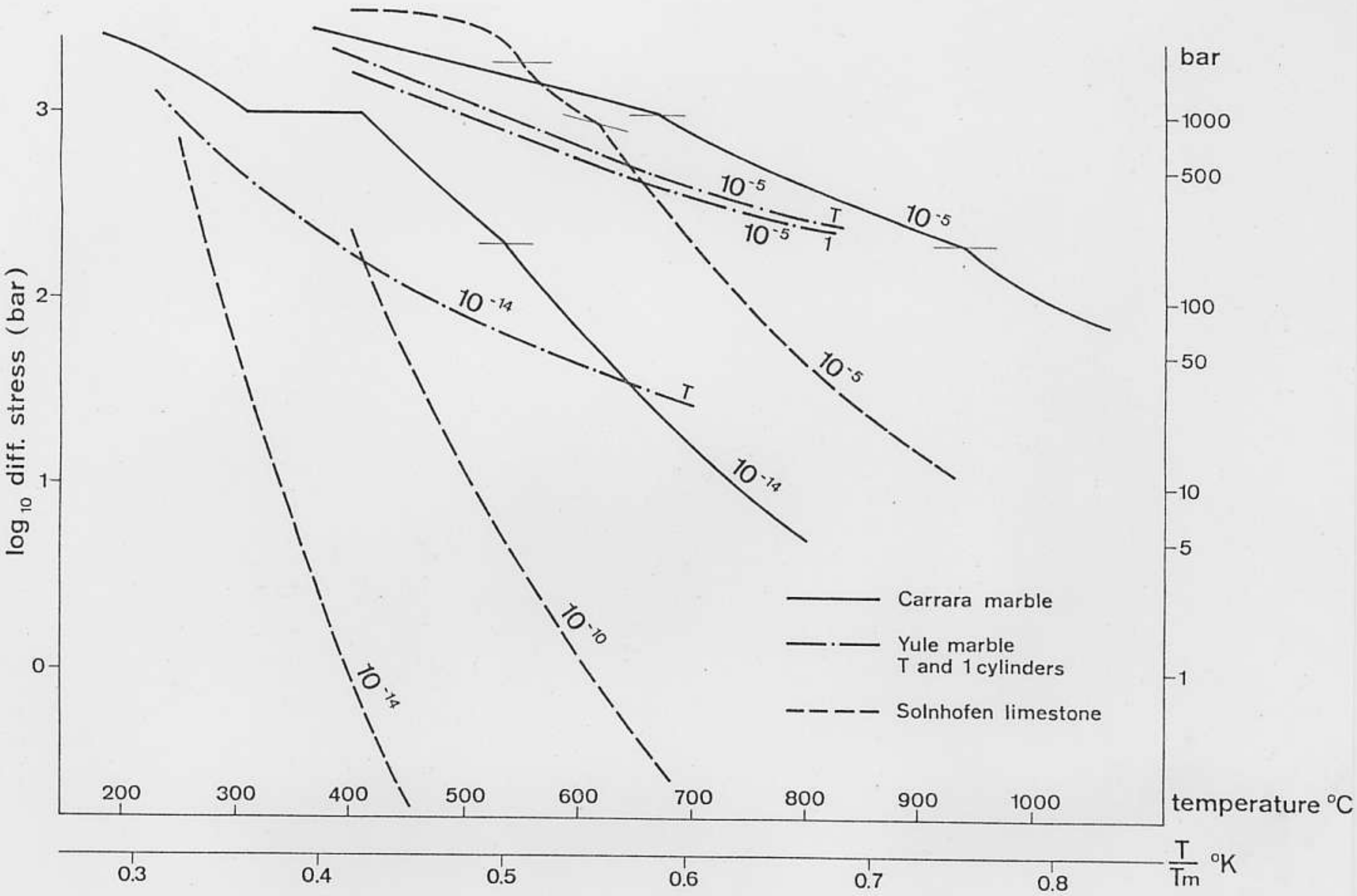

Fig. 2. The strength of different calcite rocks as a function of temperature, based on empirically determined flow laws as listed in table 1 (equations 1,2 and 3 for Solnhofen limestone, equations 5,6 and 7 for Carrara mable, equations 11 and 13 for Yule marble, table 1), taken from Schmid,Paterson and Boland, 1980.

10 μm

Fig. 3. Twinned Solnhofen limestone specimen, experimentally deformed at room temperature, 4 x 10^{-5} sec^{-1}, 1.5 kb confining pressure and at 4300 bar differential stress by 17% shortening. Compression direction vertical.

100 μm

Fig. 4 Twinned Carrara marble specimen, experimentally deformed at 600°C, $10^{-3} sec^{-1}$, 3 kb confining pressure and at 1480 bar differential stress by 20% shortening. Compression direction vertical. Note the lensoid shaped twinned domains. Host domains widen towards the grain boundary, twinned domains are constricted near grain boundaries.

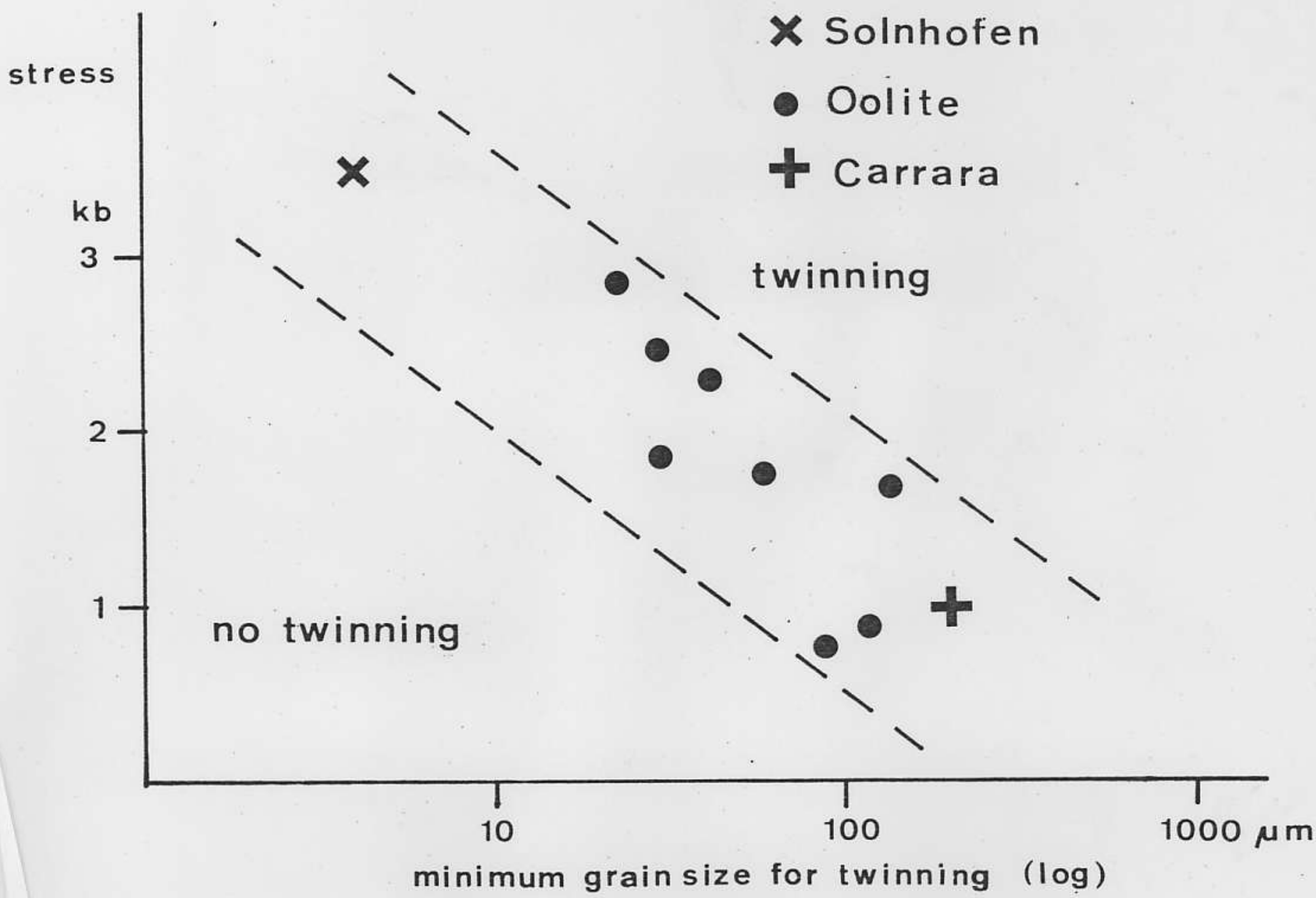

Fig. 5. Graph of differential stress vs. the logarithm of grain size, suggesting that there is a critical minimum grain size below which there is no twinning. The points labeled Solnhofen and Carrara are simply the transition stresses from twinning into glide alone at the different grain sizes of the two starting materials. The points labeled Oolite indicate the smallest grain sizes of twinned grains in a starting material of heterogeneous grain size (sparitic matrix of an experimentally deformed oolitic limestone, Schmid and Paterson 1977).

100 um

Fig. 6. Broad twin (t), causing inhomogeneous deformation in the form of a deformation band in a neighbouring grain deforming by glide. Note bent twin lamellae indicating the strain associated with the deformation band. Carrara marble, experimentally deformed at 700°C, 10^{-3} sec^{-1}, 3 kb confining pressure and at 1150 bar by 13% shortening. Compression vertical.

20 um

Fig. 7. Optically visible subgrains in Carrara marble, experimentally deformed at 1000°C, 10^{-5} sec^{-1}, 3kb confining pressure and at 132 bar differential stress by 32% shortening. Note that the misorientation at some of the subgrain boundaries is very high and this indicates recrystallization by a subgrain rotation mechanism. Compression vertical.

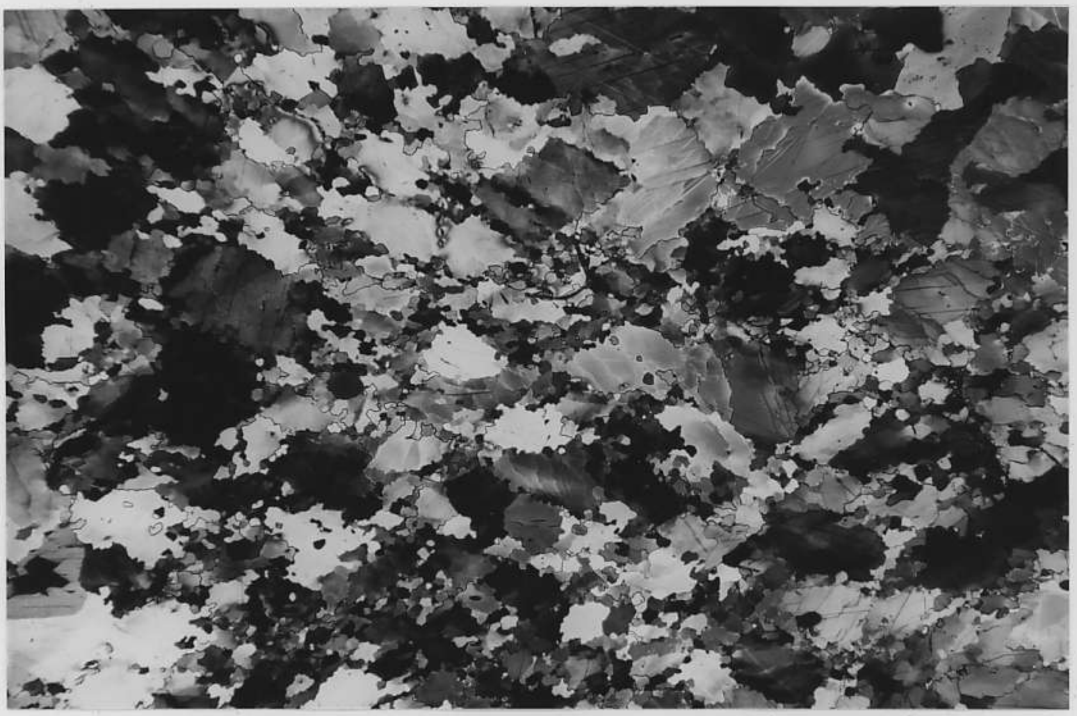

200 um

Fig. 8. Dynamic recrystallization by the rotation mechanism leads to a grain size reduction of the starting material. Carrara marble, experimentally deformed at 1000^{o}C, 10^{-4} sec^{-1}, 3 kb confining pressure, and at 165 bar differential stress by 34% shortening. Compression vertical.

200 um

Fig. 9. Recrystallization by grain boundary migration, leading to grain growth. Note that grain size reduction by subgrain rotation recrystallization occurs at the same time. Carrara marble, experimentally deformed at 1000^{o}C, 10^{-5} sec^{-1}, 3 kb confining pressure and at 151 bar differential stress by 21 % shortening. Compression vertical.

Fig. 10 :

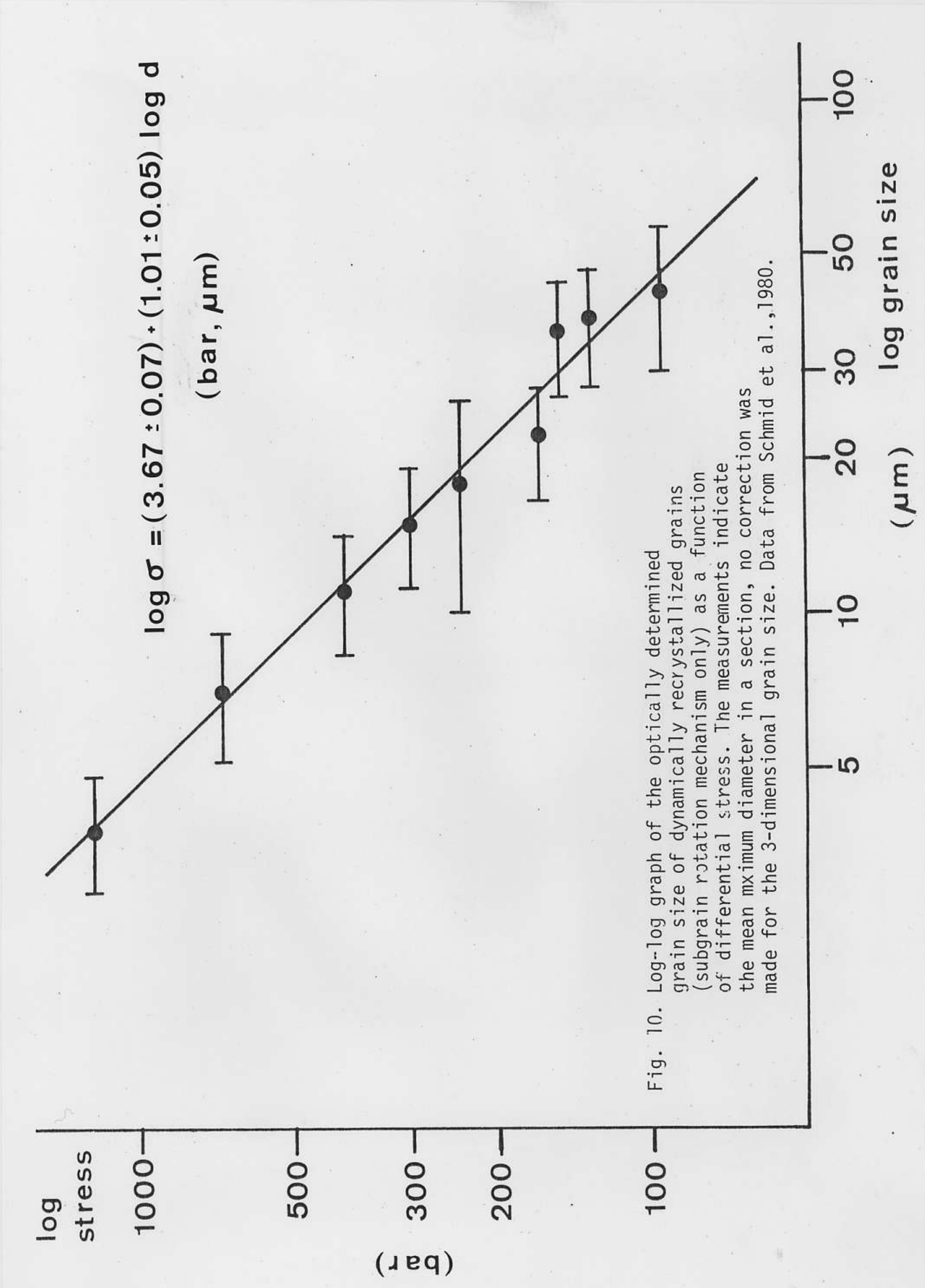

Fig. 10. Log-log graph of the optically determined grain size of dynamically recrystallized grains (subgrain rotation mechanism only) as a function of differential stress. The measurements indicate the mean mximum diameter in a section, no correction was made for the 3-dimensional grain size. Data from Schmid et al.,1980.

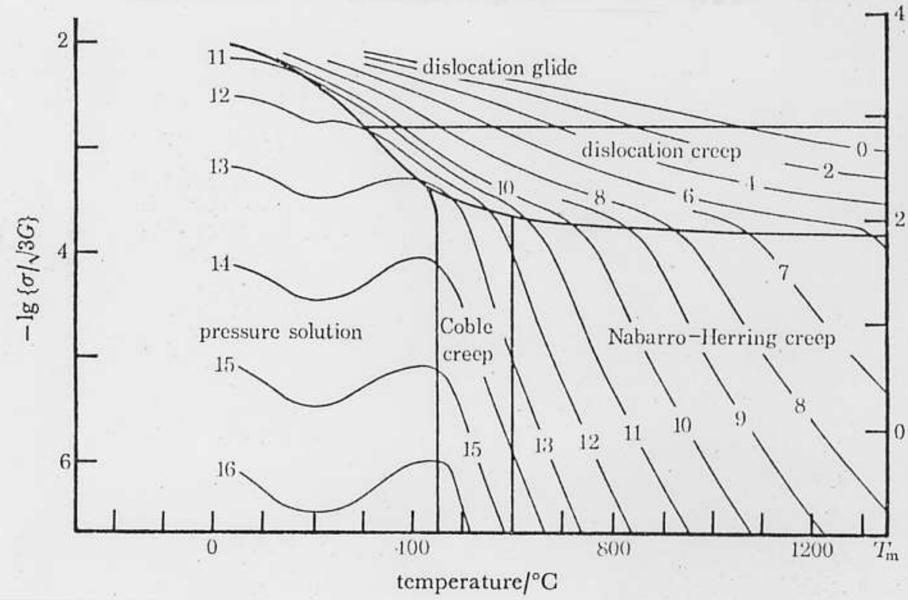

Fig. 11. Deformation mechanism map for calcite (grain size of 100 um) from Rutter (1976). Notice the subhorizontal strain rate contours in the field of pressure solution, reflecting the fact that pressure solution in calcite is not strongly temperature sensitive in the model of Rutter(1976).

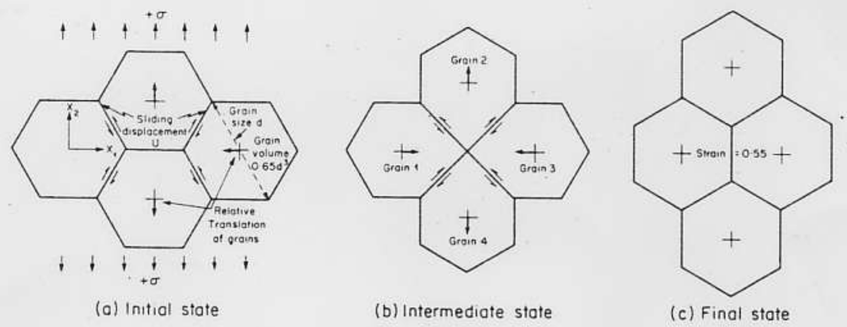

Fig. 12. Model for grain boundary sliding after Ashby and Verrall (1973). The group of four grains suffers a strain of 53% by sliding at grain boundaries and by neighbour shifting. In this particular model the necessary accommodations (intermediate step) take place by diffusional flow in the grain boundary region. There are other models invoking local crystal plastic flow in grain boundary regions (Ball and Hutchinson, 1969). Parts of the accommodation problem may also be solved by grain boundary migration.

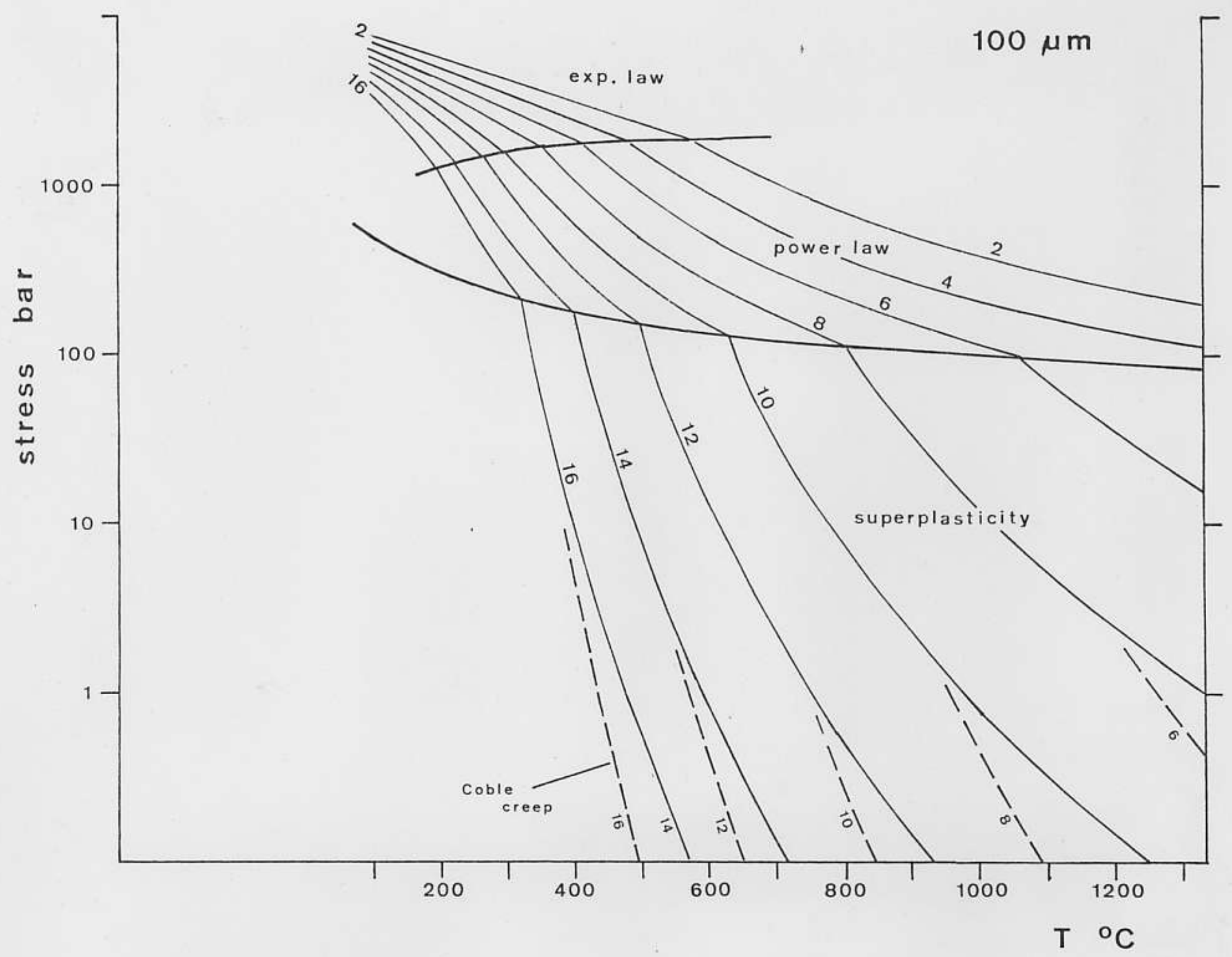

Fig. 13. Deformation mechanism map for calcite with a grain size of 100 μm, constructed entirely on the basis of empirically determined flow laws listed in table 1. The "exponential law" corresponds to equation (12), the "power law" to equation (13) for Yule marble, as listed in table 1. The field of "superplasicity" is constructed after equation (4) derived from Solnhofen limestone, compensated for grain size, also listed in table 1. The contours for Coble creep after Rutter (1976), compare fig. 11, are superimposed for comparison.

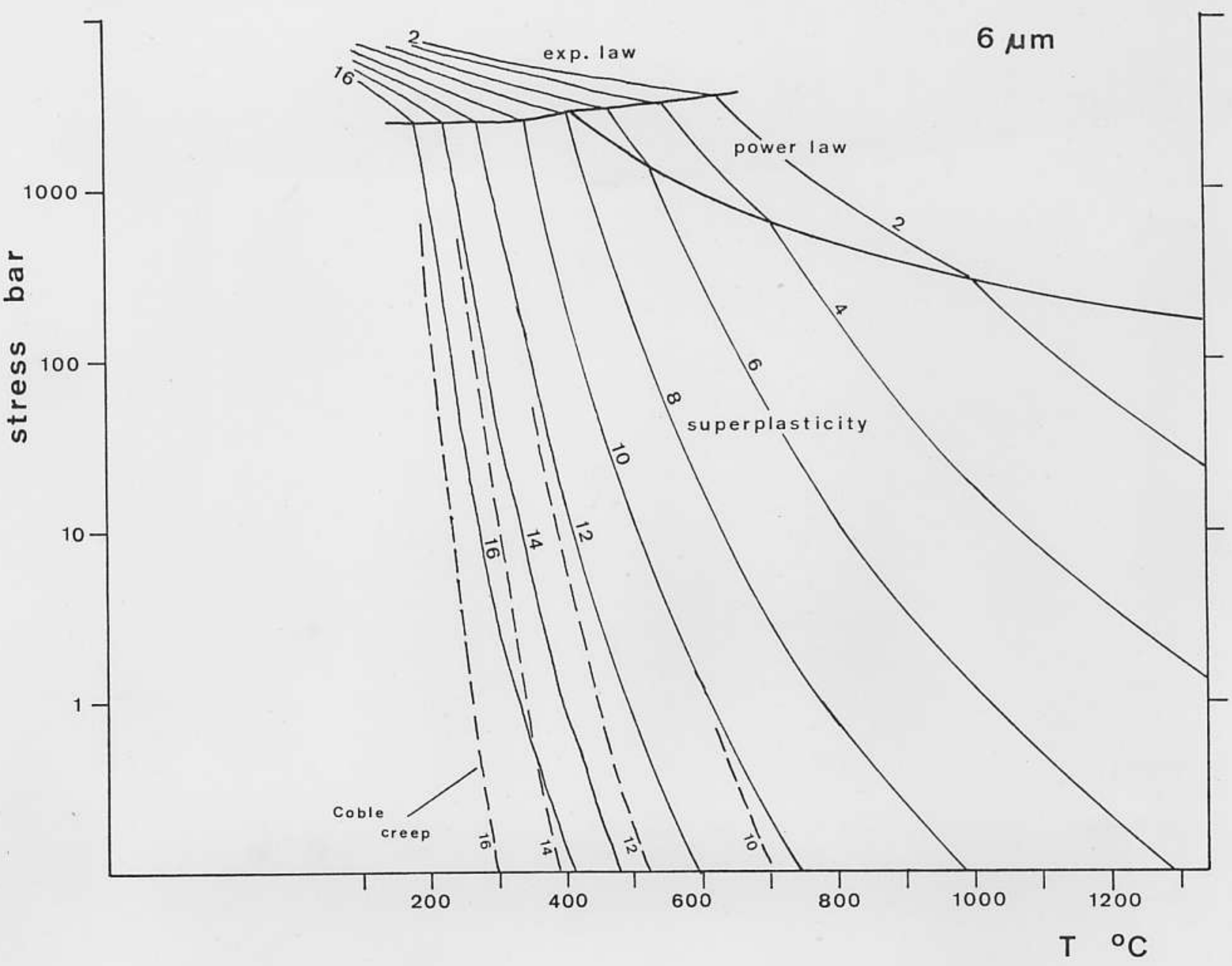

Fig. 14. Deformation mechanism map for calcite with a grain size of 6 µm, constructed entirely on the basis of empirically determined flow laws listed in table 1. The "exponential law" corresponds to equation (1), the "power law" to equation (2) and the "superplasticity" field to equation (3) in table 1, all flow laws are based on experiments with Solnhofen limestone. The contours for Coble creep after Rutter (1976) are superimposed for comparison. Note that the field of superplastic flow has expanded to higher stresses in comparison with fig. 13.

Fig. 15. Twinning is the predominant deformation mode in coarse grained marbles above 1000 bar differential stress. Under the same conditions of deformation finegrained Solnhofen limestone deforms predominantly by glide (compare fig. 18). Carrara marble experimentally deformed at 600^{0}C, 10^{-3} sec^{-1}, 3 kb confining pressure and at 1340 bar differential stress by 21% shortening. Compression vertical.

Fig. 16. "Core-mantle" structure typical for Carrara marble deformed in an intermediate stress range (200-1000bar) where equations (6) and (8) in table 1 are valid. The predominant mode of deformation is glide (the few narrow twin lamellae account for little strains only). Note the deformation bands in the grain interior and the equi-axed subgrains confined to grain boundary regions. Carrara marble experimentally deformed at 700^{0}C, 10^{-5} sec^{-1}, 3kb confining pressure, and at 685 bar differential stress by 12% shortening. Compression vertical.

Fig. 17. Equi-axed subgrains penetrate the entire region within an original grain. Increasing misorientation at subgrain boundaries results in recrystallization by subgrain rotation. This microstructure is typical for marble deformed at low stresses ($<$ 200 bar), where equations (7) and (9) in table 1 are valid. Carrara marble experimentally deformed at 1000^oC, 10^{-5} sec^{-1}, 3 kb confining pressure and at 150 bar differential stress by 21% shortening. Compression vertical.

Fig. 18. Microstructure typical for dislocation creep in Solnhofen limestone, where equation (2) in table 1 is valid. Note the absence of twinning (compare fig.15), the serrate grain boundaries inherited from the undeformed material and the large amount of flattening. Solnhofen limestone experimentally deformed at 600^oC, 10^{-4} sec^{-1}, 3kb confining pressure and at 1900 bar differential stress by 32% shortening. Compression vertical.

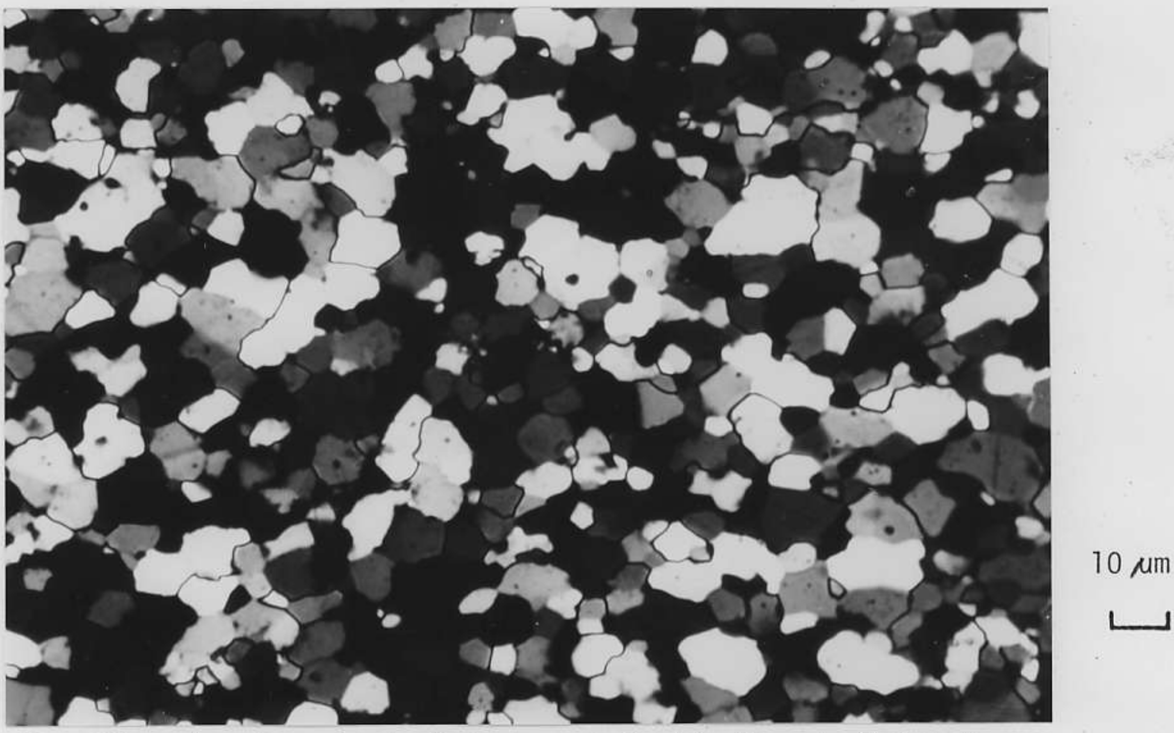

Fig. 19. Microstructure typical for superplastic flow in Solnhofen limestone, where equation (3) in table 1 is valid. Note the well equilibrated grain boundaries and the absence of grain flattening in spite of the large amount of strain (compare fig. 18). The change from serrated to straight grain boundaries coincides with the change in deformation mechanism from dislocation creep into superplastic flow. Solnhofen limestone experimentally deformed at 900°C, 7×10^{-4} sec^{-1}, 3 kb confining pressure and at 280 bar differential stress by 36% shortening. Compression vertical.

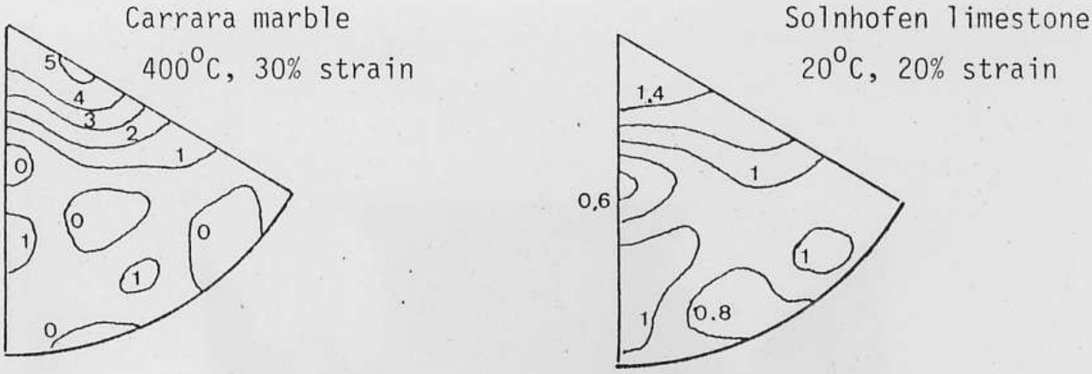

Fig. 20. "Type 1" textures associated with twinning.

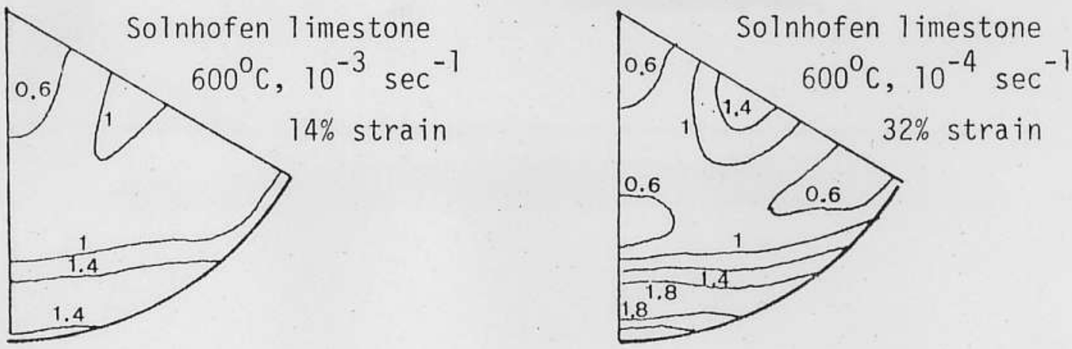

Fig. 21. "Type 2" textures associated with glide.

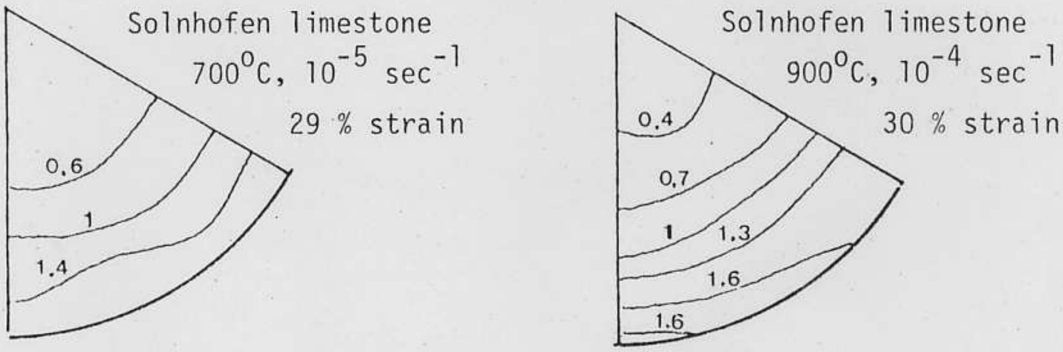

Fig. 22. "Type 3" textures associated with superplastic flow.

some important crystallographic directions in calcite:

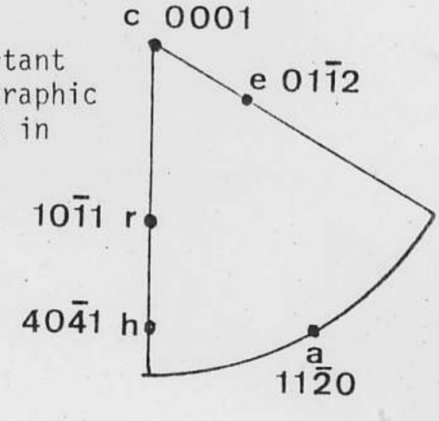

All inverse pole figures are contoured in multiples of a uniform distribution and are taken from Casey et al. 1978 .

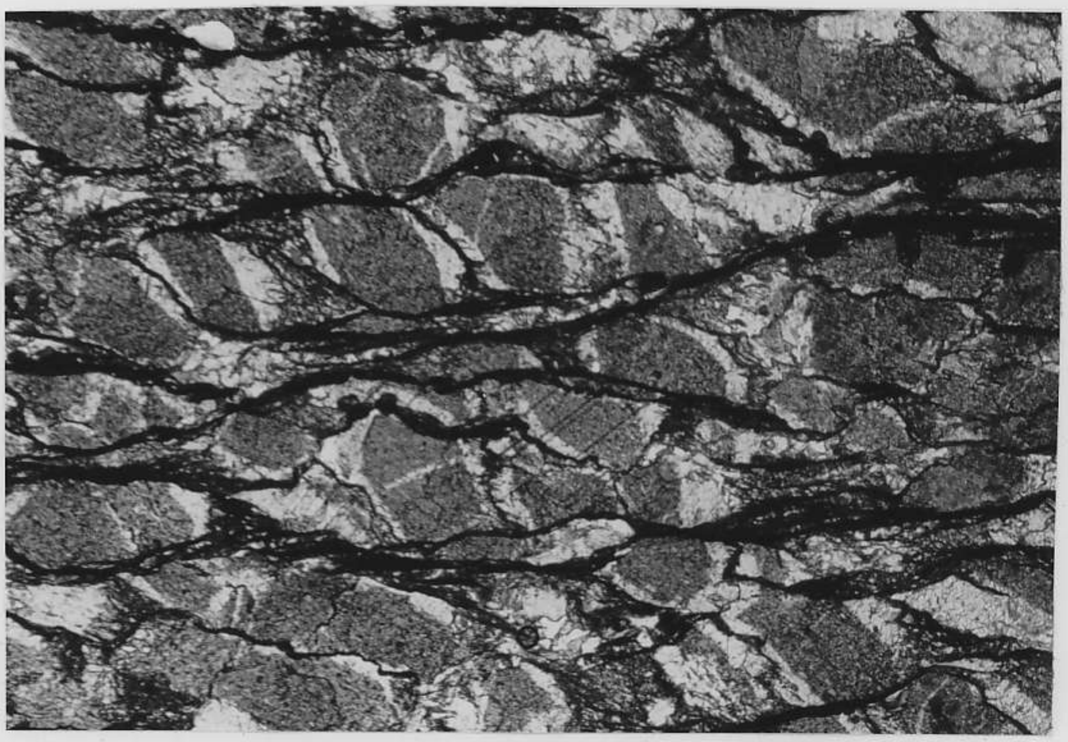

200 µm

Fig. 23. Pressure solution on the scale of individual grains in a crinoidal limestone from the schistes lustrés in Corsica. Solution took place along horizontally oriented stylolites, the white redeposition areas grow in crystallographic continuity over the dark grey inpure original single crystals of calcite. Notice that the redeposition areas form elongate domains which are not at a right angle to the stylolite orientation.

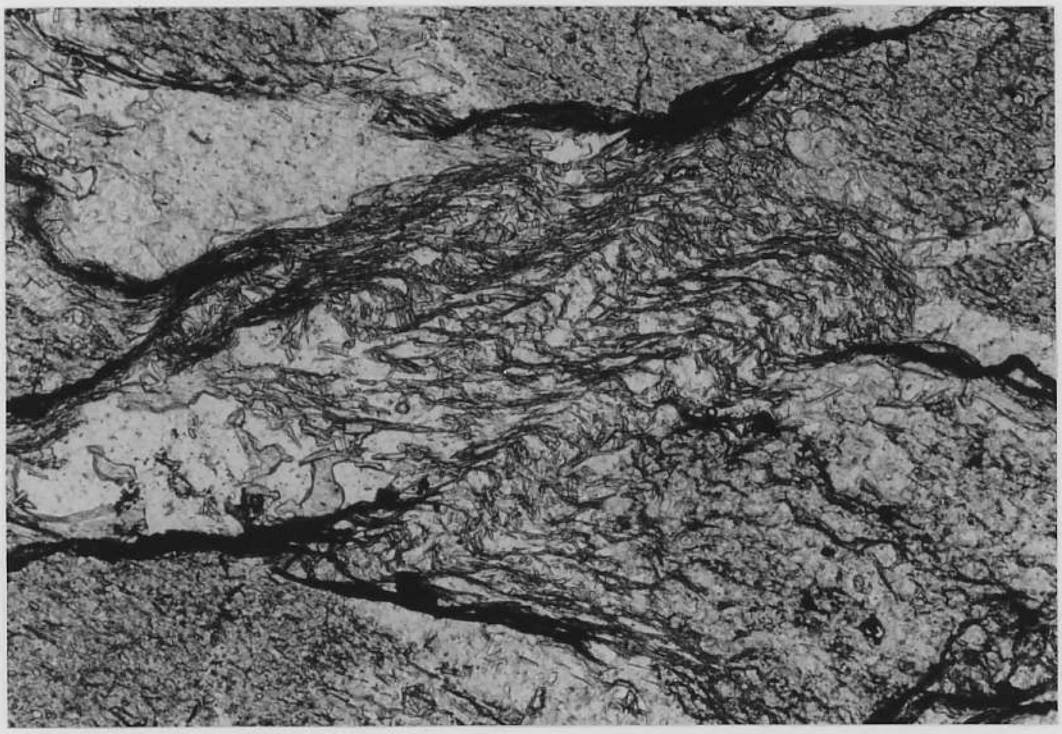

100 µm

Fig. 24. Microcrenulation in a clay-rich area of the specimen illustrated in fig. 23. The axial plane of these microfolds suggests that the direction of maximum finite shortening is not perpendicular to the plane of preferred orientation of the stylolites (horizontal in both figures 23 and 24).

Fig. 25. Specimen 71 from the inverted limb of the Morcles nappe (tertiary limestone conglomerate). A large grain in the centre of the micrograph is strongly elongated in a horizontal plane of flattening, parallel to the foliation. The finegrained domains are only slightly flattened in a plane oblique to the foliation (see fig. 27). The sense of shear as inferred from field relationships is dextral. The amount of strain as recorded by the shape of the pebbles is in the order of 50:10:1 . Only a small portion of this strain is recorded in grain aspect ratios. Glide is the main mode of deformation.

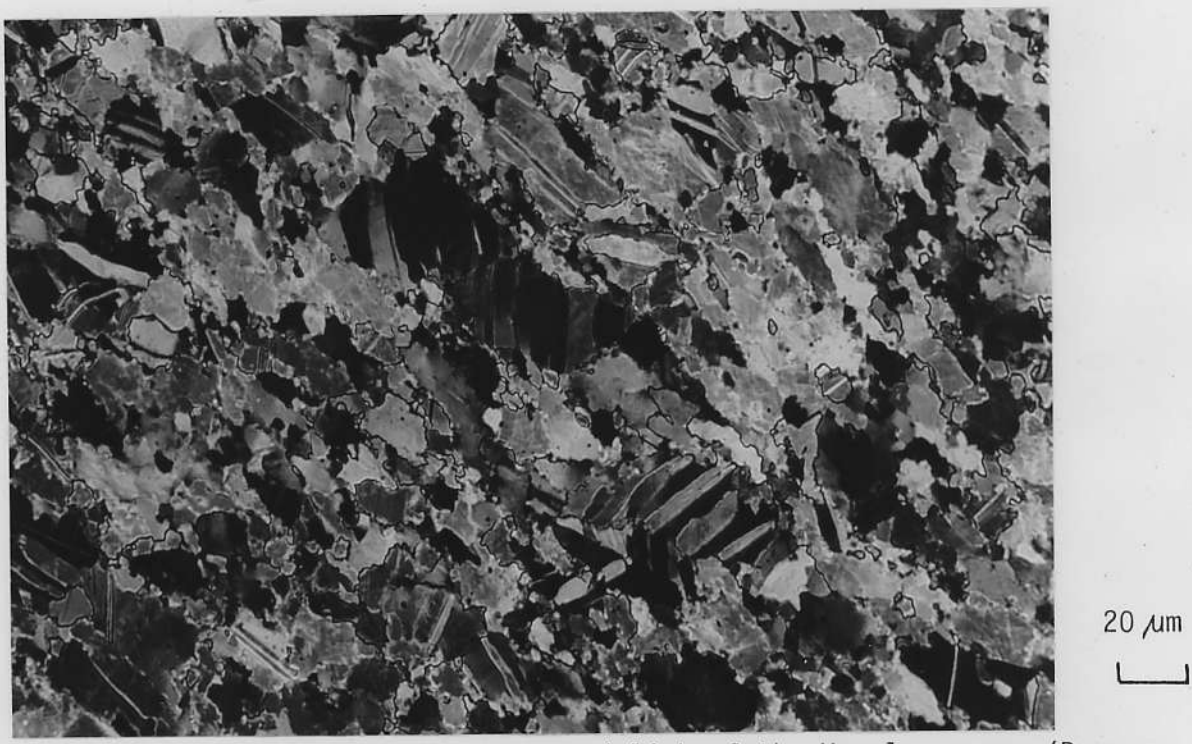

Fig. 26. Specimen 7816 from the inverted limb of the Morcles nappe (Dogger limestone). Notice that the plane of flattening of individual grains is oblique to the horizontal direction parallel to the macroscopically visible foliation (see fig. 27). The sense of shear as inferred from field relationships is sinistral in respect to this micrograph. Notice the abundance of deformation twins and the serrate grain boundaries indicative of grain boundary migration. For the texture compare fig. 34,a.

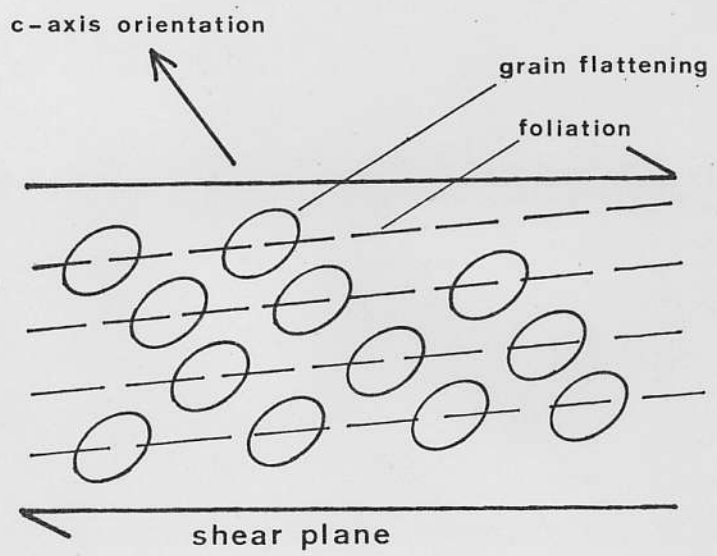

Fig. 27. Sketch illustrating the relative orientations of (i) the the macroscopic foliation tracing the orientation of the flattening plane in repect to finite strain (pebble strain in the case of specimen 71 in fig. 25), (ii) the aspect ratio and orientation of individual calcite grains tracing incremental strain and (iii) the approximate orientation of the c-axis point maximum for calcite in an environment of shearing (compare fig.34,a,b).

20 μm

Fig. 28. Coarser grained domain in specimen 7816 (compare fig. 26) illustrating lensoid shaped deformation twins comparable to the experimentally produced twins of figs. 4 and 15. The grain labelled "t" in the center of the micrograph is almost completely in a twinned orientation (white areas) and this twinned domain re-twins along a new set of dark twins. The orientation of the micrograph in repect to foliation is the same as in fig. 26. For the texture compare fig. 34 a.

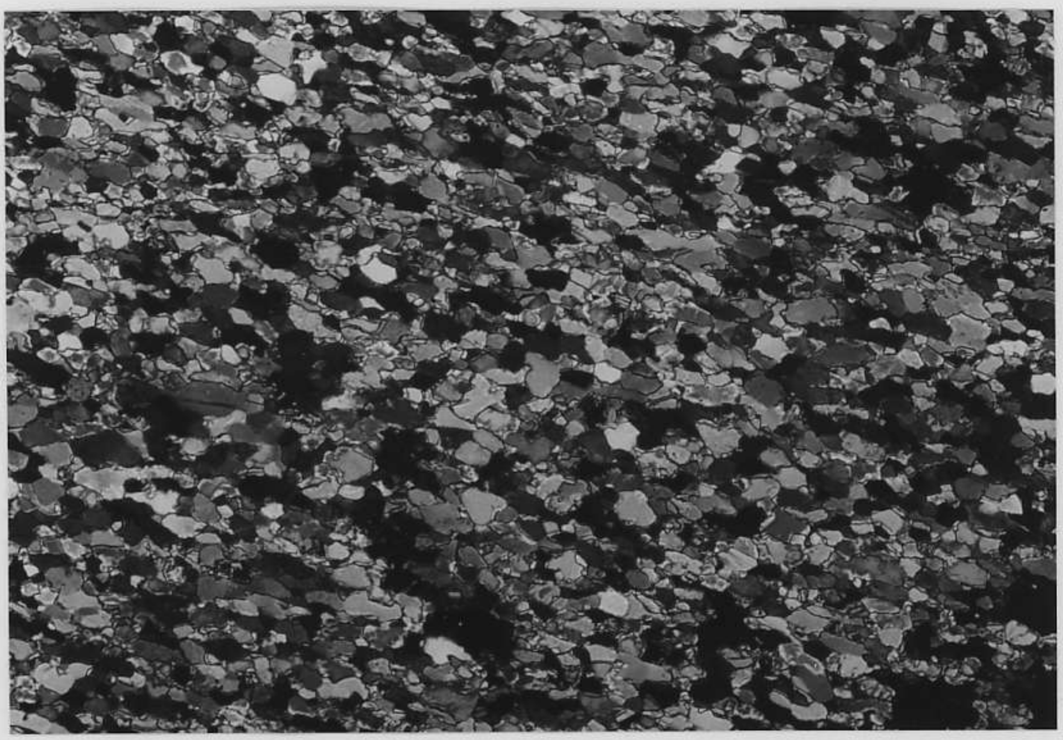

100 μm

Fig. 29. Specimen 7923 from the Saasberg Schuppe (Schrattenkalk) with well equilibrated grain boundaries. There is very little twinning to be observed and glide is the main mode of deformation. For the texture compare fig. 34c.

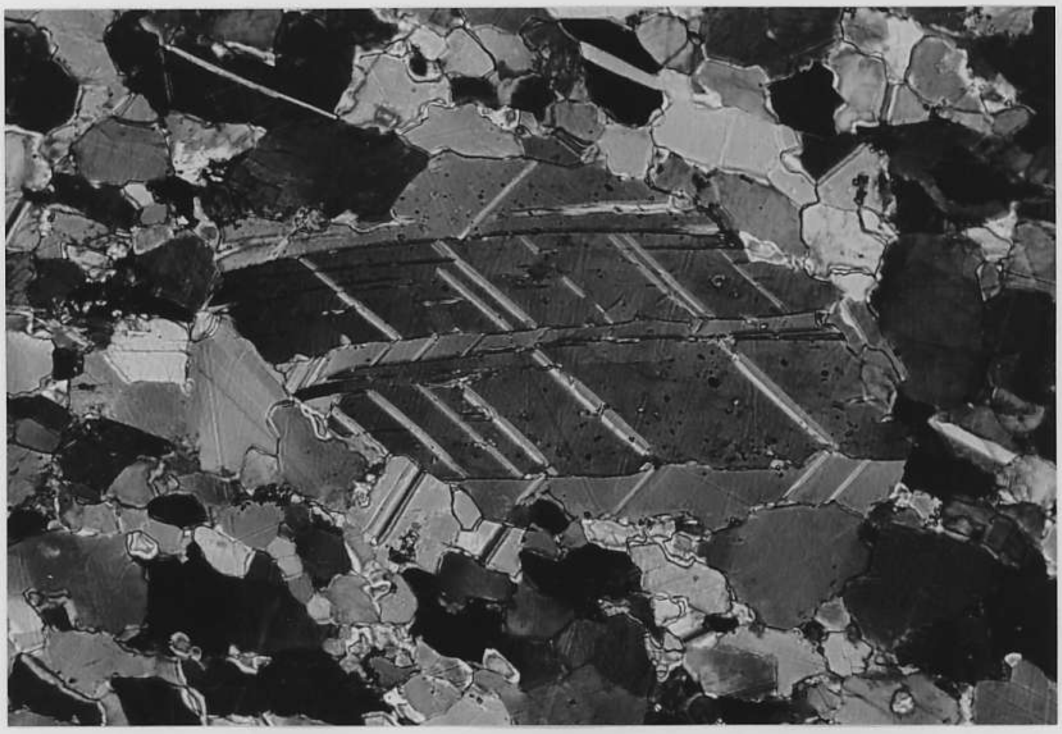

20 µm

Fig. 30. Specimen 7822 from the inverted limb of the Morcles nappe (Schrattenkalk) illustrating that twinning is restricted to the larger grains.

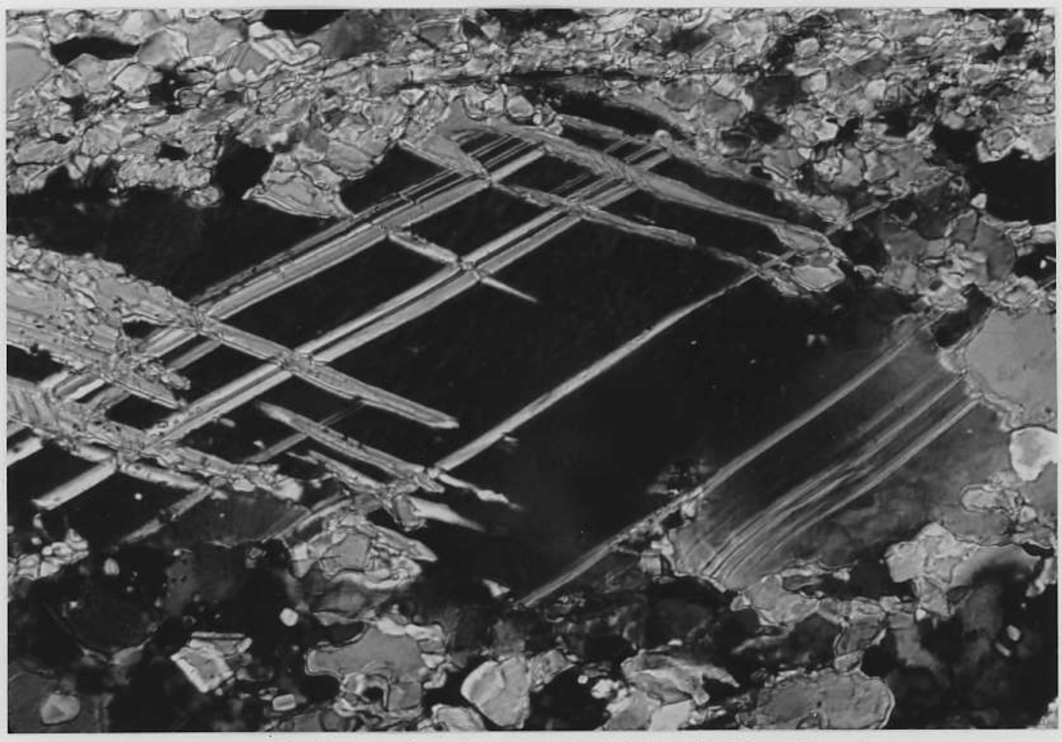

20 µm

Fig. 31. Specimen 71 from the inverted limb of the Morcles nappe (tertiary limestone conglomerate) with twinning restricted to large grains as is the case in fig. 30. Note the constriction of the twin lamellae at points of intersection, due to strain compatibility problems around twin intersection points and typical for experimentally deformed marble too (compare fig. 4).

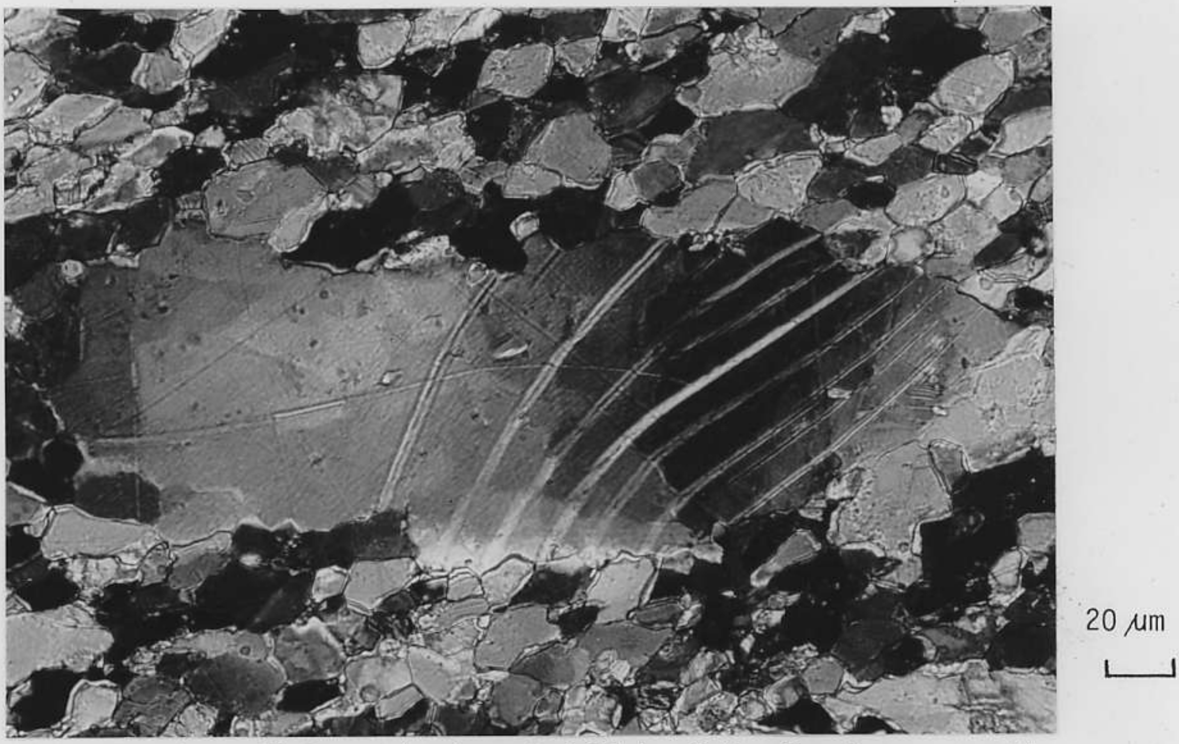

Fig. 32. Specimen 71 from the inverted limb of the Morcles nappe (tertiary limestone conglomerate, detail of fig. 25) illustrating subgrain formation within a relatively large calcite grain. Note that some of the subgrains have a grain size similar to the size of the matrix grains. The thin twin lamellae are bent and in some places suddently deflected across subgrain boundaries.

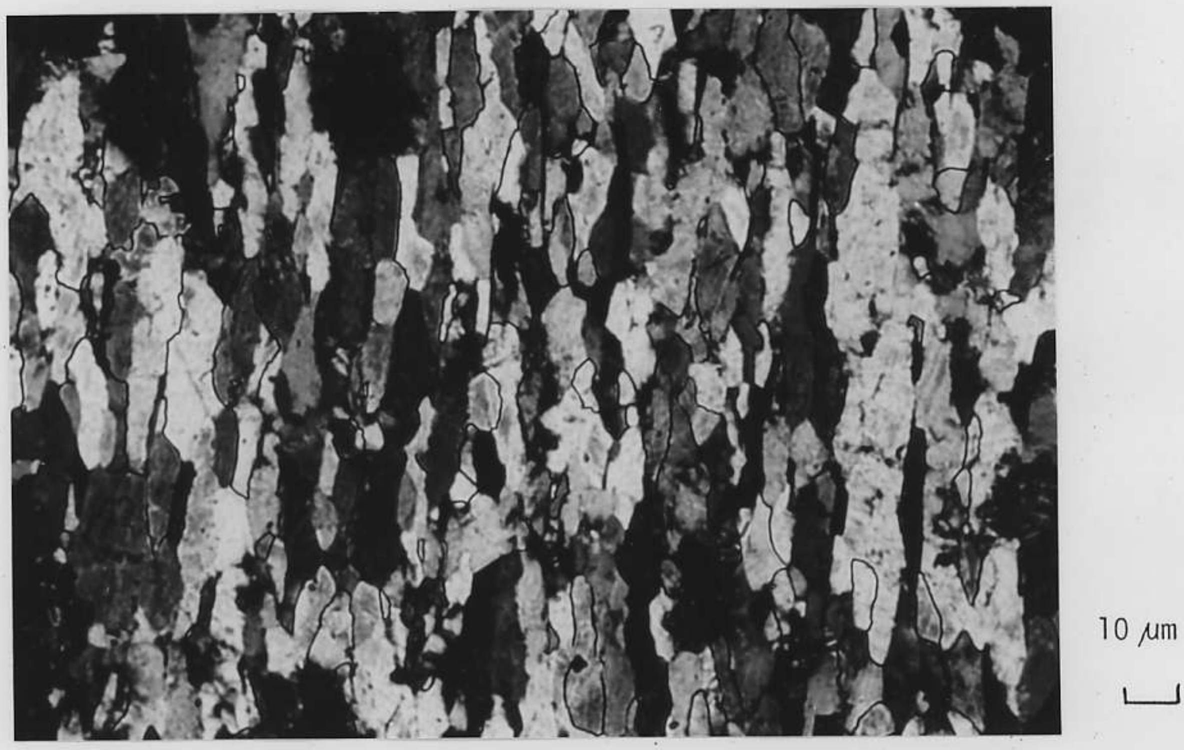

Fig. 33. Specimen 1088 from the infrahelvetic units of the Calanda region (Upper Jurassic Malm). In this specimen the individual grains are flattened in the plane of the macroscopic foliation and only the c-axis point maximum is oblique to the macroscopic fabric axes (compare the texture in fig. 34b). Glide on r is the dominant deformation mechanism as inferred from the textural evidence and there is no twinning.

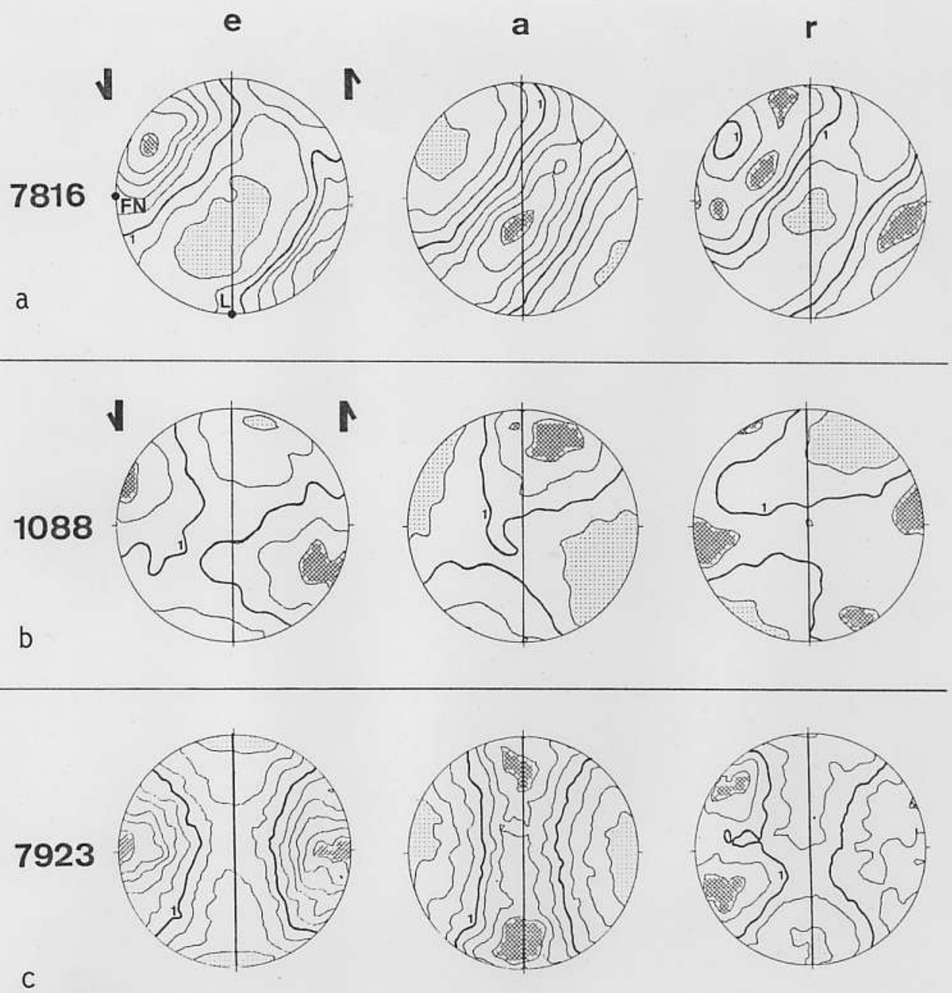

Fig. 34 a,b,c . Pole figures for the e-, a-, and r-planes in calcite for naturally deformed limestone tectonites, analysed by X-ray texture goniometry. The locations and microstructures of the specimens are described in fig. 26 and 28 for specimen 7816, in fig. 33 for specimen 1088 and in fig. 29 for specimen 7923. A complete texture analysis in terms of an orientation distribution function is given in Schmid, Casey and Starkey,1981 for specimen 7816. Note that the foliation normal (FN) is oriented E-W and that the lineation (L) is oriented N-S in all the pole figures. The contours are given in multiples of a uniform distribution with intervals of 0.2, the maxima are cross-hatched.

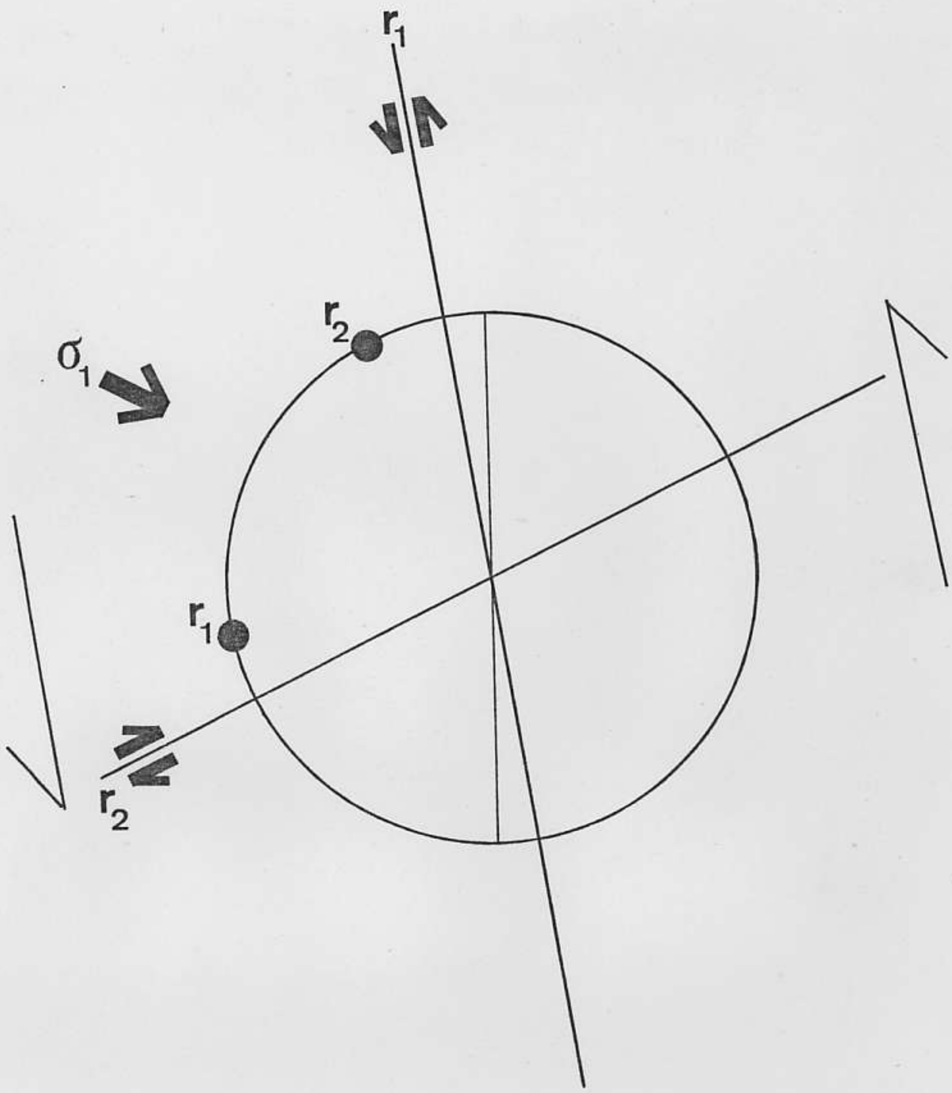

Fig. 35. Sketch illustrating the preferred alignment of calcite r-planes observed in the r-pole figure of figure 34 b. One r-plane (r_1) operates syntetically with the imposed sense of shear, the other r-plane (r_2) operates antithetically to the imposed sense of shear on the bulk rock. The third r-plane has a higher degree of freedom in terms of the exact location than r_1 and r_2 have and as a consequence no third maximum is visible in the r-pole figure of fig. 34 b allthough there are three r-planes in every calcite crystal.

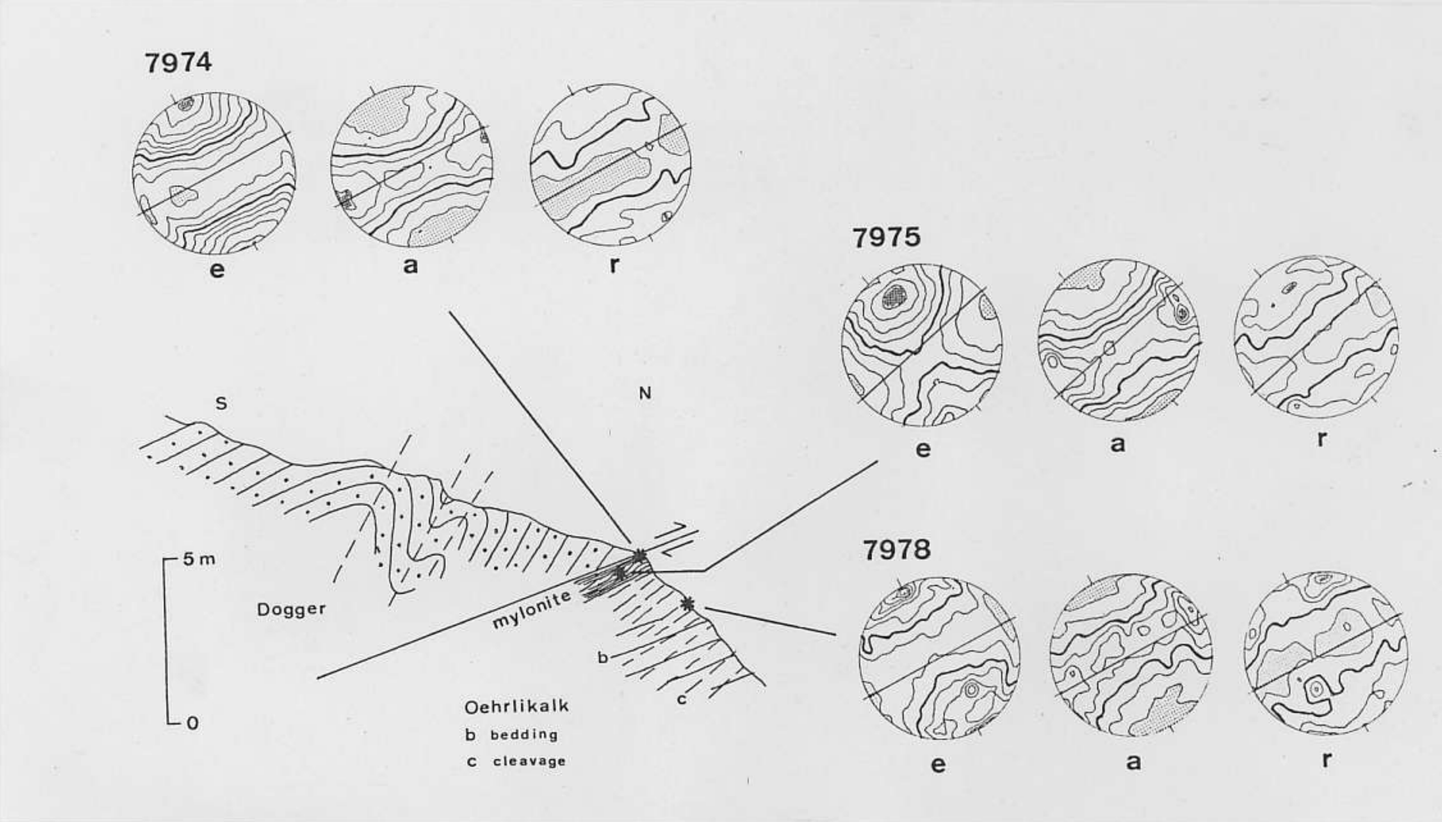

Fig. 36. Geological setting of the progressive mylonitization of Oehrlikalk at the thrust contact between the Axen-nappe (Middle Jurassic Dogger) and the Mürtschen-nappe (Lower Cretaceous Oehrlikalk) south of the eastern end of Klöntalersee (Glarus). The microstructural development is described in section 3 a. The upper hemisphere X-ray pole figures for the e-, a- and r-poles are oriented in accordance with the profile, with the foliation trace indicated. The intensities are contoured in multiples of a uniform distribution with intervals of 0.2 . The solid line is the 1.0-contour, the maximum intensities are cross-hatched, the minimum intensities are stippled. The specimen numbers refer to the specimens described in the text, specimen 7978 is not yet mylonitized, specimens 7975 and 7974 are calc-mylonites.

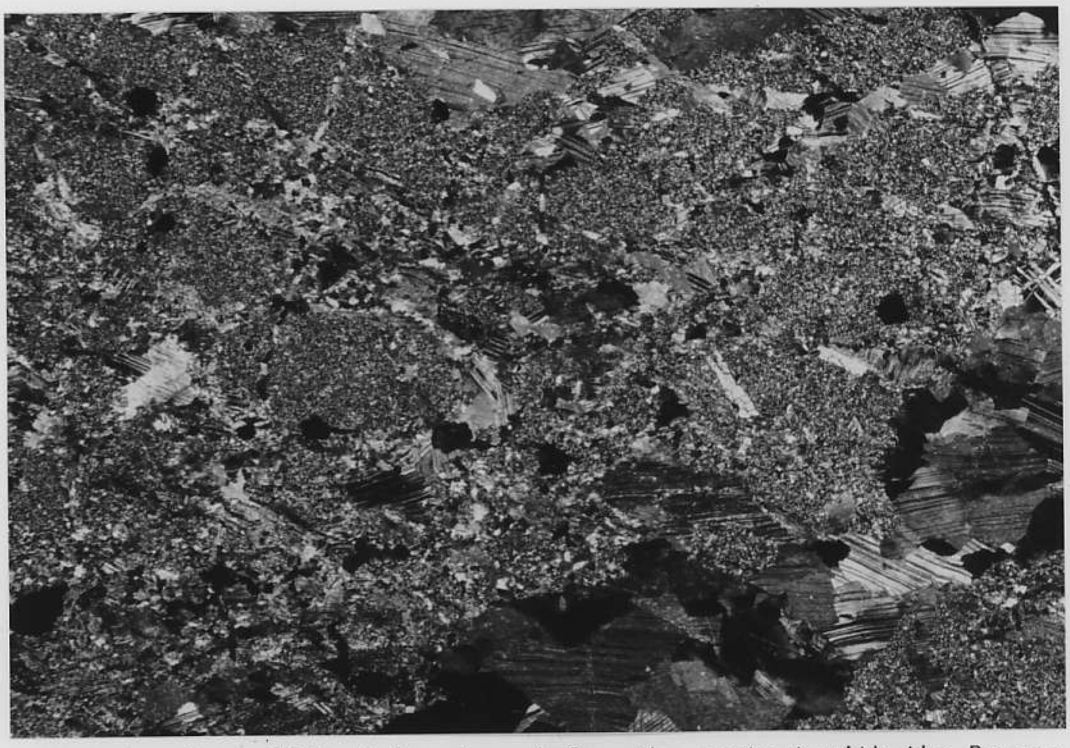

200 µm

Fig. 37. Specimen 7979 at 3 metres below the contact with the Dogger (see fig. 36): Oehrlikalk with a deformed but still well preserved original microstructure consisting of finegrained ooids in a sparitic, strongly twinned matrix. The strain indicated by the aspect ratios od the ooids is moderate.

10 µm

Fig. 38. Finegrained and untwinned microstructure within the ooids of specimen 7979 (compare fig. 37).

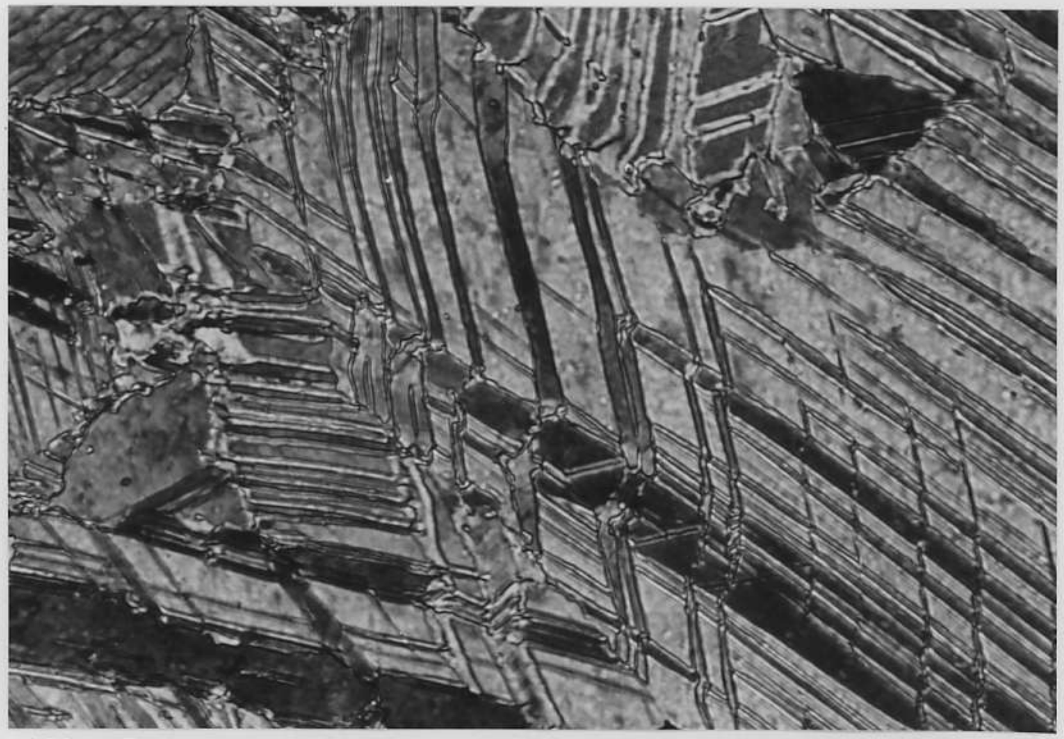

10 µm

Fig. 39. Twinning within the sparitic matrix of specimen 7979 (fig. 37). Notice the offsets of some twin lamellae produced by twinning on a second set of twin lamellae.

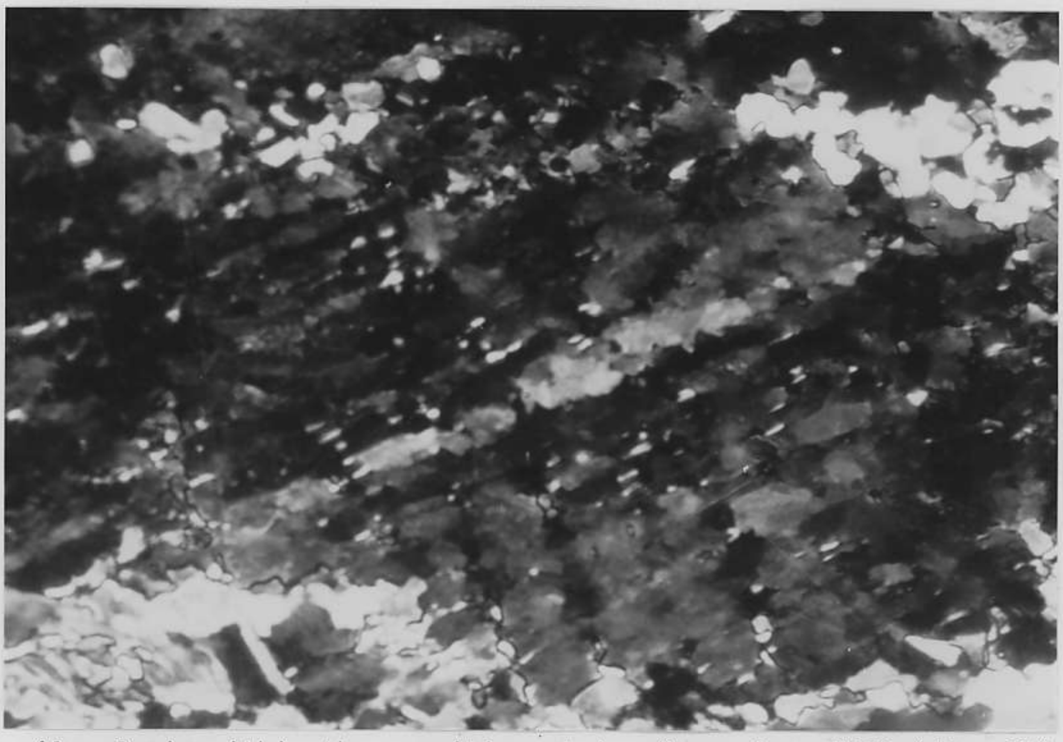

10 µm

Fig. 40. Grain within the sparitic matrix of specimen 7979 (fig. 37) which is unsuitably oriented for twinning. Glide is the main mode of deformation and subgrains form as a consequence of the rearrangement of dislocations during recovery. Parts of the crystal are recrystallized to a grain size which is similar to the size of the subgrains.

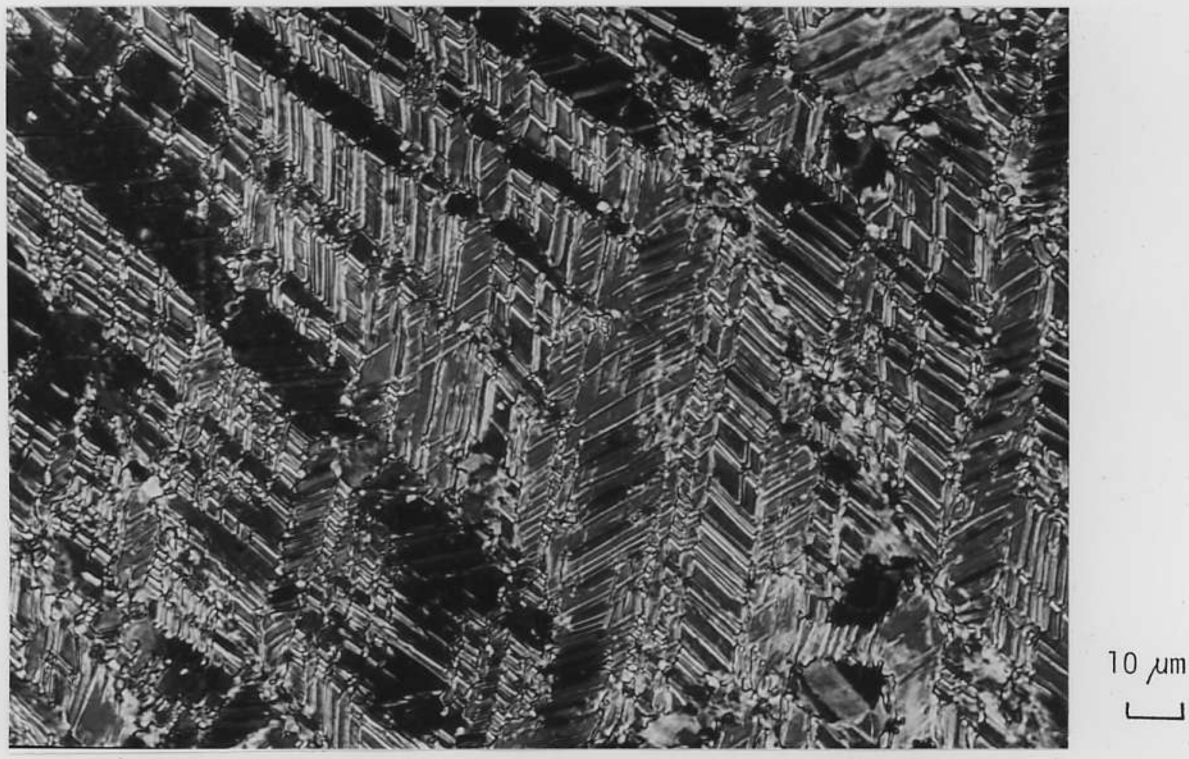

Fig. 41. Specimen 7978 (from 1.8 m below the contact, for the texture compare fig. 36): Very strongly twinned calcite grain within the sparitic matrix and nucleation of very small new grains, at the limit of optical resolution (1 µm and less).

Fig. 42. Subgrain formation and recrystallization by subgrain rotation, leading to a bigger grain size than nucleation recrystallization as illustrated in fig. 41. Both mechanisms of recrystallization occur within the same specimen. Nucleation favours twinned crystals (fig. 41), recrystallization by subgrain rotation favours untwinned or weakly twinned crystals as is the case in this micrograph.

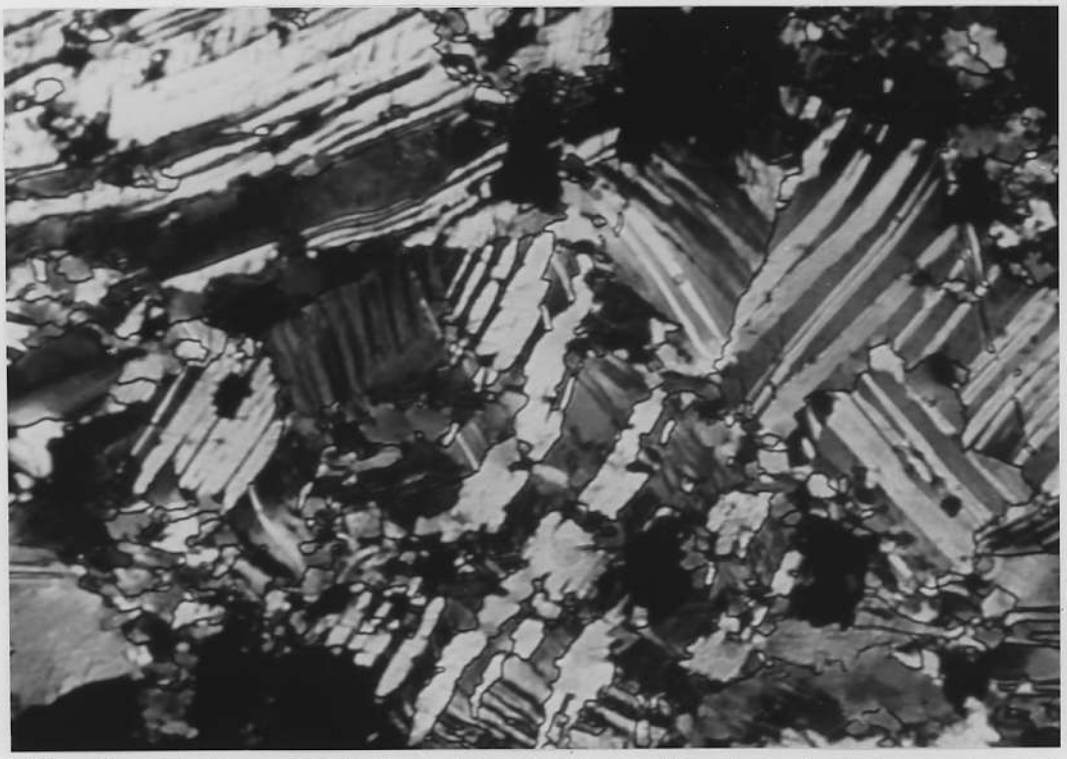

10 µm

Fig. 43. Broad, lensoid twins with evidence for twin boundary migration in specimen 7978.

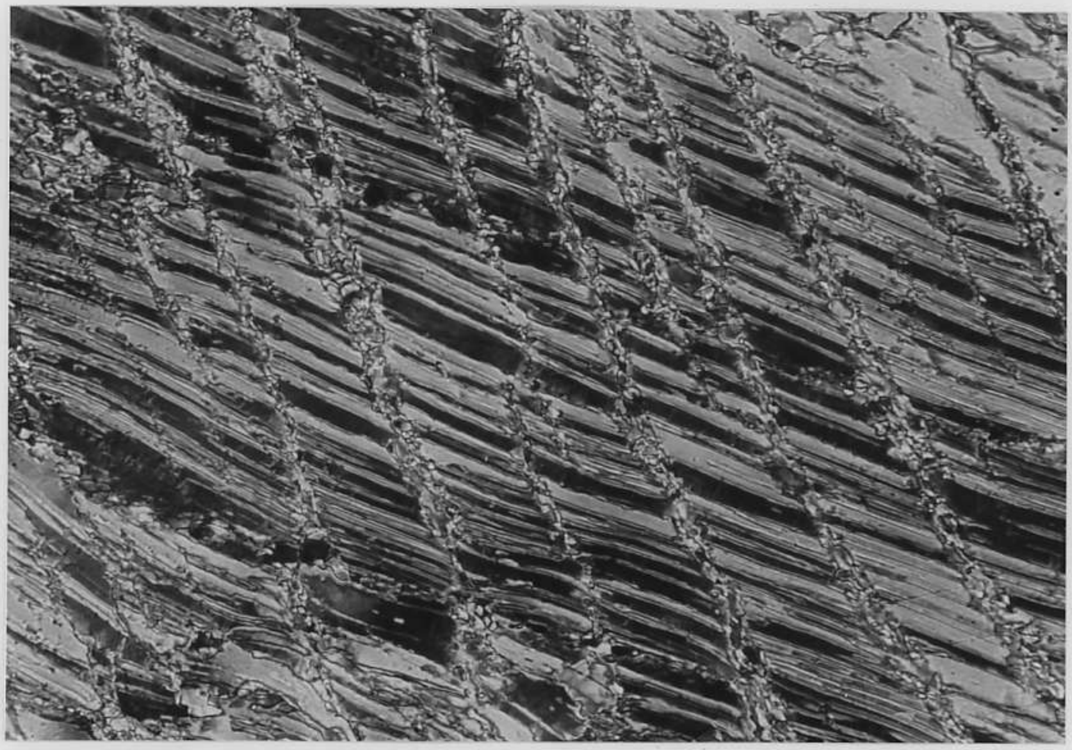

20 µm

Fig. 44. Nucleation recrystallization along traces of old twin lamellae in a relict grain (porphyroclast) within specimen 7977 taken from the base of the mylonitic layer.

100 μm

Fig. 45. Porphyroclast in specimen 7976 (mylonite layer) surrounded by a fully recrystallized finegrained matrix. This microstructure illustrates the progressive consumption of this poerphyroclast by intragranular nucleation recrystallization.

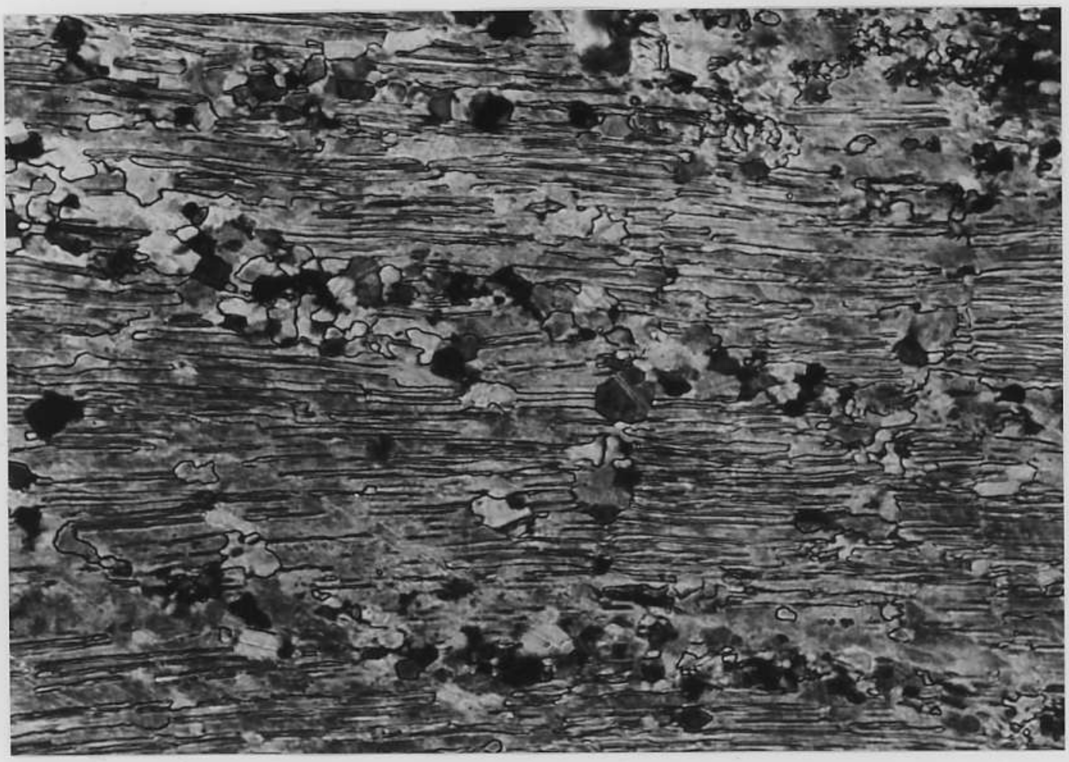

10 μm

Fig. 46. Recrystallization by subgrain rotation within an intraclast of specimen 7975 (mylonite layer).

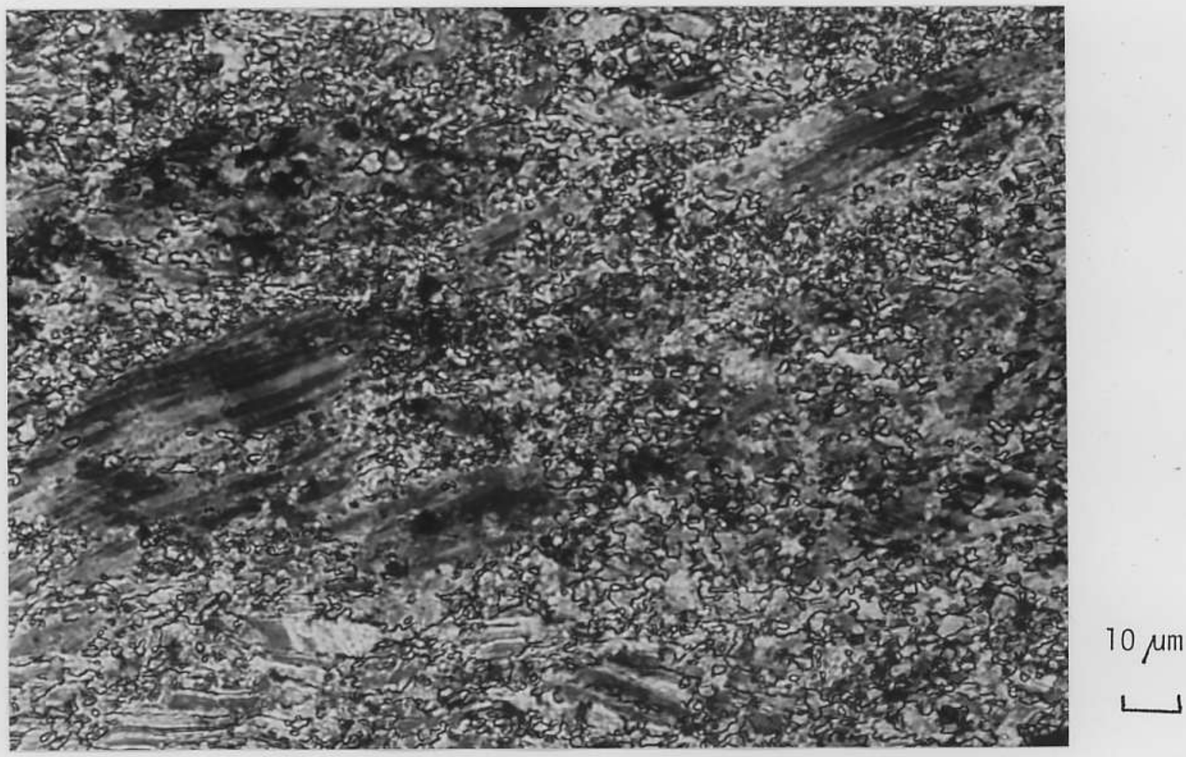

Fig. 47

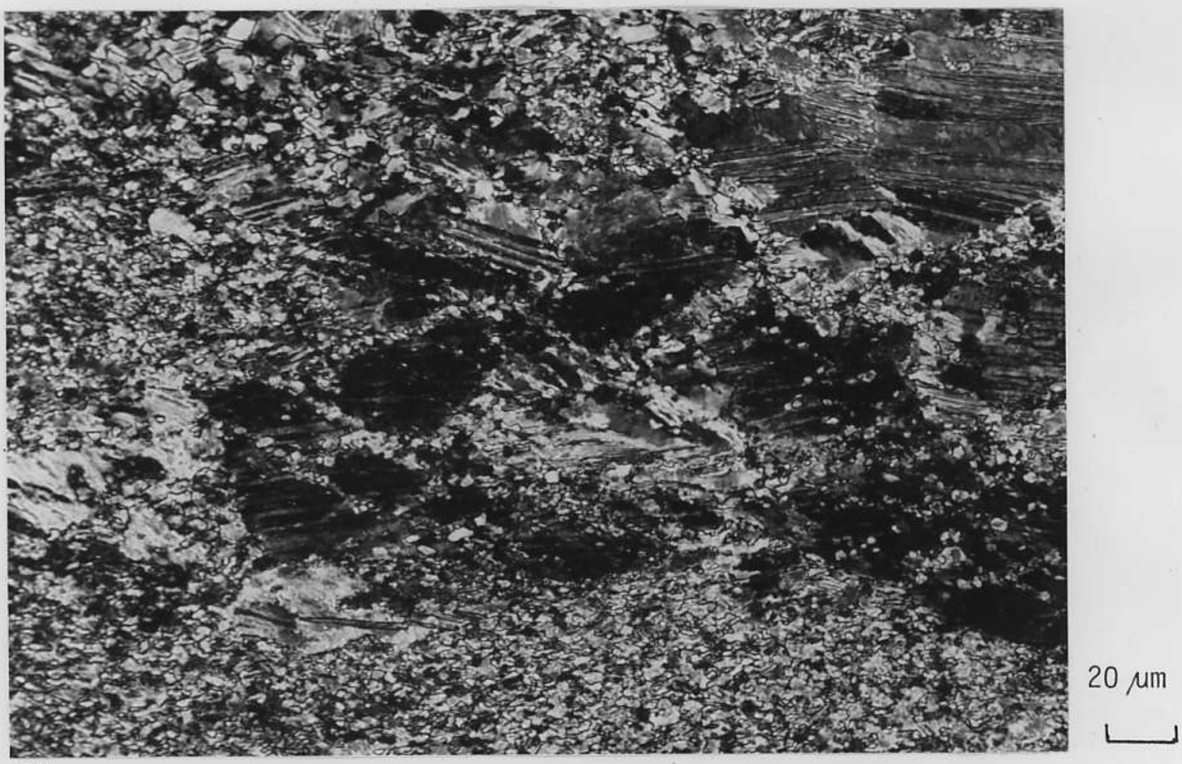

Fig. 48

Figs. 47 & 48: Typical microstructure of the calc-mylonite: a few, heavily twinned grains survive within a totally recrystallized matrix. Notice the preferred alignment of rather diffuse twin lamellae (twinning went to completion) in a subhorizontal plane parallel to the foliation (E-W in these micrographs). This strong crystallographic preferred orientation of old porphyroclasts is responsable for the texture illustrated in fig 36 to occur in specimens 7974 and 7975.

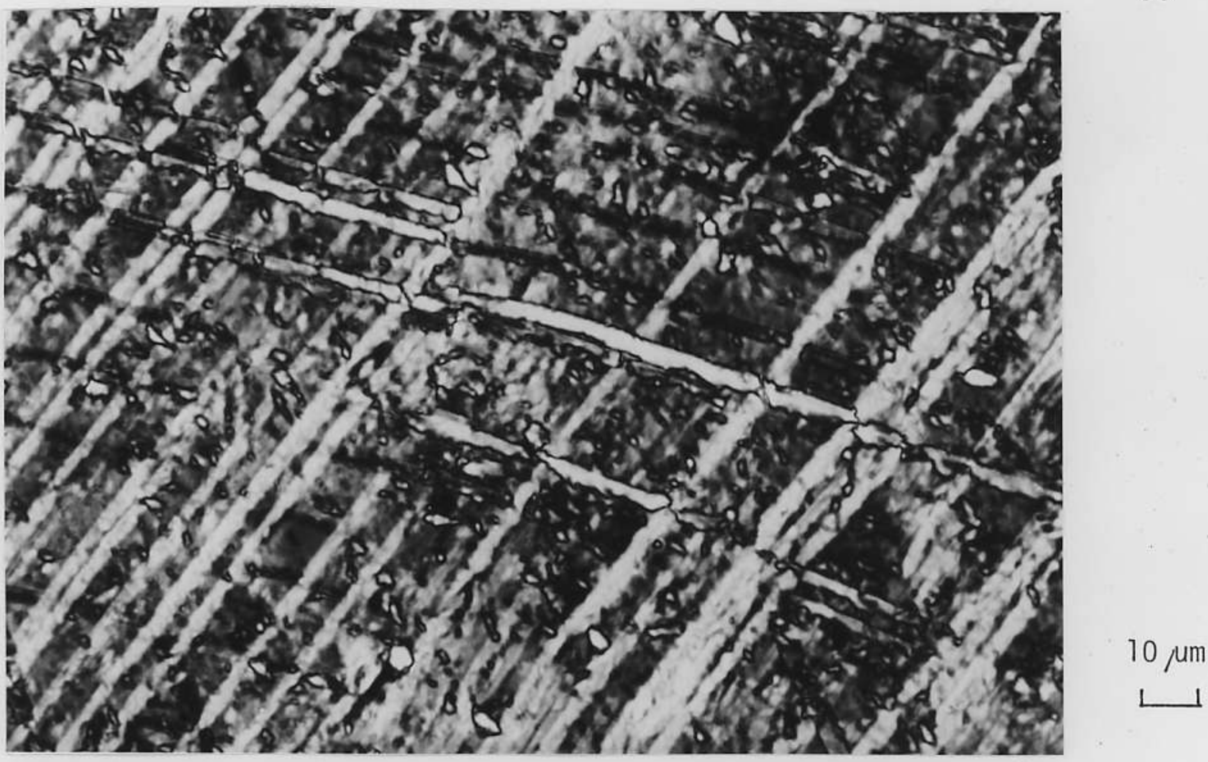

Fig. 49. Nucleation recrystallization in a twinned grain within a relatively undeformed calcite vein occuring in specimen 63 (Foostock, main Glarus overthrust).

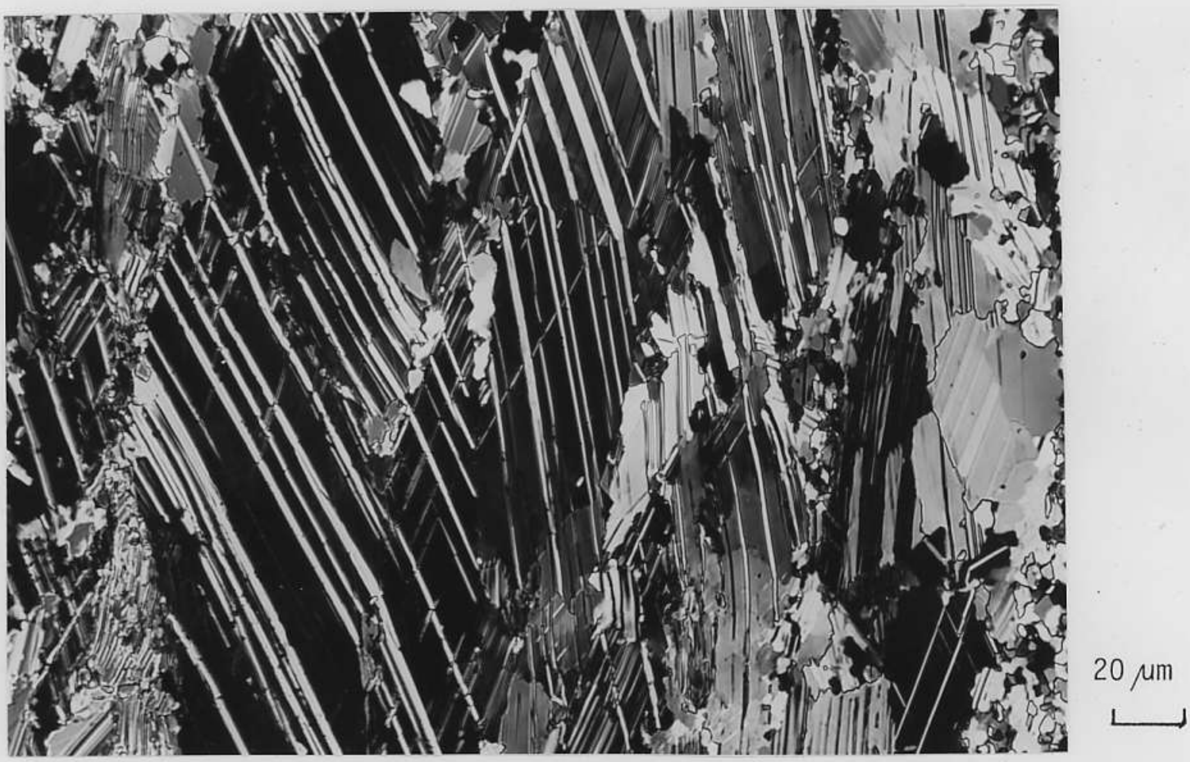

Fig. 50. Recrystallization by the subgrain rotation mechanism in specimen 64 (Foostock, main Glarus overthrust). Recrystallization is concentrated to grain boundary regions, where the strain compatibility problems lead to polygonization and operation of additional glide systems ("core-mantle" structure, compare fig. 16).

10 μm

Fig. 51. Fully recrystallized domain in specimen 64 (Foostock, main Glarus overthrust). The size of the grains is larger than in fig. 52 and the mechanism of recrystallization was probably subgrain rotation. Some of the grains are weakly twinned (late stress pulse?). The grain boundaries are well equilibrated and apart from the late (?) twinning the microstructure is similar to that of superplastically deformed Solnhofen limestone (fig. 19).

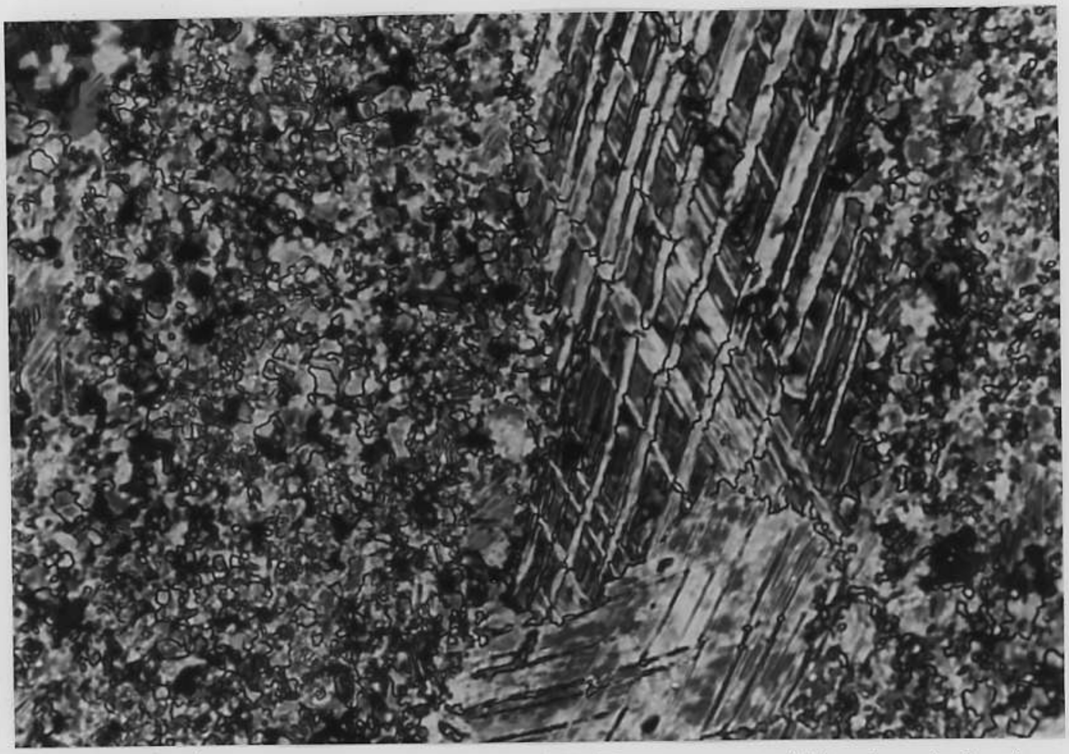

10 μm

Fig. 52. Twinned porphyroclast in a fully recrystallized matrix (specimen 63, Foostock, main Glarus overthrust). The recrystallized grain size is very much smaller than in fig. 51 and here recrystallization probably occured by a nucleation mechanism.

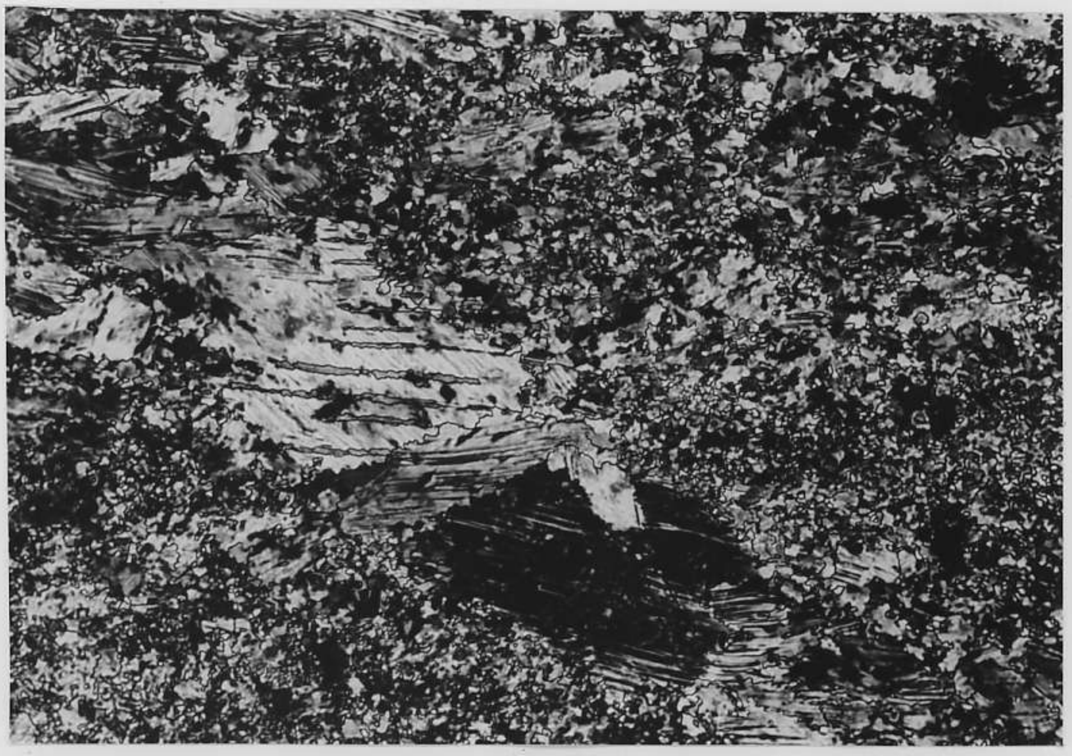

Fig. 53. Typical microstructure for the Lochseiten mylonite along the main Glarus overthrust (specimen 63, Foostock) and identical to the microstructures illustrated in figs. 47 and 48 taken from another mylonite horizon structurally above the main Glarus overthrust.

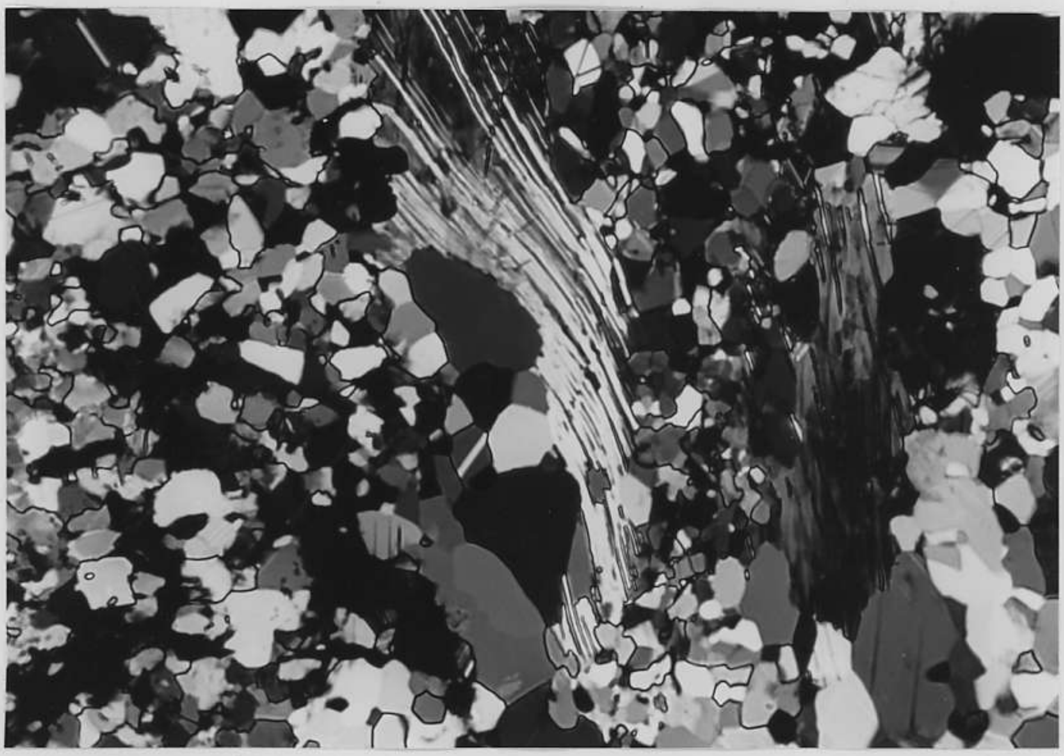

Fig. 54. Recrystallization by subgrain rotation went almost to completion in specimen 116 taken from the Ringlspitz area (main Glarus overthrust, south of Segnes Pass). The remaining old grains are heavily twinned. The new grains are free of optical strain features, the grain boundaries are well equilibrated.

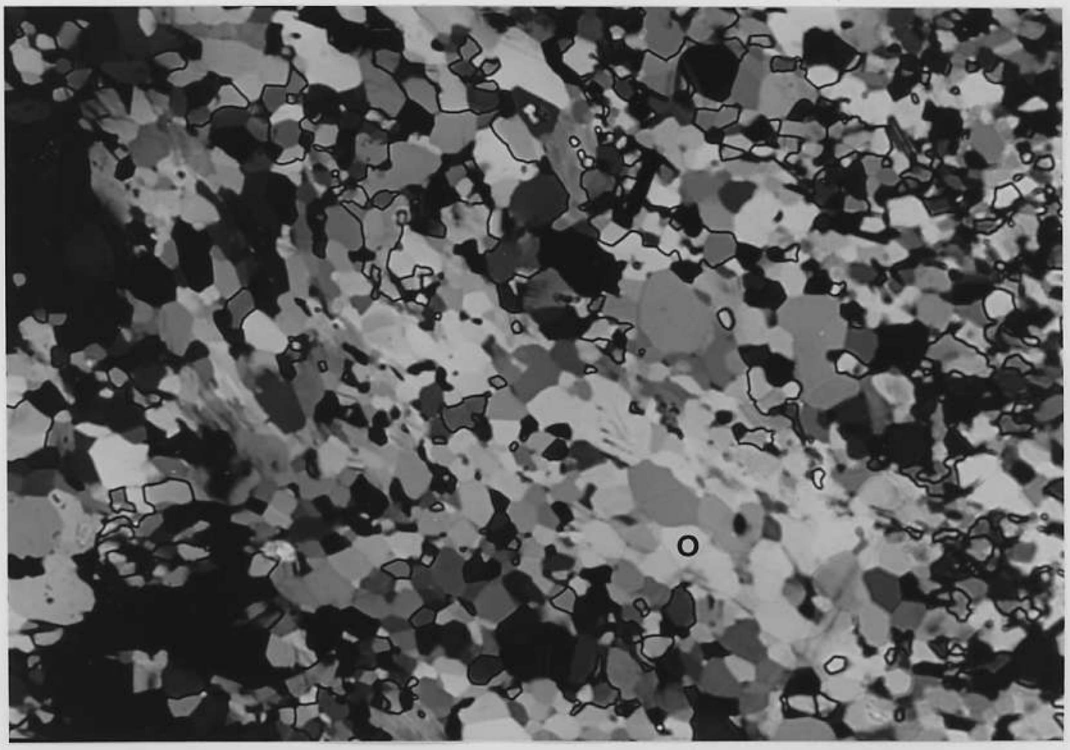

10 µm

Fig. 55. Specimen 116 (Ringlspitz, main Glarus overthrust): subgrain formation in an old grain marked "o" and recrystallization by subgrain rotation leading to a new grain size identical with the size of the subgrains. The microstructure of the recrystallized areas is strikingly similar to the microstructure of superplastically deformed Solnhofen limestone (see fig. 19).

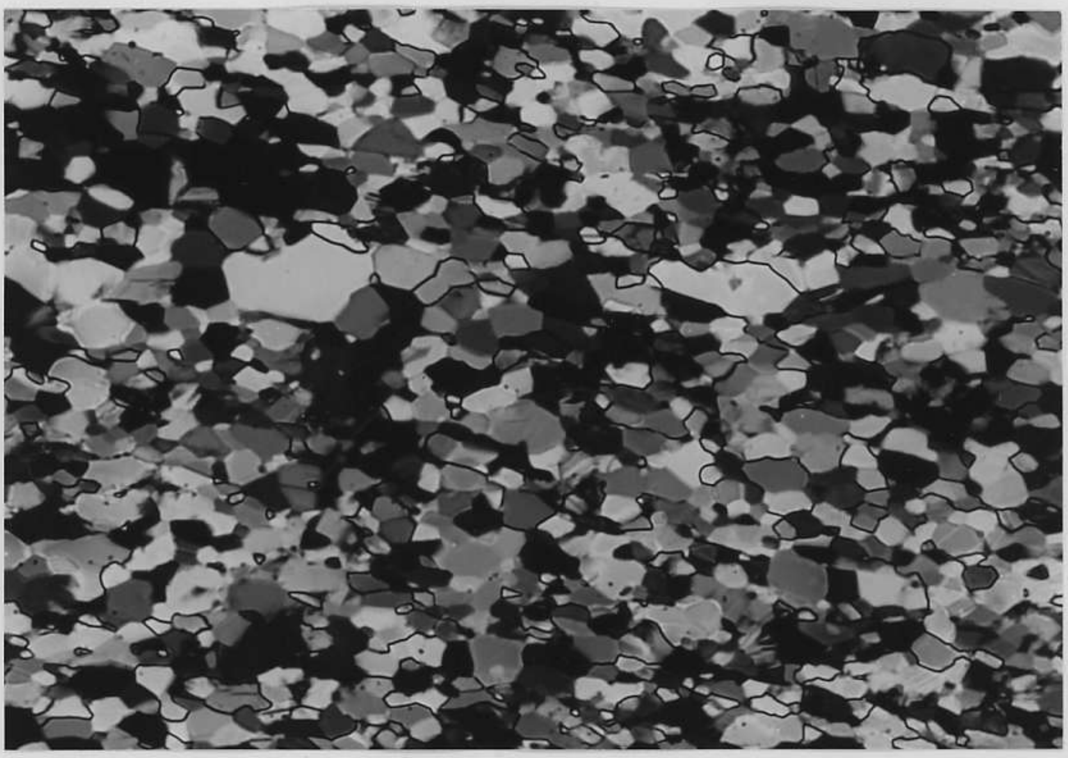

10 µm

Fig. 56. Totally recrystallized microstructure in specimen 116 (Ringlspitz, main Glarus overthrust).

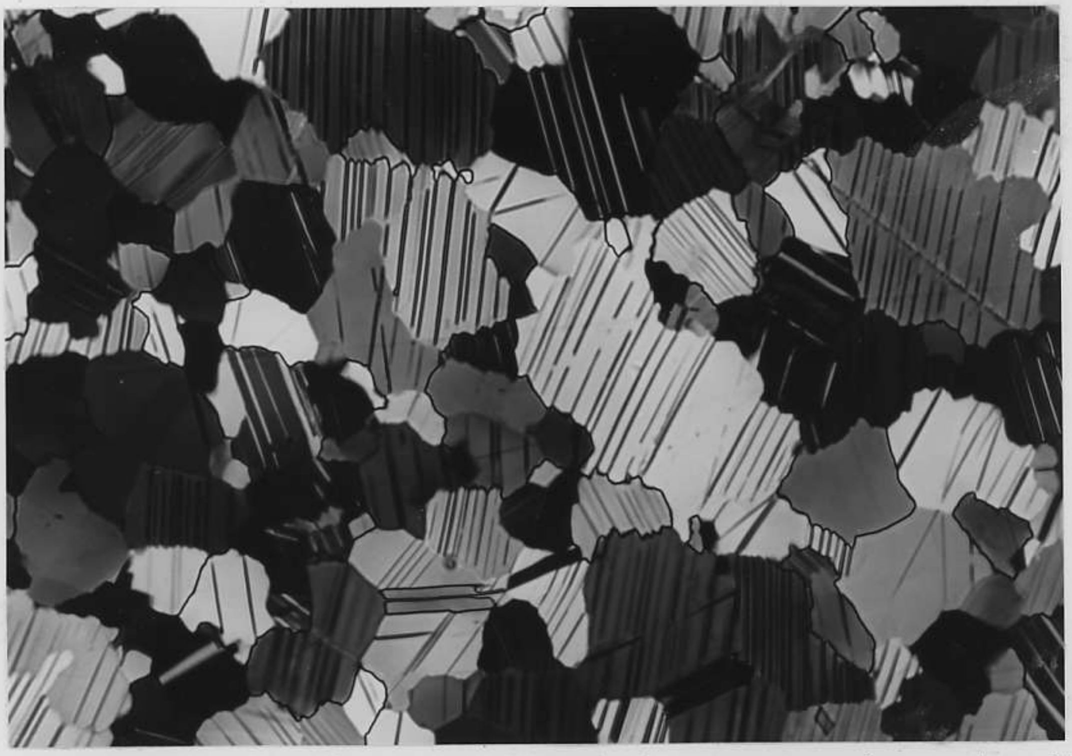

10 μm

Fig. 57. Coarser grained recrystallized microstructure in specimen 159 (Ringlspitz, main Glarus overthrust). It is likely that subsequent grain growth has occured in this specimen which in the filed has the appearance of a marble rather than that of a typical Lochseitenkalk. A late stress pulse lead to some twinning on narrow lamellae.

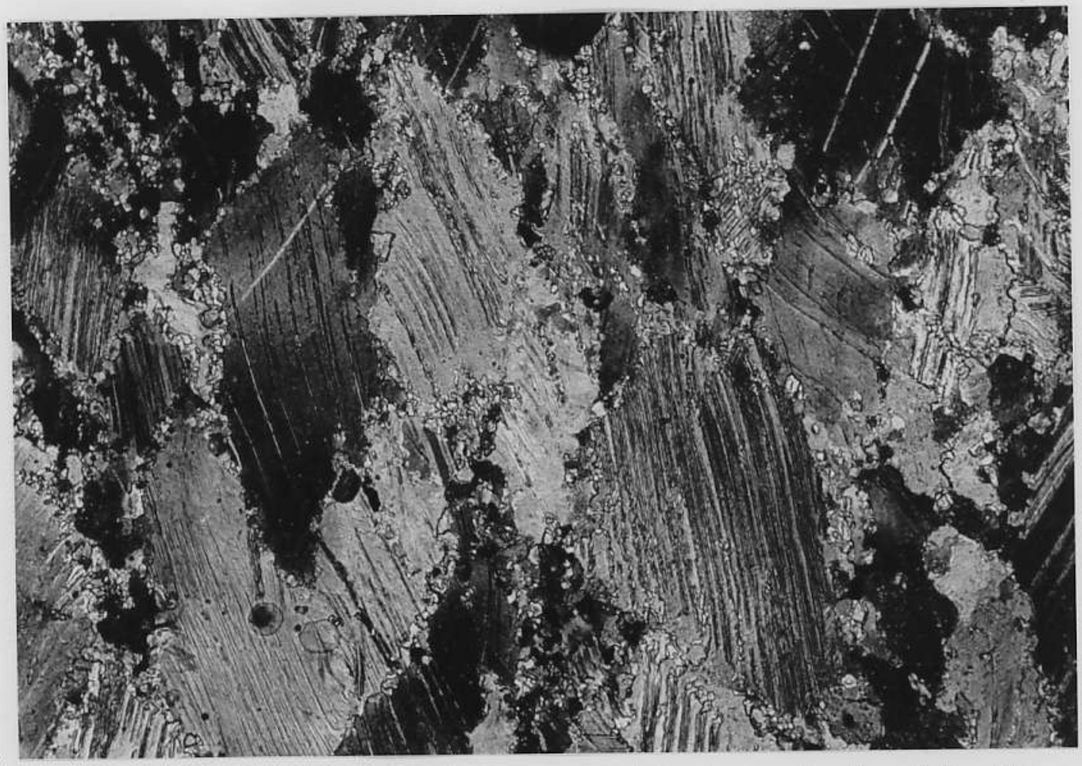

100 μm

Fig. 58. Calc-mylonite derived from a marble layer in the Valpelline Series of the Dent Blanche nappe. Heavily twinned original grains are surrounded by dynamically recrystallized grains concentrated in grain boundary areas (compare fig. 50 taken from the Lochseitenkalk).

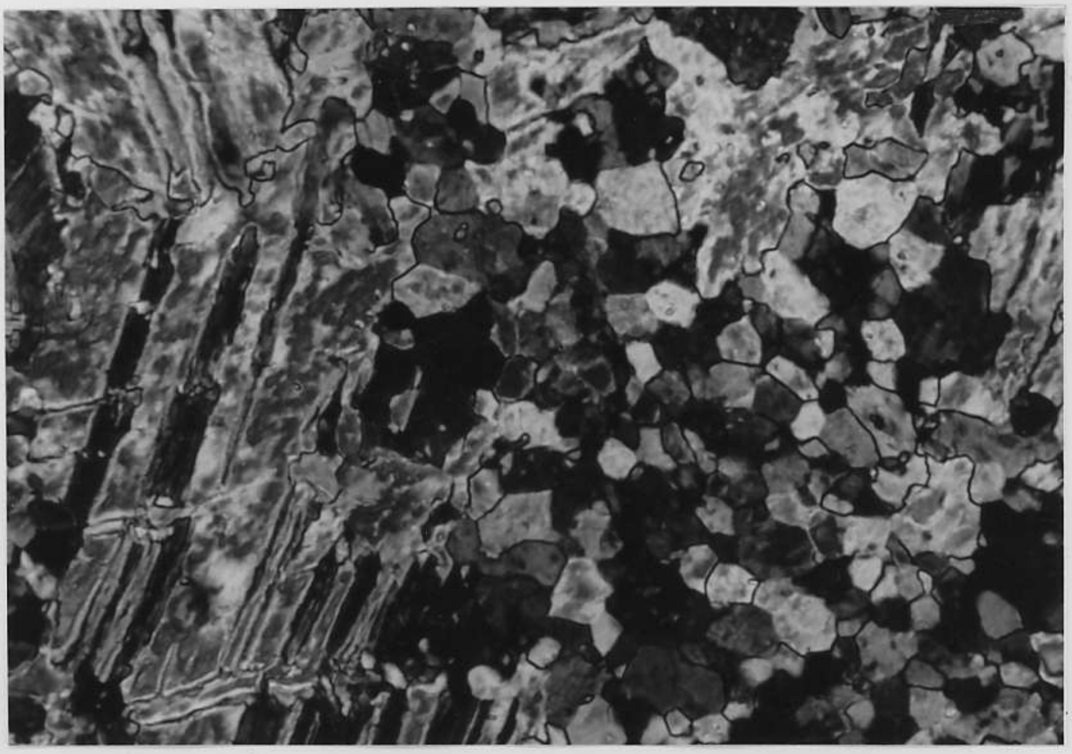

Fig. 59. Detail of a recrystallized grain boundary region in the specimen shown in fig. 58. Notice that the microstructure of these recrystallized domains is very similar to that of superplastically deformed Solnhofen limestone (fig. 19).

Fig. 60. Specimen of Lochseitenkalk, experimentally deformed at variable strain rates at 600°C, followed by stress relaxation (see chapter VI,A and fig. 65.

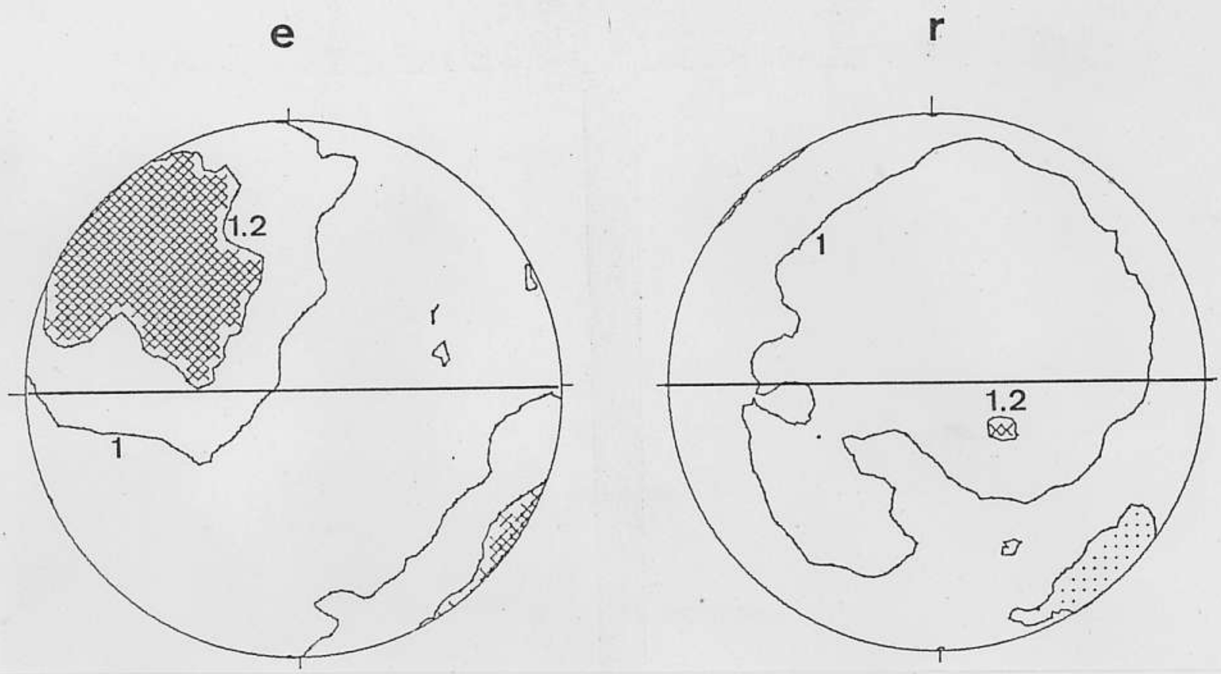

Fig. 61. Illustration of the extremely low degree of crystallographic preferred orientation in a totally recrystallized Lochseiten mylonite specimen from the Ringlspitz area

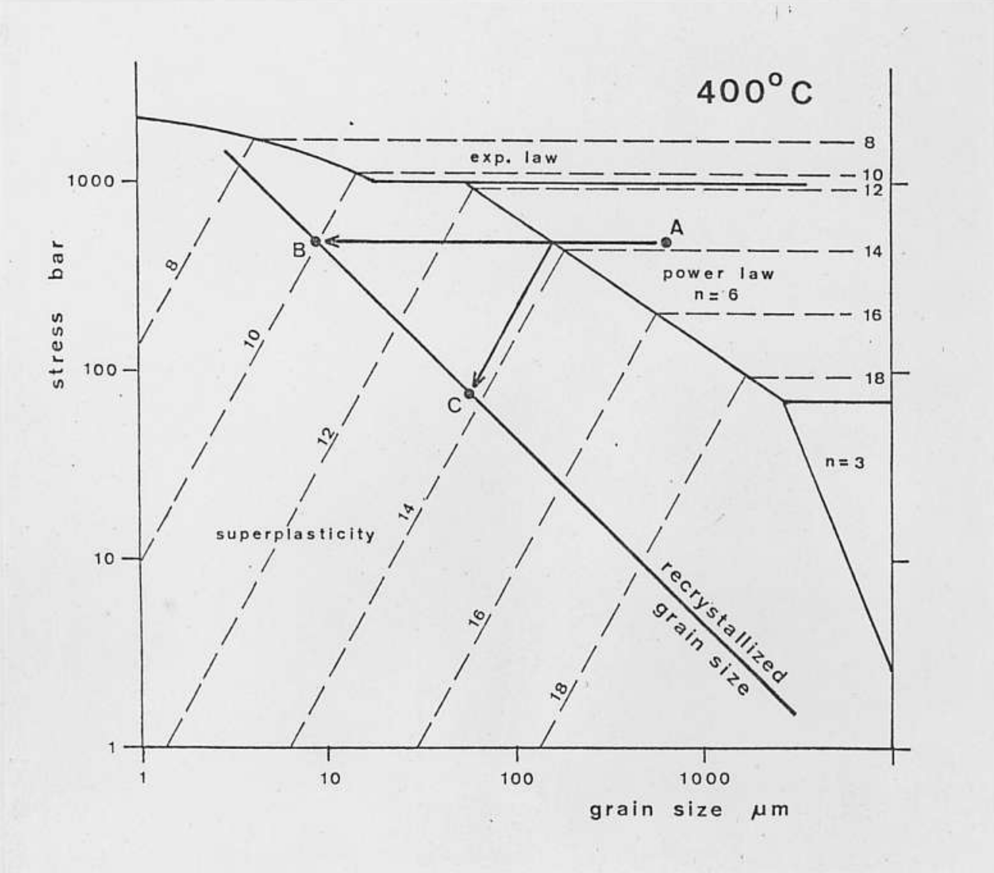
400°C
exp. law
power law
n = 6
n = 3
A
B
C
superplasticity
recrystallized grain size
stress bar
grain size μm
1
10
100
1000
8
10
12
14
16
18

Fig. 62.

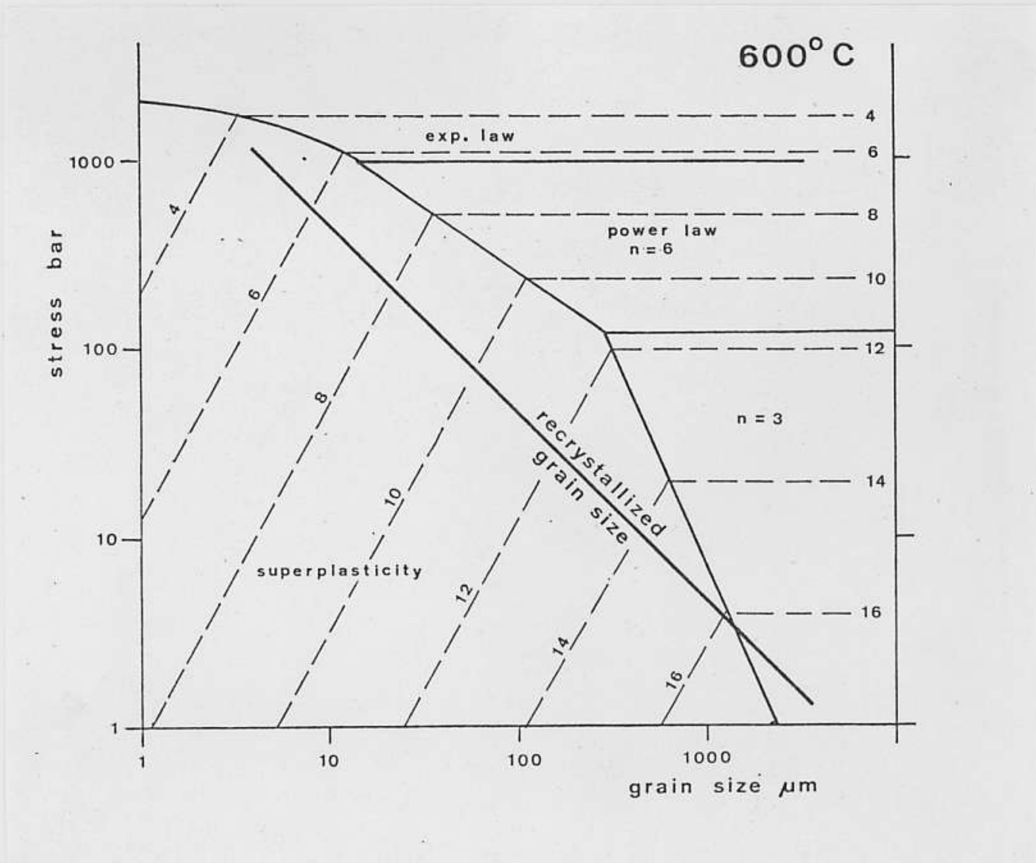
600°C
exp. law
power law
n = 6
n = 3
superplasticity
recrystallized grain size
stress bar
grain size μm
1
10
100
1000
4
6
8
10
12
14
16

Fig. 63.

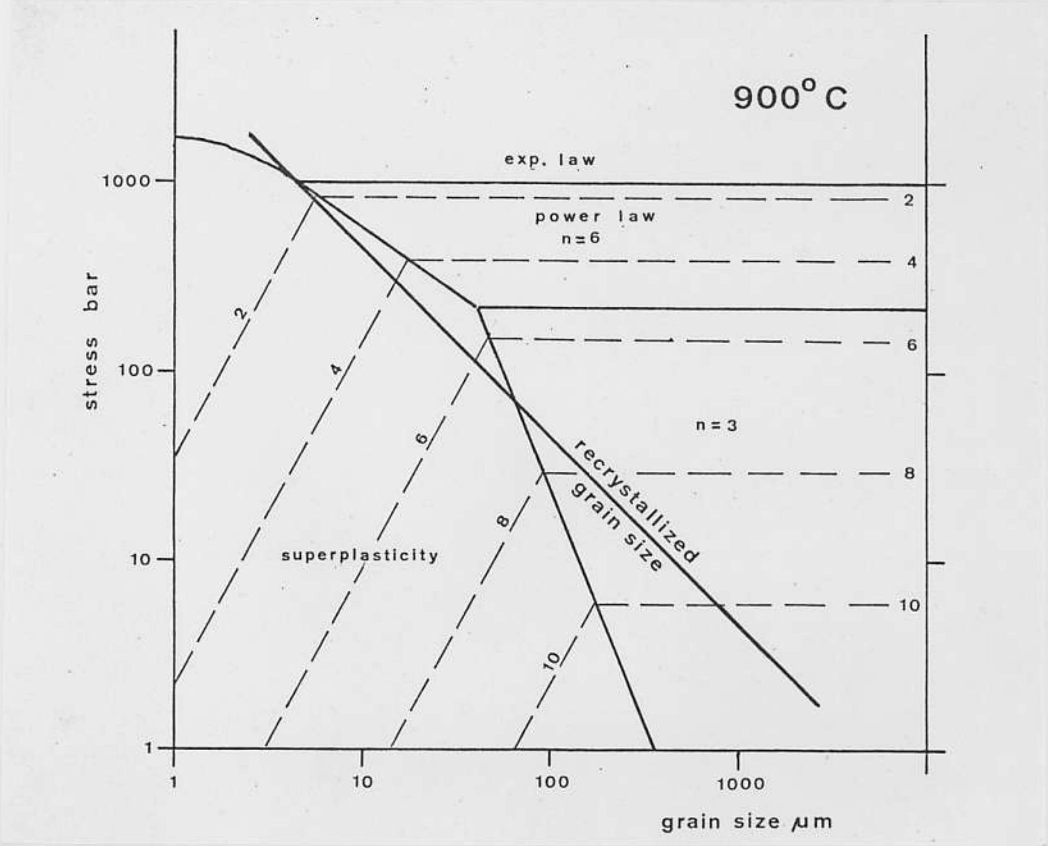

Fig. 64.

Figures 62, 63 and 64: Deformation mechanism maps for calcite at constant temperatures and represented in stress vs. grain size coordinates. The contributions from different mechanisms are taken to be non-additive for simplicity because only small errors are introduced near the mechanism boundaries. The strain rate contours are labelled with the negative exponent of the strain rate in sec^{-1}.

Superimposed on these deformation mechanism maps is the curve labelled "recrystallized grain size" taken from fig. 10.

Notice that the boundary between superplasticity and power law creep moves to lower stresses and smaller grain sizes with increasing temperature. This is due to the difference in activation energies between superplastic flow and dislocation creep.

For the explanation of points A,B,C in fig. 62 see text. These deformation mechanism maps are based on the flow laws (5), (8) and (9) for the exponential law and the power laws respectively and on flow law (4) for superplastic flow, as listed in table 1. The data on the relaxation runs on Carrara marble were preferred over the constant strain rate data because the value for the activation energy of 100 kcal $mole^{-1}$ obtained from the constant strain rate tests seems too high in comparison to all the other data on calcite (see table 1).

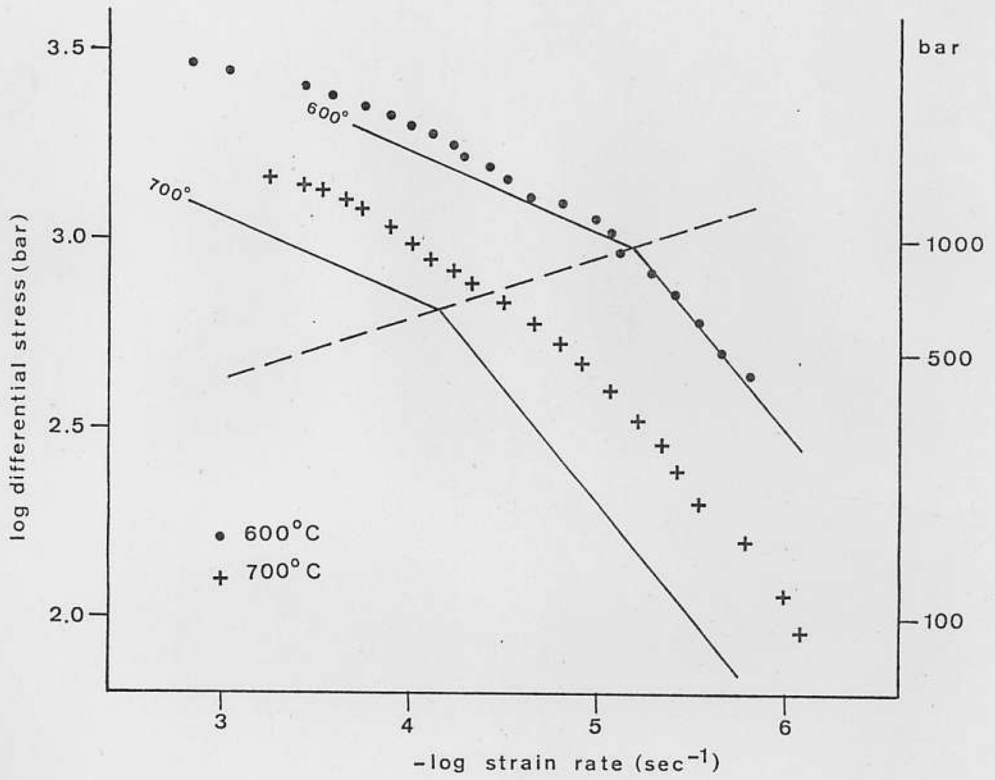

Fig. 65. Results of relaxation tests on specimens of Lochseiten mylonite. The strain rates are computed from the observed rates of stress drop by correcting for apparatus compliance. Superimposed are the best fit isotherms for Solnhofen limestone (equations (2) and (3) in table 1) for comparison. The broken line indicates the boundary between the dislocation creep and superplastic regimes. Note that a similar, although somewhat transitional change in slope of the isotherms occurs in the Lochseiten mylonite specimen.

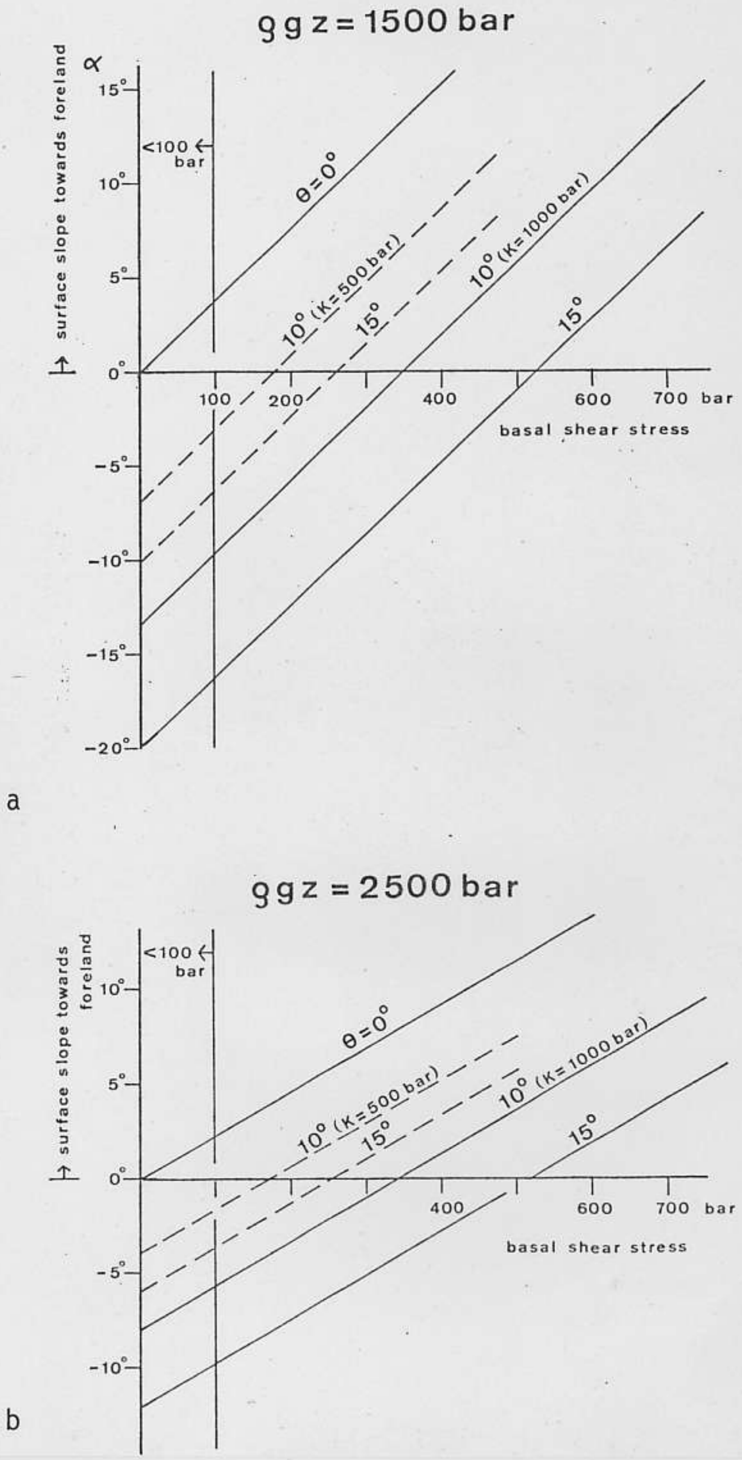

Fig. 66. Graphical representation of equation 36 in Chapple (1978) discussed in the text. This graph illustrates the dependence of the surface slope α on the absolute value of the basal shear stress in the mylonite or decollement horizon. Two sets of contours are given for a 0^0, 10^0 and 15^0 slope θ of the basal decollement horizon away from the foreland: the solid and broken lines assume a yield stress K of 1000 bar and 500 bar respectively. The top figure (a) refers to a thickness of the overthrust block of 6 km, the bottom figure (b) assumes lo km overburden. Notice that positive surface slopes, and consequently a component of gravity spreading are only obtained for relatively strong decollement horizons (far in excess of the 100 bars considered to be the maximum possible shear strength of the Lochseiten mylonite.